UNCLASSIFIED

CENTRAL RESEARCH LIBRARY

CENTRAL RESEARCH LIBRARY
DOCUMENT COLLECTION

MARTIN MARIETTA ENERGY SYSTEMS LIBRARIES

3 4456 0350444 7

ORNL-2204
Progress
cy. 4

PHYSICS DIVISION

SEMIANNUAL PROGRESS REPORT

FOR PERIOD ENDING SEPTEMBER 10, 1956

REFERENCE COPY

OAK RIDGE NATIONAL LABORATORY
OPERATED BY
UNION CARBIDE NUCLEAR COMPANY
A Division of Union Carbide and Carbon Corporation
UCC
POST OFFICE BOX X • OAK RIDGE, TENNESSEE

UNCLASSIFIED

Printed in USA. Price 50 cents. Available from the

Office of Technical Services
U. S. Department of Commerce
Washington 25, D. C.

LEGAL NOTICE

This report was prepared as an account of Government sponsored work. Neither the United States, nor the Commission, nor any person acting on behalf of the Commission:

A. Makes any warranty or representation, express or implied, with respect to the accuracy, completeness, or usefulness of the information contained in this report, or that the use of any information, apparatus, method, or process disclosed in this report may not infringe privately owned rights; or

B. Assumes any liabilities with respect to the use of, or for damages resulting from the use of any information, apparatus, method, or process disclosed in this report.

As used in the above, "person acting on behalf of the Commission" includes any employee or contractor of the Commission to the extent that such employee or contractor prepares, handles or distributes, or provides access to, any information pursuant to his employment or contract with the Commission.

UNCLASSIFIED

ORNL-2204

Contract No. W-7405-eng-26

PHYSICS DIVISION

SEMIANNUAL PROGRESS REPORT

for Period Ending September 10, 1956

A. H. Snell, Director
J. L. Fowler and E. O. Wollan, Associate Directors

DATE ISSUED

JAN 29 1957

OAK RIDGE NATIONAL LABORATORY
Operated by
UNION CARBIDE NUCLEAR COMPANY
A Division of Union Carbide and Carbon Corporation
Post Office Box X
Oak Ridge, Tennessee

MARTIN MARIETTA ENERGY SYSTEMS LIBRARIES

UNCLASSIFIED

3 4456 0350444 7

ORNL-2204
Progress

INTERNAL DISTRIBUTION

1. C. E. Center
2. Biology Library
3. Health Physics Library
4-6. Central Research Library
7. Reactor Experimental Engineering Library
8-19. Laboratory Records Department
20. Laboratory Records, ORNL R.C.
21. A. M. Weinberg
22. L. B. Emlet (K-25)
23. J. P. Murray (Y-12)
24. J. A. Swartout
25. E. H. Taylor
26. E. D. Shipley
27. E. J. Murphy
28. M. L. Nelson
29. A. H. Snell
30. A. Hollaender
31. K. Z. Morgan
32. F. L. Culler
33. M. T. Kelley
34. E. M. King
35. E. O. Wollan
36. D. W. Cardwell
37. A. S. Householder
38. L. D. Roberts
39. R. B. Briggs
40. R. N. Lyon
41. W. C. Koehler
42. E. P. Blizard
43. M. E. Rose
44. G. E. Boyd
45. W. H. Sullivan
46. R. W. Stoughton
47. C. E. Winters
48. W. H. Jordan
49. E. C. Campbell
50. D. S. Billington
51. M. A. Bredig
52. R. S. Livingston
53. C. P. Keim
54. F. C. Maienschein
55. C. E. Clifford
56. R. C. Block
57. C. D. Susano
58. C. J. Borkowski
59. M. J. Skinner
60. M. K. Wilkinson
61. J. W. Cable
62. P. M. Reyling
63. D. D. Cowen
64. W. M. Good
65. G. C. Williams
66. J. L. Fowler
67. R. W. Johnson
68. J. R. McNally, Jr.
69. J. L. Gabbard
70. R. A. Charpie
71. E. P. Wigner (consultant)
72. G. G. Slaughter
73. Eugene Guth
74. R. W. Peelle
75. P. R. Bell
76. G. G. Kelley
77. C. C. Harris
78. H. G. MacPherson
79. P. H. Stelson
80. J. E. Sherwood
81. W. Zobel
82. R. B. Murray
83. H. B. Willard
84. J. Schenck
85. J. H. Neiler
86. J. A. Harvey
87. C. F. Barnett
88. N. H. Lazar
89. R. R. Dickison
90. A. Simon
91. J. H. Gibbons
92. J. J. Pinajian
93. S. Bernstein
94. H. A. Bethe (consultant)
95. ORNL – Y-12 Technical Library, Document Reference Section

EXTERNAL DISTRIBUTION

96. W. G. Pollard, ORINS
97. W. K. H. Panofsky, Stanford University
98. L. C. Biedenharn, Rice Institute
99. R. F. Bacher, California Institute of Technology
100. John Dunning, Columbia University
101. Phillips Petroleum Co., Attn: Librarian
102. R. L. Heath, Phillips Petroleum Company
103. S. DeBenedetti, Carnegie Institute of Technology
104. Massachusetts Institute of Technology, Department of Electrical Engineering
105. A. von Hippel, Laboratory for Insulation Research, MIT
106. M. Goodrich, Louisiana State University
107. Truman S. Grey, Massachusetts Institute of Technology
108. V. C. Wilson, General Electric Co., Schenectady
109. D. S. Hughes, University of Texas
110. E. A. Rollor, ANP Project Office, Fort Worth
111. S. Frankel, Physics Dept., University of Pennsylvania
112. G. Griffith, Westinghouse Research Laboratory, E. Pittsburgh, Pennsylvania
113. F. Allison, Emory and Henry University, Emory, Virginia
114. J. A. Sauer, Physics Dept., Pennsylvania State College, State College, Pennsylvania
115. J. E. Goldman, Dept. of Physics, Carnegie Institute of Technology
116. R. Stephenson, Dept. of Chemical Engineering, New York University
117. M. Goldhaber, Brookhaven National Laboratory
118. M. N. Saha, c/o Library, Institute of Nuclear Physics, 92 Upper Circular Road, Calcutta, India
119. J. A. Wheeler, Palmer Physical Laboratory, Princeton University
120. R. S. Christy, California Institute of Technology
121. T. J. Turner, Wake Forrest College
122. T. Lauritsen, California Institute of Technology
123. N. F. Ramsey, Harvard University
124. University of Notre Dame (Attention: Library)
125. J. H. Van Vleck, Harvard University
126. A. Glassgold, University of Minnesota
127. P. M. Steir, National Carbon Research Laboratories, P. O. Box 6087, Cleveland, Ohio
128. Boeing Airplane Company
129. Division of Research and Development, AEC, ORO
130. John Manley, Physics Dept., University of Washington, Seattle
131. C. L. McGinnis, Nuclear Data Project, National Research Council, Washington
132. J. Rotblat, The Medical College of St. Bartholomew's Hospital, Charterhouse Square, London ECI, England

133-731. Given distribution as shown in TID-4500 (12th ed.) under Physics Category

Physics Division progress reports previously issued in this series are as follows:

ORNL-325 Supplement	December, January, and February, 1948-1949
ORNL-366	Period Ending June 15, 1949
ORNL-481	Period Ending September 25, 1949
ORNL-577	Period Ending December 15, 1949
ORNL-694	Period Ending March 15, 1950
ORNL-782	Period Ending June 15, 1950
ORNL-865	Period Ending September 20, 1950
ORNL-940	Period Ending December 20, 1950
ORNL-1005	Period Ending March 20, 1951
ORNL-1092	Period Ending June 20, 1951
ORNL-1164	Period Ending September 20, 1951
ORNL-1278	Period Ending December 20, 1951
ORNL-1289	Period Ending March 20, 1952
ORNL-1365	Period Ending June 20, 1952
ORNL-1415	Period Ending September 20, 1952
ORNL-1496	Period Ending December 20, 1952
ORNL-1620	Period Ending September 10, 1953
ORNL-1705	Period Ending March 10, 1954
ORNL-1798	Period Ending September 10, 1954
ORNL-1879	Period Ending March 20, 1955
ORNL-1975	Period Ending September 10, 1955
ORNL-2076	Period Ending March 10, 1956

TABLE OF CONTENTS AND SUMMARY

RELATIVISTIC TWO-BODY WAVE EQUATION
D. A. Geffen and T. A. Welton 1

The relativistic two-body wave equation has been studied with the aim of using it for improved calculations of the two-nucleon problem.

FINITE RESULTS FOR MASS AND COUPLING-CONSTANT RENORMALIZATIONS
T. A. Welton 1

A procedure for obtaining finite mass corrections in all interesting relativistic quantum field theories has been found.

WIGNER-EISENBUD RELATION FOR THE R MATRIX
G. T. Trammell 5

A new derivation is given for the energy dependence of the Wigner-Eisenbud R matrix.

EXPONENTIALLY DECAYING STATES IN QUANTUM MECHANICS
G. T. Trammell 7

It is shown that a quantum mechanical state will decay no more rapidly than some inverse power of the time for sufficiently large times.

POTENTIAL WELLS FOR LIGHT NUCLEI
J. L. Fowler 10

Simple static potential wells with diffuse boundaries have been used to calculate the s-wave phase shift for elastic neutron scattering from light zero-spin nuclei. The same potentials can also be used to obtain the correct energy position of the $2s$ bound states.

NONLINEAR ACCELERATOR ORBIT CODES
T. A. Welton and T. I. Arnette 12

A set of Oracle codes of increasing flexibility and accuracy has been constructed for the purpose of carrying out calculations on linear and nonlinear orbit behavior in accelerators with constant orbital frequency as well as with constant momentum compaction.

ANALYTICAL TREATMENT OF ACCELERATION THROUGH RESONANCES
M. M. Gordon and T. A. Welton 14

Analytical and numerical studies of the phenomena encountered in passage through imperfection resonances have been largely completed.

CYCLOTRON MODEL DESIGN STUDY
T. I. Arnette, H. G. Blosser, H. C. Owens, and G. T. Trammell 15

Oracle calculations pertaining to the design of an electron model for a straight four-sector Thomas type of cyclotron are described.

ANGULAR DISTRIBUTIONS AND POLARIZATION OF GAMMA RAYS FROM COULOMB EXCITATION
F. K. McGowan and P. H. Stelson 20

Angular distributions and polarization-direction correlations have been measured for the gamma rays following coulomb excitation in Tl^{205}, Tl^{203}, Au^{197}, Ir^{193}, Ir^{191}, Os^{188}, $Os^{190,192}$, Ag^{109}, Ag^{107}, and Mo^{95}. Polarization-direction measurements of several transitions have resolved the ambiguity in the values of $(E2/M1)1/2$ and of the spins of the excited state.

THE REACTION $N^{14}(p,p'\gamma)N^{14}$
J. K. Bair, H. O. Cohn, J. D. Kington, and H. B. Willard 23

The yield of the 2.31-Mev gamma rays resulting from the inelastic scattering of protons by the first excited state of N^{14} has been measured for bombarding energies ranging from 2.5 to 5.1 Mev.

THE $C^{13}(p,\gamma)N^{14}$ REACTION
H. B. Willard, J. K. Bair, and H. O. Cohn 25

A detailed spectrum of the $C^{13}(p,\gamma)N^{14}$ reaction at the 3.11-Mev resonance shows that this level in N^{14} at 10.43-Mev excitation decays mainly to the ground state, with about a 10% cascade through the 6.44-Mev level.

PRELIMINARY YIELD OF THE REACTION $C^{13}(p,p'\gamma)C^{13}$
H. O. Cohn, J. K. Bair, and H. B. Willard 26

A preliminary yield curve for the gamma rays resulting from the reaction $C^{13}(p,p'\gamma)C^{13}$ has been obtained for incident proton energies between 3.6 and 5.0 Mev.

THRESHOLDS AND CROSS SECTIONS FOR (p,n) REACTIONS IN INTERMEDIATE NUCLEI
C. H. Johnson, A. Galonsky, and J. Ulrich 28

Absolute (p,n) cross sections are reported for Ti^{49}, V^{51}, Mn^{55}, Ga^{71}, and As^{75} for proton energies from threshold to 500 kev above threshold. The threshold for the $Se^{77}(p,n)Br^{77}$ reaction was observed at 2176 kev; that for $Se^{82}(p,n)Br^{82}$ is not greater than 970 kev, while that for $Nb^{93}(p,n)Mo^{93}$ is not greater than 1310 kev.

THE 2.07-Mev RESONANCE IN THE NEUTRON TOTAL CROSS SECTION OF C^{12}
H. B. Willard, J. K. Bair, and H. O. Cohn 30

The total cross section of C^{12} has been remeasured in the region of the 2.07-Mev resonance. When corrections are made for background, in-scattering, energy resolution, and the second group of neutrons from the $Li^7(p,n)$ reaction, the result is in good agreement with the assignment of $D_{5/2}$ to the 6.86-Mev excited state of C^{13}.

ELASTIC NEUTRON SCATTERING DIFFERENTIAL CROSS SECTIONS FOR OXYGEN AND BERYLLIUM
H. O. Cohn and J. L. Fowler 32

Elastic neutron scattering differential cross sections for oxygen and beryllium at $E_n = 0.73$ and 1.50 Mev are presented.

NEUTRON RESONANCE PARAMETERS OF Eu^{151} AND Eu^{153}
J. A. Harvey and R. C. Block 33

The parameters of the resonances in Eu^{151} and Eu^{153} have been determined from 1 to 10 ev from transmission measurements with enriched isotopes with the ORNL fast chopper.

MEASUREMENT OF THERMAL-NEUTRON RELAXATION TIMES IN SUBCRITICAL SYSTEMS
E. C. Campbell and P. H. Stelson 34

Additional measurements on the decay rate of a subcritical reactor following exposure to bursts of fast neutrons are described and interpreted. Thermal-neutron flux distribution measurements, made with a small LiI probe, are in agreement with theory.

ENERGY LOSS OF PROTONS IN SILVER AND GOLD
P. H. Stelson and F. K. McGowan 36

Measurements of coulomb excitation in thick and thin targets of silver and gold have furnished information on the energy loss of protons in these materials.

CROSS SECTIONS FOR ELECTRON LOSS BY HYDROGEN ATOMS AND THE EQUILIBRIUM CHARGE DISTRIBUTION OF A HYDROGEN BEAM

C. F. Barnett, H. K. Reynolds, and R. G. Reinhardt 39

Cross sections were determined for electron loss by fast hydrogen atoms in various stopping gases in the energy range 250 kev to 1 Mev. Also, determinations were made of the equilibrium charge distribution of a hydrogen beam after it had passed through a thick gas target.

MOLECULAR BREAKUP FOLLOWING BETA DECAY OF TRITIUM HYDRIDE

A. H. Snell, F. Pleasonton, and H. E. Leming 42

The charge spectrometer has been applied to the study of the breakup of the HT molecule following beta decay. There is a probability of more than 90% that the molecule will hold together as the helium hydride ion, $(He^3H)^+$. An upper limit of 1.6% is placed upon the frequency of electron shake-off resulting from the nuclear charge change that accompanies the beta decay.

NEUTRON DIFFRACTION BY RARE-EARTH COMPOUNDS

W. C. Koehler, E. O. Wollan, M. K. Wilkinson, and J. W. Cable 44

Neutron-diffraction evidence for antiferromagnetic ordering of rare-earth ions in $ErFeO_3$ and Er_2O_3 is described. Possible correlations with the general problem of antiferromagnetic ordering in oxidic substances are discussed.

METHODS FOR SINGLE-CRYSTAL MAGNETIC NEUTRON-DIFFRACTION STUDIES AT LOW TEMPERATURES

E. O. Wollan, W. C. Koehler, M. K. Wilkinson, and J. W. Cable 49

A goniometer has been incorporated in the low-temperature cryostat associated with the neutron-diffraction spectrometer in order to permit the magnetic scattering properties of single crystals to be studied at low temperatures.

ANTIFERROMAGNETISM IN $MnCl_2$

M. K. Wilkinson, J. W. Cable, E. O. Wollan, and W. C. Koehler 51

Neutron-diffraction measurements from single crystals of $MnCl_2$ have confirmed previous specific-heat and magnetic-susceptibility measurements which suggested two antiferromagnetic transitions at low temperatures.

MAGNETIC NEUTRON SCATTERING FROM $CoCl_2$ AND $FeCl_2$

M. K. Wilkinson and J. W. Cable 53

Investigations of the diffuse scattering of neutrons from $FeCl_2$ and $CoCl_2$ near the Néel temperatures have shown that ferromagnetic coupling is predominant in these antiferromagnetic structures. This result explains the abnormal behavior found in previous measurements of the magnetic susceptibilities.

THE A-8 LINEAR AMPLIFIER

G. G. Kelley 55

A new amplifier has been developed for pulse spectrometry. It features extremely good overload tolerance, fast pulse response, high gain, stability, and linearity.

VARIATION OF NaI(Tl) DETECTION EFFICIENCIES WITH CRYSTAL SIZE AND GEOMETRY FOR MEDICAL RESEARCH

J. E. Francis, C. C. Harris, and J. I. Trombka 57

The variation of detection efficiencies with crystal size and geometry for medical research has been measured. These measurements show that a 3 × 3 in. crystal and the spectrometry method of counting yield the best detection efficiency.

TABLES OF SOLID ANGLES AND ACTIVATIONS
A. V. H. Masket, R. L. Macklin, and H. W. Schmitt 59

Tables of solid angles and linear activations for right circular cylinders have been prepared. These include the solid angle subtended by a circular disk and cover a wide range of dimensions and spacings.

NUCLEAR ORIENTATION OF Np^{237}, U^{233}, AND U^{235} NUCLEI
L. D. Roberts, J. W. T. Dabbs, and G. W. Parker 60

Further angular-distribution measurements on alpha particles emitted by partially oriented Np^{237} and U^{233} nuclei have been made. A theoretical discussion of the results is given.

PUBLICATIONS

W. S. Lyon and N. H. Lazar, "Decay of Mg^{27}," *Phys. Rev.* **101,** 1524 (1956).

C. H. Johnson and H. E. Banta, "Tritium Gas Target for Neutron Production," *Rev. Sci. Instr.* **27,** 132 (1956).

C. C. Harris, "The 'Hard Bottoming' Technique in Nuclear Instrumentation Circuit Design," *Inst. Radio Engrs. – Trans. on Nuclear Science* **NS-3**(2), 5 (1956).

D. A. Geffen and F. L. Scarf, "Spurious Solutions of a Bethe-Salpeter Equation," *Phys. Rev.* **101,** 1829 (1956).

G. D. O'Kelley, N. H. Lazar, and E. Eichler, "Decay of Rb^{89}," *Phys. Rev.* **102,** 223 (1956).

J. L. Fowler and J. E. Brolley, Jr., "Monoenergetic Neutron Techniques in the 10–30 Mev Range," *Revs. Mod. Phys.* **28,** 103 (1956).

E. D. Klema, "Gamma-Gamma Angular Correlation in Sr^{88}," *Phys. Rev.* **102,** 449 (1956).

R. L. Macklin, H. W. Schmitt, and J. H. Gibbons, "Neutron Absorption Cross Sections of U^{235} and Pu^{239} in the 5- to 50-kev Energy Range," *Phys. Rev.* **102,** 797 (1956).

S. Bernstein, M. M. Shapiro, C. P. Stanford, T. E. Stephenson, J. B. Dial, S. Freed, G. W. Parker, A. R. Brosi, G. M. Herbert, and T. W. DeWitt, "The Neutron Cross Section of Xe^{135} as a Function of Energy," *Phys. Rev.* **102,** 823 (1956).

J. E. Francis and P. R. Bell, "Medical Scintillation Spectrometer," *Proceedings of the International Conference on the Peaceful Uses of Atomic Energy,* vol 14, p 193, United Nations, New York, 1956.

G. G. Kelley, "Methods of Pulse Analysis," *Proceedings of the International Conference on the Peaceful Uses of Atomic Energy,* vol 14, p 260, United Nations, New York, 1956.

S. Bernstein and E. C. Smith, "The Cross Section of the Fission Product Poison Xe^{135} as a Function of Energy," *Proceedings of the International Conference on the Peaceful Uses of Atomic Energy,* vol 4, p 153, United Nations, New York, 1956.

A. H. Snell, "The Nuclear Reactor in Basic Science," *Proceedings of the International Conference on the Peaceful Uses of Atomic Energy,* vol 2, p 248, United Nations, New York, 1956.

E. O. Wollan and C. G. Shull, "Neutron Diffraction Research in the United States," *Proceedings of the International Conference on the Peaceful Uses of Atomic Energy,* vol 2, p 66, United Nations, New York, 1956.

N. H. Lazar, "Decay of Sb^{125}," *Phys. Rev.* **102,** 1058 (1956).

L. D. Roberts, book review ("Quantum Theory of Solids," by R. E. Peierls, Oxford University Press, New York, 1955), *Phys. Today* **9,** 29 (1956).

C. G. Shull and E. O. Wollan, "Applications of Neutron Diffraction to Solid State Problems," *Solid State Physics,* vol II, p 137–217, Academic Press, New York, 1956.

R. L. Macklin and H. S. Pomerance, "Resonance Capture Integrals," *Progress in Nuclear Energy,* vol I, chap. 6, McGraw-Hill, New York, 1956.

J. A. Harvey and J. E. Sanders, "Summary of Data on the Cross Sections and Neutron Yields of U^{233}, U^{235}, and Pu^{239}," *Progress in Nuclear Energy,* vol I, chap. 1, McGraw-Hill, New York, 1956.

A. H. Snell and F. Pleasonton, "Multiple Ionization in Xenon Following Internal Conversion," *Phys. Rev.* **102,** 1419 (1956).

J. H. Gibbons, "Neutron Resonances in the kev Region," *Phys. Rev.* **102,** 1574 (1956).

H. W. Newson, J. H. Gibbons, H. Marshak, R. M. Williamson, R. A. Mobley, A. L. Toller, and R. Block, "Neutron Resonances in the kev Region: The Heavy Even Elements," *Phys. Rev.* **102,** 1580 (1956).

M. E. Rose, book review ("Applications of Spinor Invariants in Atomic Physics," by H. C. Brinkman, Interscience, New York, 1956), *Phys. Today* **9**(7), 17 (1956).

C. H. Johnson and C. C. Trail, "Proton-Recoil Neutron Spectrometer," *Rev. Sci. Instr.* 27, 468 (1956).

A. H. Snell, book review ("Proceedings of the International Conference on the Peaceful Uses of Atomic Energy," vols 2 and 14, United Nations, New York, 1956), *Am. Scientist* **44,** 200A (1956).

M. K. Wilkinson and C. G. Shull, "Neutron Diffraction Studies on Iron at High Temperatures," *Phys. Rev.* **103,** 516 (1956).

H. A. Gersch, C. G. Shull, and M. K. Wilkinson, "Critical Magnetic Scattering of Neutrons by Iron, *Phys. Rev.* **103,** 525 (1956).

A. E. Glassgold and A. Galonsky, "Alpha-Particle Model of C^{12}," *Phys. Rev.* **103,** 701 (1956).

E. D. Klema and R. K. Osborn, "Empirical Determination of Nuclear Moments of Inertia and Intrinsic Quadrupole Moments," *Phys. Rev.* **103,** 833 (1956).

T. A. Welton, book review ("Science and the Human Imagination," by M. B. Hesse, Philosophical Library, New York, 1955), *Phys. Today* **9**(8), 39 (1956).

C. C. Harris and P. R. Bell, "Filamentary Subminiature Scalers," *Rev. Sci. Instr.* **27,** 608 (1956).

P. M. Stier and C. F. Barnett, "Charge Exchange Cross Sections of Hydrogen Ions in Gases," *Phys. Rev.* **103,** 896 (1956).

F. K. McGowan and P. H. Stelson, "Evidence for Reduction of *M*1 *K*-Shell Internal Conversion Coefficient," *Phys. Rev.* **103,** 1133 (1956).

A. H. Snell, book review ("Proceedings of the International Conference on the Peaceful Uses of Atomic Energy," vols 4 and 16, United Nations, New York, 1956), *Phys. Today* **9**(9), 25 (1956).

PAPERS PRESENTED AT SCIENTIFIC MEETINGS

American Physical Society, Southeastern Section Meeting, Nashville, Tennessee, March 29–31, 1956

W. C. Koehler (invited paper), "Neutron-Diffraction Studies of Magnetic Interaction."

F. K. McGowan (invited paper), "Yields, Angular Distributions, and Polarization of Gamma Rays from Coulomb Excitation."

T. A. Welton (invited paper), "A Survey of Fixed-Frequency High-Energy Accelerators,"

E. C. Campbell and P. H. Stelson, "Fast-Decay Measurements with Pulsed Neutron Source."

C. H. Johnson and J. P. Judish, "Compound Electrostatic Lens for the ORNL 3-Mv Van de Graaff."

R. L. Macklin, "Neutron Activation of Iodine near 25 kev."

C. D. Moak and R. F. King, "The ORNL 625-kv Cascade Accelerator."

A. H. Snell and F. Pleasonton, "Charge States of Rb^{85} Following Beta Decay of 9.4-year Kr^{85}."

P. H. Stelson and F. K. McGowan, "Polarization of γ-Rays in Ta^{181}."
H. B. Willard, J. K. Bair, H. O. Cohn, and J. D. Kington, "The $Si^{28}(p,p'\gamma)Si^{28}$ Reaction."

High Energy Nuclear Physics Conference, Rochester, New York, April 3–7, 1956

T. A. Welton, "On the Possibility of a Finite Fermion Mass Renormalization."

Spring Meeting of Optical Society of America, Philadelphia, Pennsylvania, April 5–7, 1956

P. R. Bell (invited paper), "Optical Problems and Scintillation Counters."

American Physical Society Meeting, Washington, D. C., April 26–28, 1956

A. H. Snell (invited paper), "Charge States in Rare Gases Following Internal Conversion and Beta Emission."
E. C. Campbell and P. H. Stelson, "Relaxation Times of Subcritical Reactor by Pulsed-Neutron Techniques."
H. O. Cohn and J. L. Fowler, "Differential Elastic Scattering of Neutrons from Neon."
J. W. T. Dabbs, L. D. Roberts, and G. W. Parker, "Alpha-Particle Emission from U^{233} Nuclei Aligned by the Pound Method."
W. C. Koehler and E. O. Wollan, "Magnetic Neutron Diffraction Study of $MnBr_2$ and $FeBr_2$."
N. H. Lazar and G. D. O'Kelley, "Decay of Nb^{90}."
F. K. McGowan, P. H. Stelson, and M. M. Bretscher, "Angular Distribution of Gamma Rays Following Coulomb Excitation in Pt^{194}, Cd^{114}, Pd^{110}, Ru^{104}, Cd^{113}, and Cd^{111}."
C. D. Moak and A. Galonsky, "Search for Level in C^{12} Predicted by the Alpha-Particle Model."
V. E. Pilcher, D. J. Hughes, and J. A. Harvey, "Neutron Resonance Parameters of U^{234} and U^{236}."
L. D. Roberts, J. W. T. Dabbs, G. W. Parker, and R. D. Ellison, "Alpha-Particle Emission from Oriented Np^{237} Nuclei and the Spheroidal Shape of This Nucleus."
P. H. Stelson and F. K. McGowan, "Polarization of Gamma Rays Following Coulomb Excitation."
M. K. Wilkinson and J. W. Cable, "Antiferromagnetic Structures of $FeCl_2$ and $CoCl_2$."
J. E. Wills, Jr., "The Scattering of Neutrons from F^{19} and C^{12} Between 0.5 and 5 Mev."

American Nuclear Society Meeting, Chicago, Illinois, June 6–8, 1956

E. C. Campbell and P. H. Stelson, "Reactor Parameters of Small Subcritical Reactor by Pulsed-Neutron Techniques."

Annual Meeting of the American Crystallographic Association, French Lick, Indiana, June 11–15, 1956

W. C. Koehler, "Magnetic form Factors by Neutron Scattering."
M. K. Wilkinson, W. C. Koehler, J. W. Cable, and E. O. Wollan, "Magnetic Scattering of Neutrons from Hexagonal Layer Structures."

Annual Meeting of Society of Nuclear Medicine, Salt Lake City, Utah, June 21–23, 1956

C. C. Harris, J. E. Francis, and P. R. Bell, "High-Resolution Scanning of Radioactivity in Vivo on Minimum Dosages."

Gordon Research Conference, Meriden, New Hampshire, June 25–29, 1956

F. K. McGowan and P. H. Stelson (invited paper), "Coulomb Excitation Studies."
P. R. Bell (invited paper), "Precision Scintillation Spectrometry."

International Conference on Nuclear Reactions, Amsterdam, The Netherlands, July 2–7, 1956

J. L. Fowler, "Differential Elastic Scattering of Neutrons from Light Elements."

P. H. Stelson and F. K. McGowan (paper presented by J. L. Fowler), "Yields, Angular Distributions, Polarization, and Internal Conversion of Gamma Rays from Coulomb Excitation."

Eleventh Annual Calorimetry Conference, The Johns-Hopkins University, Baltimore, Maryland, September 14–15, 1956

L. D. Roberts, J. W. T. Dabbs, and G. W. Parker, "Specific Heat Due to Nuclear Quadrupole Coupling in the $U^{235}O_2^{++}$ Group."

ANNOUNCEMENTS

Additions to the Physics Division staff during this period were as follows: H. C. Owens (Accelerator Studies), and G. P. Boicourt and D. P. Hamblen (Scintillation Spectrometry).

Summer personnel included the following research participants and visitors: A. E. S. Green (Associate Professor, Florida State University), T. A. Green (Assistant Professor, Wesleyan University), M. Gordon (Associate Professor, University of Florida), and F. Rohrlich (summer visitor, State University of Iowa), Theoretical Physics; J. H. Henkel (Assistant Professor, University of Florida), H. A. Gersch (summer visitor, Georgia Institute of Technology), and U. H. Bents (summer visitor, former ORINS Fellow), Neutron Diffraction; H. L. Reaves (Assistant Professor, Hampden-Sydney College) and H. K. Reynolds (summer visitor, University of Houston), High Voltage; and J. I. Trombka (summer visitor, ORINS), Scintillation Spectrometry.

University students here for the summer were as follows: V. E. Barnes, II (Harvard University), J. P. Ulrich (University of Michigan), and D. R. Bitzer (University of Richmond), High Voltage; G. R. Burleson (Stanford University), Scintillation Spectrometry; P. J. Haigh (Carson-Newman College) Theoretical Physics; H. E. Leming (University of Arkansas), Recoil Spectrometry; W. V. Weyhmann (Duke University), Low-Temperature Physics; and J. M. Winter, Jr. (Massachusetts Institute of Technology), Atomic-Beam Spectroscopy.

W. I. Linlor has returned to the University of California Radiation Laboratory at Berkeley, California, after spending six months on loan to the Physics Division (Project Sherwood).

Terminations: U. H. Bents, ORINS Fellow (Neutron Diffraction); J. E. Wills, ORINS Fellow (High Voltage); D. A. Geffen (Theoretical Physics); and E. D. Klema (Scintillation Spectrometry).

S. Bernstein returned to the Laboratory in June 1956 from Haifa, Israel, where he spent the past year in teaching and research at the Israel Institute of Technology.

PHYSICS DIVISION
SEMIANNUAL PROGRESS REPORT

RELATIVISTIC TWO-BODY WAVE EQUATION

D. A. Geffen T. A. Welton

A study has been completed of the relativistic two-body wave equation (Bethe-Salpeter equation), aimed at providing a more adequate foundation for a relativistic theory of the two-nucleon system. The equation, with spin included and with the interaction kernel calculated in the ladder approximation, has been reduced to four coupled partial differential equations (relative distance and relative time) for the case of the $^1S_0$ state. The behavior for small times and distances has been deduced, and it has been shown that the singularity of the kernel does not preclude the existence of a well-behaved solution of the equation. This is true both for positronium and for the two-nucleon system, assuming symmetrical pseudoscalar meson theory with pseudoscalar coupling. It is hoped that future numerical work can give detailed properties of the state.

FINITE RESULTS FOR MASS AND COUPLING-CONSTANT RENORMALIZATIONS

T. A. Welton

Relativistic field theories, in general, yield infinite results which must be reinterpreted in terms of infinite alterations of mass and coupling constant. In many cases these corrections can be treated as finite and ignored (renormalization), and, in fact, it has been proposed that only those theories be regarded as physically possible which are capable of renormalization. It is, however, quite unsatisfactory to have unexplained divergences in a theory, even though they can be circumvented in practical computation. In addition, one of the two most attractive meson theories (pseudoscalar mesons with pseudovector coupling) has been ruled out, mainly because it is not renormalizable.

It is therefore of interest to attempt to reformulate the quantum field theories in such a way that the divergences appear as mathematical defects, if possible, and such that finite values replace the previous divergent values. This reformulation has been largely accomplished in work here previously reported. It has been shown that a problem can be set up containing the elements of the known problem, but capable of solution by new methods which admit well-defined answers.

As an example, consider the mass correction for a nucleon interacting with the symmetrical pseudoscalar meson field through the pseudovector (gradient) coupling. The wave equation is

$$n\psi = \gamma p \psi + \frac{f}{\mu} \gamma_5 \tau_i \gamma \frac{\partial A_i}{\partial x} \psi \ . \tag{1}$$

The formalism has been previously described, with x referring to four Cartesian coordinates. The mass constant of the nucleon ("bare mass") is the analytical continuation to the imaginary axis of n. The quantity A_i is one I-space component of the pseudoscalar field and is conveniently written

$$A_i = \frac{1}{\sqrt{4\pi^3}} \int \frac{dk}{\sqrt{k^2 + \mu^2}} \mathcal{A}_i(k)\, e^{ikx} \ , \tag{2}$$

with μ = the meson mass and $\mathcal{A}_i(k)$ a *classical* random variable satisfying

$$\langle \mathcal{A}_i(k)\, \mathcal{A}_j(k') \rangle = \delta_{ij}\, \delta(k + k') \ . \tag{3}$$

The computation procedure is to assume a definite value for the four-momentum P of the nucleon-meson system, calculate the value of n for a definite choice of $\mathcal{A}_i(k)$, and then calculate $\langle n \rangle$, using Eq. 3. This average must then be suitably analytically continued and interpreted as the nucleon bare mass m required to give experimental mass $|P|$. If the first and second terms of the operator on the right of Eq. 1 are denoted by N_0 and N_1, a variational principle for n can be written

$$n = \frac{(\psi^\star N_0\, \psi) + (\psi^\star N_1\, \psi)}{(\psi^\star\, \psi)} \ , \tag{4}$$

with parentheses indicating integrations and summations over the spin and the coordinate space. The correct value of n is obtained by varying ψ to make n stationary, but a presumably convergent sequence of approximate wave functions can be obtained by the iteration procedure. Let ψ_0 be the correct function (plane wave with four-momentum P) as $f \to 0$. A sequence of functions can then be defined by

$$\begin{cases} \psi_1 = \left[1 + (n - N_0)^{-1} N_1\right] \psi_0 \ , \\ \psi_2 = \left[1 + (n - N_0)^{-1} N_1 + (n - N_0)^{-1} N_1 (n - N_0)^{-1} N_1\right] \psi_0 \ , \\ \cdots \ . \end{cases} \tag{5}$$

It is simple to show that ψ_1, for example, is the best (in the varictional sense) trial function with the general form of the first-order perturbed wave function. In the above, however, it is not assumed that the correction of ψ_0 is small compared with ψ_0. If perturbation theory were valid, n could be set equal to $n_0 = |P|$. This will not be so, in general, and Eq. 4 is a complicated implicit equation for n. Actually, the average of Eq. 4 over the possible values of the random amplitude variables is required. This complicated average can be very much simplified by the observation that

$$\left\langle \frac{u}{v} \right\rangle = \frac{\langle u \rangle}{\langle v \rangle} \ , \tag{6}$$

with an error which goes to zero as a reciprocal power of the length of the four-dimensional quantization volume (assumed infinite).

If ψ_1 is used for ψ, Eq. 4 becomes, with the use of Eqs. 5 and 6,

$$\langle n \rangle = \frac{\left(\psi_0^\star \left[N_0 + \left\langle N_1 \dfrac{N_0}{(n - N_0)^2} N_1 \right\rangle + 2 \left\langle N_1 \dfrac{1}{n - N_0} N_1 \right\rangle\right] \psi_0\right)}{\left(\psi_0^\star \left[1 + \left\langle N_1 \dfrac{1}{(n - N_0)^2} N_1 \right\rangle\right] \psi_0\right)} \ . \tag{7}$$

There is some ambiguity as to what value to insert for n where it appears in the denominators on the

right. It will, however, appear that the value, if finite, is irrelevant, so that n and $\langle n \rangle$ will be denoted by the same symbol, n.

Because of the singular nature of the theory, the integrals in both numerator and denominator will diverge strongly. It is therefore convenient to keep only the most strongly divergent terms, so that Eq. 7 becomes

$$n = \frac{\left(\psi_0 \left\langle N_1 \frac{2n - N_0}{(n - N_0)^2} N_1 \right\rangle \psi_0\right)}{\left(\psi_0^* \left\langle N_1 \frac{1}{(n - N_0)^2} N_1 \right\rangle \psi_0\right)} . \tag{8}$$

By use of Eqs. 2 and 3, Eq. 8 can be transformed to

$$n = \frac{\frac{f^2}{4\pi^3\mu^2}\left(\psi_0^* \int \frac{dk}{k^2 + \mu^2} \tau_i \gamma_5 \gamma k \frac{2n - \gamma p + \gamma k}{(n - \gamma p + \gamma k)^2} \gamma k \gamma_5 \tau_i \psi_0\right)}{\frac{f^2}{4\pi^3\mu^2}\left(\psi_0^* \int \frac{dk}{k^2 + \mu^2} \tau_i \gamma_5 \gamma k \frac{1}{(n - \gamma + \gamma)^2} \gamma k \gamma_5 \tau_i \psi_0\right)} . \tag{9}$$

Note that the coupling constant cancels, the value of n being therefore independent of the strength of the coupling. This unexpected result follows from the divergence of the integrals retained in the numerator and denominator. Very similar integrals conspire to yield an infinite mass in the conventional theory.

If some obvious reductions are performed, Eq. 9 becomes

$$n = \frac{\left(\psi_0^* \int \frac{dk}{k^2} \frac{\gamma k(k^2 \gamma p - k^2 \gamma k + 2pk\gamma k)\, \gamma k}{(k^2 - 2pk)^2} \psi_0\right)}{\left(\psi_0^* \int \frac{dk}{k^2} \frac{\gamma k k^2 \gamma k}{(k^2 - 2pk)^2} \psi_0\right)} , \tag{10}$$

where n, p, and μ have been neglected in comparison with k, since the divergence of the integrals comes for large k. The ψ_0 will be omitted, it being understood that $\gamma p = |P|$ and $p^2 = P^2$ wherever they stand in the final result. The standard method can now be used to obtain integrands with a single denominator:

$$n = \frac{\int_0^1 u\, du \int dk \frac{\gamma k(k^2 \gamma p - k^2 \gamma k + 2pk\gamma k)\, \gamma k}{(k^2 - 2upk)^3}}{\int_0^1 u\, du \int dk \frac{\gamma k k^2 \gamma}{(k^2 - 2upk)^3}} . \tag{11}$$

The usual shift of origin in k space can now be made, to obtain k integrals with spherically symmetric

denominators. With up added to k, and p^2 dropped in comparison with k^2, Eq. 11 becomes

$$(12)\quad n = \frac{\displaystyle\int_0^1 u\,du \int_0^\infty k^3\,dk \int d\Omega\, \frac{-k^4\gamma_\alpha k_\alpha - 2uk^4\gamma p + (1-u)\,k^2 k_\alpha k_\beta \gamma_\alpha \gamma p \gamma_\beta - 2(1-u)\,k^2 k_\alpha k_\beta \gamma_\alpha p_\beta}{k^6}}{\displaystyle\int_0^1 u\,du \int_0^\infty k^3\,dk \int d\Omega\, \frac{k^2 k_\alpha k_\beta \gamma_\alpha \gamma_\beta}{k^6}} .$$

The $\int d\Omega$, over the polar angles in four-momentum space, is easily done by use of

$$(13)\quad \int d\Omega k_\alpha k_\beta = \frac{k^2}{4}\,\delta_{\alpha\beta} \int d\Omega \quad ,$$

$$\int d\Omega k_\alpha = 0 \quad ,$$

and Eq. 12 becomes

$$(14)\quad n = \frac{-\displaystyle\int_0^1 u\,du \int_0^\infty k\,dk\,(1+u)\,\gamma p}{\displaystyle\int_0^1 u\,du \int_0^\infty k\,dk} .$$

The diverging integrals in the numerator and the denominator can be canceled with any reasonable sort of limiting procedure. The result finally is

$$(15)\quad n = -\tfrac{5}{3}\cdot|P| = -\tfrac{5}{3}(P_1^2 + P_2^2 + P_3^2 + P_4^2)^{1/2} .$$

The analytic continuation required to give a bare mass value is then trivial, P_4 being replaced by iP_0, and n by im:

$$(16)\quad m = -\tfrac{5}{3}(P_0^2 - P_1^2 - P_2^2 - P_3^2)^{1/2} = -\tfrac{5}{3}\,m_0 .$$

The observed or experimental mass is m_0, while the theoretical mass constant appearing in the fundamental equations is m. The negative sign is irrelevant, while the factor $\tfrac{5}{3}$ represents the effect of the meson field in altering the inertia of the nucleon.

Exactly the same procedure has been used in calculating the relation between m and m_0 for a number of other interesting cases. It is found that all cases of definite physical interest yield finite mass corrections. Some field theories, however, which have a quite similar mathematical form, give a truly divergent mass correction. It is suggested that nonfiniteness of the mass correction rather than nonrenormalizability be used as a criterion for rejecting a possible theory.

Closed-loop contributions have been ignored in the above discussion. Divergence troubles from this source are completely independent of those studied here. On the other hand, alterations of the effective coupling constant (vertex operator) can be handled exactly as above, with similar results.

WIGNER-EISENBUD RELATION FOR THE R MATRIX

G. T. Trammell

If, for simplicity, a case is considered in which an s-wave neutron incident on a nucleus in its ground state has insufficient energy to leave the nucleus in an excited state, then the wave function is asymptotically

$$\psi_k(x,r) \sim \chi_0(x) \sin [kr + \eta(k)] \quad . \tag{1}$$

The Wigner-Eisenbud relation for the R matrix then takes the form

$$\tan [kR + \eta(k)] = k \sum \frac{C_\lambda^2}{E_\lambda - E} \quad , \tag{2}$$

where R is a radius outside of which Eq. 1 is assumed to hold as an equality, namely,

$$\psi_k(x,r) = \chi_0(x) \sin [kr + \eta(k)] \quad , \qquad r > R. \tag{1a}$$

It is interesting to see that condition 2 on the allowable form of $\eta(k)$ is just the condition implied by the requirement that a superposition of states satisfying Eq. 1a be capable of representing a neutron, external to R, in an arbitrary state with the nucleus in its ground state:

$$f(r)\, \chi_0(x) = \chi_0(x) \int_0^\infty a(k) \sin [kr + \eta(k)]\, dk \quad , \tag{3}$$

where $f(r)$ vanishes for $r < R$ but is otherwise arbitrary; for from the orthogonality of the ψ_k's,

$$a(k) = \int_0^\infty f(r) \sin [kr + \eta(k)]\, dr \quad . \tag{4}$$

It is sufficient to take $f = \delta(r - r_0)$, $r_0 > R$, then Eq. 3 becomes

$$\begin{aligned} \delta(r - r_0) &= \int_0^\infty \sin [kr_0 + \eta(k)] \sin [kr + \eta(k)]\, dk \\ &= \int_0^\infty \tfrac{1}{2}[\cos k(r - r_0) - \cos k(r + r_0) + 2\eta(k)]\, dk \\ &= \delta(r - r_0) - \int_0^\infty \cos [k(r + r_0) + 2\eta(k)]\, dk \quad , \end{aligned} \tag{3a}$$

or

$$\int_0^\infty \cos 2[ky + \phi(k)]\, dk = 0 \quad , \tag{5}$$

for $y > 0$ where $\phi(k) = kR + \eta(k)$. We now define

$$\phi(-k) \equiv -\phi(k) \quad , \tag{6}$$

then Eq. 5 becomes

$$\int_{-\infty}^\infty e^{iky}\, e^{i2\phi(k)}\, dk = 0 \quad , \qquad y > 0. \tag{5a}$$

By expanding the function $e^{i2\phi(k)}$ into a Fourier integral,

(7) $$e^{i2\phi(k)} = \int_{-\infty}^{\infty} a(x)\, e^{ixk}\, dx \ ,$$

and inserting Eq. 7 into Eq. 5a (assuming orders of integrations may be reversed), the condition that $a(x) = 0$ for $x < 0$ is obtained; therefore Eq. 7 becomes

(7a) $$e^{i2\phi(k)} = \int_{0}^{\infty} a(x)\, e^{ixk}\, dx \ ,$$

which represents a function analytic in the upper half of the complex plane of k. Writing

(8) $$k\zeta(k^2) = \tan \phi(k)$$

gives

(9) $$e^{i2\phi(k)} = \frac{1 + ik\zeta(k^2)}{1 - ik\zeta(k^2)} \ .$$

According to Eq. 7a, $\zeta(k^2)$ must be free from singularities except for simple poles, and

(10) $$w(k) = 1 - ik\zeta(k^2) \neq 0$$

for k in the upper half of the complex plane. With the additional restriction from Eq. 8 that $\zeta(k^2)$ be real for k real,

(11) $$\zeta(k^2) = P(k^2) + \sum \frac{C_n}{(k^2 - \Lambda_n^2)^{\lambda_n}} + \frac{\bar{C}_n}{(k^2 - \bar{\Lambda}_n)^{\lambda_n}} \ ,$$

where $P(k^2)$ is a polynomial in k^2 with real coefficients, the C_n's and Λ_n's are complex constants, and the λ_n are positive integers. If Eq. 11 is rewritten, calling the Λ_n which are real k_n and those which are complex Λ_n, then

(11a) $$\zeta(k^2) = A_m k^{2m} + \ldots + A_0 + \sum_n \frac{C_n}{(k^2 - k_n^2)^{\lambda_n}} + \sum_i \left[\frac{C_i}{(k^2 - \Lambda_i^2)^{\alpha_i}} + \frac{\bar{C}_i}{(k^2 - \bar{\Lambda}_i^2)^{\alpha_i}} \right] \ .$$

From the Nyquist procedure, then, the number of roots of $w(k)$, defined by Eqs. 10, 11, and 11a, in the upper half plane is

(12) $$m + 1 - S\left(\frac{A_m}{|A_m|}\right) + \sum_{\text{real}} \left\{ \left[\frac{\lambda_n - 1 + S\left(\frac{C_n}{|C_n|}\right)}{2} \right] + \left[\frac{\lambda_n - 1 + S\left(\frac{C_n}{|C_n|}(-1)^{\lambda_n + 1}\right)}{2} \right] \right\} + 2 \sum_{\text{complex}} \alpha_i \ ,$$

where $[a] \equiv a$ if a is an integer, otherwise $[a]$ is the smallest integer larger than a; $S(x) = 1$ if $x \geqq 0$, otherwise it is zero.

Therefore if Eq. 10 is to hold,

$$m = 0, \qquad A_0 \gtrless 0, \qquad \lambda_n = 1, \qquad C \lesseqgtr 0, \tag{13}$$

and there must be no complex poles of $\zeta(k^2)$. If $A_0 > 0$, $e^{i2\phi(+i\infty)} = -1$. From Eq. 7*a*, $a(x) \to -2\delta(x)$ at $x = 0$. Therefore by insisting that Eq. 5 hold for $y \geqq 0$, $A_0 = 0$, and the following is obtained as the condition on $\eta(k)$:

$$\tan\left[kR + \eta(k)\right] = k \sum \frac{C_\lambda^2}{k_\lambda^2 - k^2} \quad . \tag{14}$$

From Eqs. 7*a* and 9 the sum rule is obtained:

$$\lim\,(k \to \infty)\; k \sum_\lambda \frac{C_\lambda^2}{k_\lambda^2 + k^2} = 1 \quad . \tag{15}$$

Equation 14 contains no contributions from the k_λ^2's which are negative. This is because no account was taken of negative-energy stationary states similar to Eq. 1. Also, the accuracy of Eq. 14 is restricted because in the derivation Eq. 1 was assumed to hold for arbitrarily large k.

This work was suggested by a paper by Wigner,[1] who derived Eq. 14 from the principle of causality by considering the motion in time of wave packets incident on the internal region; however, earlier, van Kempen[2] considered the same problem from a standpoint similar to that of Wigner's and with perhaps more mathematical rigor than is used here.

[1] E. P. Wigner, *Am. J. Phys.* **23**, 371 (1955).
[2] N. G. van Kempen, *Phys. Rev.* **91**, 1267 (1953).

EXPONENTIALLY DECAYING STATES IN QUANTUM MECHANICS

G. T. Trammell

If a quantum mechanical system is described by $|\psi(t)\rangle$, then the amplitude that it will be found in a state $|A\rangle$ is $F_a(t) = \langle A|\psi(t)\rangle$. In studying the quasi-stationary states of nuclear physics it is natural to inquire into the possibility of choosing $|A\rangle$ and $|\psi(t)\rangle$ such that

$$F_a(t) \sim e^{-iE_0 t}\, e^{-\alpha t} \quad .$$

The general condition on $F_a(t)$ is

$$F_a(t) = \sum_i f(E_i)\, e^{-iE_i t} + \int_0^\infty f(E)\, e^{-iEt}\, dE \quad .$$

The sum is over the discrete states. If, for small E, $f(E) = E^\beta f_0 + \ldots$, the $f(E_i)$ are assumed to be zero; then for large t

$$F_a(t) \sim t^{-\beta-1} f_0 + f_0' t^{-\beta-2} + \ldots \quad .$$

Thus for large times the decay is slower than for any exponential.

It is not surprising that a particle put in a region from which it may leak out exhibits, after a sufficiently long time, a probability of being found in that region which decays only as some inverse power of the time, because there is dispersion of the particle waves.

For an atom decaying from an excited state, though, there is no dispersion as such for the electromagnetic waves which carry off the energy, and it is perhaps somewhat surprising that, if initially the atom is prepared in an excited state, with no photons in the field, then a long time later the probability that this state has been preserved will decrease only as some inverse power of the time.

Rather than study the atom it is simpler to consider an oscillator coupled to an infinite string. This system, as is well known, admits of a simple decomposition into normal modes of the complete Hamiltonian. The normal coordinates and momenta may be quantized, and the stationary states may be found without an expansion in the coupling constant. Although a thoroughgoing treatment is yet to be made, it is thought that a rough, intuitive consideration brings out the main point.

If $y(t)$ is the displacement of the oscillator, and $\xi(x,t)$ is that of the string, then the equations of motion are

$$M(\ddot{y} + \omega_0^2 y) = -\epsilon\left(y - \xi(0,t)\right) ,$$

$$\rho(\ddot{\xi} - c^2 \xi'') = \epsilon\left(y - \xi(0,t)\right) \delta(x) .$$

If initially the string is at rest and the oscillator is given a displacement, then the subsequent motion of the oscillator is represented by a damped sinusoid with complex frequency:

$$\omega \cong \pm i\omega_0 \left(1 + \frac{\epsilon}{2M\omega_0^2}\right) - \frac{\epsilon^2}{4M\rho c\omega_0} .$$

If the oscillator is coupled to a bar instead of to a string, then the equations of motion become

$$M(\ddot{y} + \omega_0^2 y) = -\epsilon\left(y - \xi(0,t)\right) ,$$

$$\rho\ddot{\xi} + K^2 \frac{d^4\xi}{dx^4} = +\epsilon\left(y - \xi(0,t)\right) \delta(x) \quad \text{(ref 1)} .$$

[1]See, for example, P. M. Morse, *Vibration and Sound*, McGraw-Hill, New York, 1948.

Now, in addition to the damped sinusoid there is a term which for large times is inversely proportional to the time. The string and the bar differ in this respect: energy delivered at a point to the string immediately travels off down the string (with velocity c), so that when the force stops, the motion of the string at the point of application ceases. Because of dispersion the bar continues to exhibit motion at the point of application after the force has stopped. The situation for the oscillator coupled to the bar is, then, that initially the amplitude of the oscillator is large relative to that of the bar at the point of coupling; energy is given up to the bar at a rate proportional to the energy of the oscillator. This energy imparted to the bar does not propagate down the bar at a finite rate, but, rather, spreads as the energy moves, which results in a continuing motion at the coupling point, which motion serves to force the oscillator and makes the rate of loss of amplitude of the oscillator to be limited by the rate at which energy can be propagated down the bar.

If the string motion is quantized and if the propagation of a phonon on the string is considered, the situation is quite different from the propagation of an unquantized disturbance. Although fundamentally the phonon also is quite different from a disturbance on a bar, it does exhibit the property of spreading out, but not because of dispersion.

If $|\psi(\xi(x),t)\rangle$ is the state vector for the string and

$$\bar{\xi}(x,t) = \langle\psi(\xi,t)\,|\,\xi(x)\,|\,\psi(\xi,t)\rangle$$

is the expected value of the string displacement at x and t, then it is well known that

$$\frac{d^2}{dt^2}\bar{\xi}(x,t) - c^2 \frac{d^2}{dx^2}\bar{\xi}(x,t) = 0 .$$

Further, $\bar{\xi}(x,t)$ and $d\bar{\xi}(x,0)/dt$ may (in principle) be chosen arbitrarily, and so a packet may be made with $\bar{\xi}(x,0)$ arbitrary that will travel with the velocity c without change of shape:

$$\bar{\xi}(x,t) = \bar{\xi}(x - ct,0) .$$

However, this property is restricted to $\bar{\xi}(x,t)$; $\overline{\xi^2}(x,t)$ does not exhibit it. More to the point: let

$$|\psi(\xi,t)\rangle = \int_{-\infty}^{\infty} \zeta(k)\,|k\rangle\, e^{-i|k|t}\, dk$$

describe a phonon packet. Here $|k\rangle$ is the state vector describing a phonon of wave number k on the string with no other phonon present. If

$$\int_{-\infty}^{\infty} |\zeta|^2 \, dk = 1 \quad ,$$

then $|\psi(\xi,t)\rangle$ represents one phonon on the string with a probability $|\zeta(k)|^2$ of its having wave number k. Here

$$\bar{\xi}(x,t) = 0 \quad .$$

It is possible to take the energy density as a measure of a phonon being at a point x; however, it seems better to imagine a system which can be coupled to any point on the string with coupling energy $\epsilon\xi(x)\, y$, where y is the coordinate of the measuring system, then the amplitude that the system has absorbed the phonon at x and t is proportional to

$$\xi_{01}(x,t) \equiv \langle 0 | \xi(x) | \psi(\xi,t) \rangle \quad ,$$

where $|0\rangle$ is the ground state of the string. In terms of the creation and destruction operators $\bar{a}_k$ and a_k,

$$\xi(x) = \int_{-\infty}^{\infty} dk \sqrt{\frac{\hbar}{2k}} \, (a_k + \bar{a}_{-k}) \, e^{ikx} \quad ;$$

then

$$\xi_{01}(x,t) = \int_{-\infty}^{\infty} \sqrt{\frac{\hbar}{2k}} \, \zeta(k) \, e^{ikx} \, e^{-i|k|t} \, dk \quad .$$

The $\sqrt{\hbar/2k}$ will be absorbed in $\zeta(k)$; $\xi_{01}(x,t)$ obeys the wave equation and is therefore expressible as

$$\xi_{01}(x,t) = f(x - ct) + g(x + ct) \quad ,$$

as is seen from the above expression. However, $\xi_{01}(x,0)$ and $d\xi_{01}(x,0)/dt$ can no longer be chosen independently. In fact, if it is desired to have only waves which travel to the right (with velocity c and hence preserve their shape), then

$$\xi_{01}(x,0) = \int_0^{\infty} \zeta(k) \, e^{ikx} \, dk \quad ,$$

which represents a spreadout packet whose amplitude at large $|x|$ is $\propto |x|^{-\beta}$, where β is a small number depending on the behavior of $\zeta(k)$ near $k = 0$, and hence whose amplitude at given x for large $t \propto t^{-\beta}$. On the other hand, a packet which is initially well confined will contain both waves traveling to the right and to the left, each of which have amplitudes $\propto |x|^{-\beta}$ at large $|x|$ and hence will give an amplitude at given $x \propto t^{-\beta}$ at large times. In fact,

$$\xi_{01}(0,t) = \int_0^{\infty} \left(\zeta(k) + \zeta(-k) \right) e^{-i|k|t} \, dk \sim t^{-\beta} \, .$$

Hence, roughly, a photon emitted by an atom is available for readsorption with an amplitude $\sim t^{-\beta}$, and therefore the amplitude that the atom be found in an excited state with no photon in the field $\sim t^{-\beta}$.

The above arguments are heuristic, and perhaps a more rigorous analysis is worthwhile in the future.

If the Breit-Wigner one-level formula is used to determine the properties of a decaying state, then the probability for no decay after time t is asymptotically

$$e^{-\Gamma t} - \left(\frac{\Gamma}{E_0}\right)^{5/2} \frac{1}{(\Gamma t)^{3/2}} \quad .$$

The anomalous behavior would not take over until

$$e^{-\Gamma t} \cong \left(\frac{\Gamma}{E_0}\right)^{5/2} \quad .$$

If typical values are inserted for natural alpha emitters,

$$e^{-\Gamma t} \cong 10^{-80} \quad ,$$

when the anomalous behavior would take over. This compares unfavorably with 10^{52} particles in the earth. On the other hand, taking $\Gamma/E_0 \cong 10^{-5}$ and $E_0 = 1$ ev, $e^{-\Gamma t} \cong 10^{-14}$, when the anomalous behavior might be expected to take over. More thoroughgoing analysis is necessary before it can be definitely established whether or not this effect is measurable.

POTENTIAL WELLS FOR LIGHT NUCLEI

J. L. Fowler

It was pointed out at the Amsterdam Conference that the s-wave phase shifts for elastic neutron scattering from light nuclei with zero spin can be calculated from simple static potentials.[1] In Fig. 1 the solid curves are theoretical s-wave phase shifts due to the square well potentials, with the characteristics listed beside each curve. For He^4 neutron scattering a similar well can be used to explain the experimental data.[2]

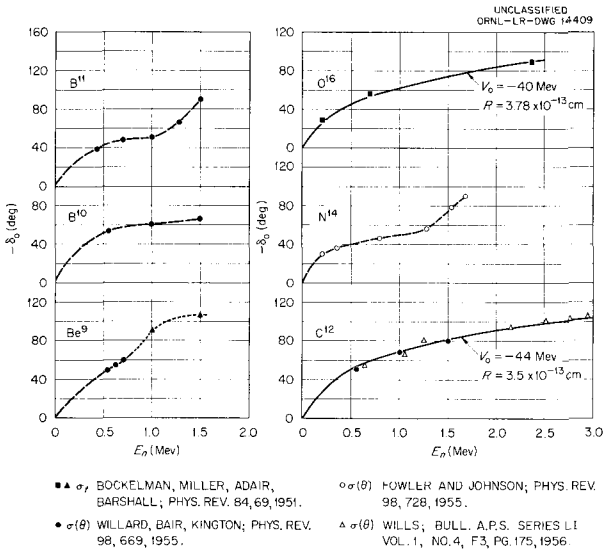

Fig. 1. The s-Wave Phase Shifts for Neutron Scattering from Light Nuclei. Dashed curves are through experimental points. Solid curves are theoretical phase shifts calculated for the potential wells indicated beside each curve.

In the case of carbon and oxygen, with the wells indicated in Fig. 1, the $2s$ bound states should be found in compound nuclei, C^{13} and O^{17}. For the case of carbon, the well used would give the $2s$ level at -4.4 Mev. In C^{13} there is a $J = \frac{1}{2}+$ level at -1.86 Mev, with a reduced width approaching that for a single particle.[3] It is reasonable to identify this level with the $2s$ state for a neutron moving in the potential due to the C^{12} core.

Of course, the highly idealized potential used for the curves in Fig. 1 should not be expected to give the correct position of the $2s$ bound state, since the detailed variation of the potential with distance affects the bound states much more than it affects the phase shifts for scattering at higher energies. In fact, the information on the bound states can be used, together with the scattering phase shifts, to deduce additional information concerning the static potential. When a potential is introduced with a diffuse boundary in the form of an exponential tail,[4] the parameters can be adjusted so as to fit both the energy position of the bound state as well as the s-wave phase shifts. A fairly close fit to these two sets of data for carbon is obtained with the following well:

$$V = -48.8 \text{ Mev}, \quad r < 2.67 \times 10^{-13} \text{ cm},$$

$$V = -48.8\, e^{-(r-2.67\times10^{-13})/(0.75\times10^{-13})}, \quad r > 2.67 \times 10^{-13} \text{ cm}.$$

For this potential the $2s$ state of C^{13} lies in the neighborhood of -2 Mev (ref 4). The calculated s-wave phase shifts compare favorably with experiment, as shown in Fig. 2. The diffuseness parameter (0.75×10^{-13} cm) is in the range to be expected from other work.[5]

In calculating the s-wave phase shifts the exponential well was approximated by a well having six steps such that for each step the well strength,[5] S_i,

$$\left[S_i = \int_{r_i}^{r_{i+1}} V(r)\, r\, dr \right]$$

is the same as it is for the corresponding interval in the exponential well. Similar calculation with a four-step well gives about the same result and indicates that the step approximation is reasonably accurate.

[1] J. L. Fowler, "Differential Elastic Scattering of Neutrons from Light Elements." A paper presented at the International Conference on Nuclear Reactors, Amsterdam, The Netherlands, July 2–7, 1956.

[2] E. Van der Spuy, *Nuclear Physics* 1, 381 (1956).

[3] F. Ajzenberg and T. Lauritsen, *Revs. Mod. Phys.* 27, 77 (1955).

[4] A. E. S. Green and K. Lee, *Phys. Rev.* 99, 772 (1955).

[5] A. E. S. Green, *Phys. Rev.* 102, 1325 (1956).

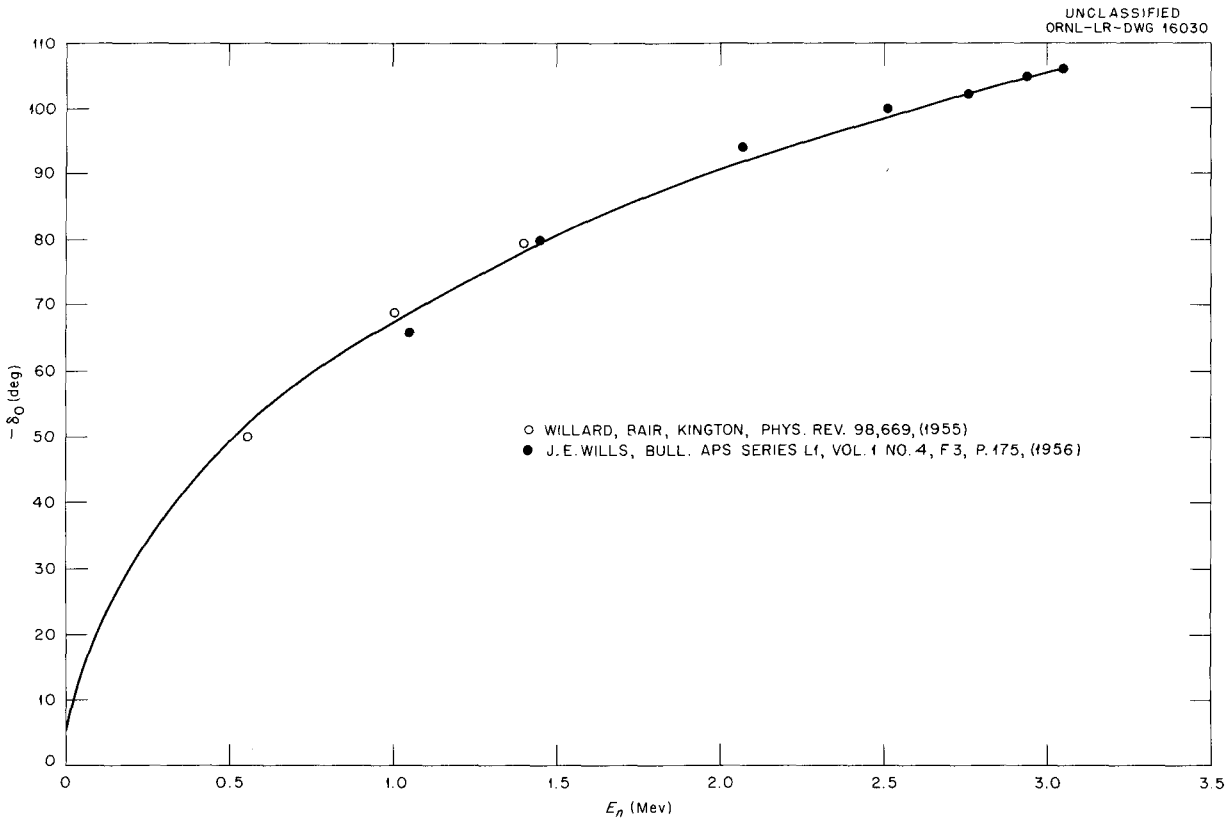

Fig. 2. The *s*-Wave Phase Shifts for Neutron Scattering from Carbon. The solid curve is calculated for a potential well with an exponential tail.

In the case of O^{17} there is a $J = \frac{1}{2}+$ level at −3.27 Mev below the $O^{16} + n$ unbound state.[3] With this information, together with neutron scattering data[6] for O^{16}, it should be possible to find a similar set of parameters for the static potential due to the O^{16} core. By a slight readjustment of the parameters in the case of carbon and oxygen, allowance could be made for the change of effective potential depth with energy which Brueckner's calculations have suggested.[7] No simple static potential has been found to give the *s*-wave phase shifts observed from the light nonzero-spin nuclei (Fig. 1).

The author is indebted to A. E. S. Green for many helpful discussions of the exponential well.

[6]C. K. Bockelman, *Phys. Rev.* **84**, 69 (1951); A. Okazaki, *Phys. Rev.* **99**, 55 (1955); H. O. Cohn and J. L. Fowler, p 32, this report.

[7]K. A. Brueckner, R. J. Eden, and N. C. Francis, *Phys. Rev.* **100**, 891 (1955).

NONLINEAR ACCELERATOR ORBIT CODES

T. A. Welton T. I. Arnette

Over the past year, a series of Oracle codes was developed for the calculation of properties of orbits in accelerators with azimuthal field variation, but possessing a median plane. The main applications have been to fixed-frequency cyclotrons, but the same codes will also handle orbits in machines with variable orbit frequency and fixed focusing frequencies.

In all these codes one aim has been to achieve an automatic graphical display of the orbit dynamics. This was first done by the use of the curve plotter output of the Oracle, by which portions of the desired curves were obtained on successive frames of film. These frames could then be glued together to form a continuous strip chart of radial and vertical displacements as functions of angle. This form of output proved to be insufficiently flexible, largely because of the difficulty of monitoring runs as they occurred. The Oracle curve plotter makes available two voltages (for beam deflection purposes) which are proportional to any desired machine numbers (digitally represented). These voltages can then be used to actuate two Brown recorders, thus giving a continuous and immediate graphical output, which greatly facilitates the obtaining and interpretation of orbit data.

Codes 244.1 and 244.2 have been completed for some time. In both of these the following equations of motion are integrated:

$$(1a) \qquad \dot{r} = \frac{rp_r}{\sqrt{p^2 - p_r^2 - p_z^2}} ,$$

$$(1b) \qquad \dot{z} = \frac{rp_z}{\sqrt{p^2 - p_r^2 - p_z^2}} ,$$

$$(1c) \quad \dot{p}_r = \sqrt{p^2 - p_r^2 - p_z^2} - r(B_z + \delta_z) + \frac{rp_z}{\sqrt{p^2 - p_r^2 - p_z^2}} (B_\theta + \delta_\theta) ,$$

$$(1d) \quad \dot{p}_z = r(B_r + \delta_r) - \frac{rp_r}{\sqrt{p^2 - p_r^2 - p_z^2}} (B_\theta + \delta_\theta) ,$$

where $\dot{r} \equiv dr/d\theta$, etc. These equations are not Hamiltonian, in spite of the notation. They are simply the Lagrangian equations written in a form more convenient for computation. The parameter p is the particle momentum in units of m_0c, and the radial and vertical kinetic momenta (p_r, p_z) are in the same units. The coordinates (r, z) and the magnetic field components (B_z, B_r, B_θ) are measured in units such that $e/m_0c^2 = 1$. The symbols (B_r, B_θ, B_z) are that part of the magnetic field which has the theoretically desirable N-fold repetition in a revolution, while $(\delta_r, \delta_\theta, \delta_z)$ are that part of the field which repeats only after one revolution – the so-called error field.

In addition to the above equations,

$$(2) \qquad \frac{dt}{d\theta} = \frac{p}{\beta} \frac{r}{\sqrt{p^2 - p_r^2 - p_z^2}}$$

is simultaneously integrated to obtain the time of the particle as a function of angle. The parameter β is just the particle speed in units of the light speed $\left(\beta = p/\sqrt{p^2 + 1}\right)$, and t is measured in the previously defined length units, the conversion to normal time units being accomplished by division by the light speed.

The equations are integrated by the Runga-Kutta procedure, with 16 steps per sector being found to give good accuracy. With a mathematical process of such complexity, considerable thought has been devoted to making the computation time per sector as low as possible, consistent with the need for accuracy in runs which continue for many revolutions. This sector time (which comes out in the neighborhood of 8 sec) is largely dependent on the complexity of the process used for supplying the magnetic field components. The general form used is

$$(3) \quad B_z(r,\theta,0) \equiv B(r,\theta) = B_0(r) + B_1(r) \cos N(\theta - \zeta)$$

for the main field in the median plane. The term $B_0(r)$ determines mainly the orbit timing and the radial focusing, while $B_1(r)$ determines the vertical focusing, in conjunction with the spiral angle $\zeta(r)$ and the vertical focusing supplied by the gradient of B_0.

For simplicity, it is assumed that B_r, B_θ, and B_z for $z \neq 0$ are given simply as components of the gradient of the magnetostatic potential which gives Eq. 3:

$$\begin{aligned} \psi &= Bz \ , \\ B_z &= \frac{\partial \psi}{\partial z} = B \ , \\ B_r &= \frac{\partial \psi}{\partial r} = z \frac{\partial B}{\partial r} \ , \\ B_\theta &= \frac{\partial \psi}{r \partial \theta} = \frac{z}{r} \frac{\partial B}{\partial \theta} \ . \end{aligned} \tag{4}$$

This is suitable for small vertical amplitudes, but, since ψ fails to satisfy the Laplace equation, $\nabla \cdot B$ is not zero. This defect would be remedied by a term in B_z of order z^2, which will not contribute appreciably in cases which have been studied. In codes 244.1 and 244.2, B_0 and B_1 are supplied as tables of values at uniform increments of radius, while $\zeta(r)$ is supplied in the form of coefficients of a polynomial:

$$\zeta(r) = \zeta_0 + \zeta_1 r + \zeta_2 r^2 \ . \tag{5}$$

In practice, B_0 and B_1 are supplied either from analytical approximations or from another code (265) which calculates the magnetic field required to give constant orbit time and prescribed vertical focusing. Unfortunately, neither the analytical ("smooth") approximation nor the code 265 are sufficiently accurate to guarantee that the prescribed fields will give suitable vertical focusing (a *very* sensitive function) when used in codes 244.1 or 244.2. It has, however, been found that a small empirical adjustment of ζ_1 and ζ_2 will give satisfactory performance.

The code 244.1 takes $p = p_0$ (a specified initial value), $z = p_z = 0$, $\delta_r = \delta_\theta = \delta_z = 0$. Approximately correct values of r and p_r for the equilibrium orbit are then automatically introduced, and Eqs. 1 are integrated through a sector $(2\pi/N)$. The resulting r and p_r values are stored, and the sector is integrated through twice more with, first, an altered initial r value and then with an altered p_r value. The resulting information is sufficient to predict quite closely the true equilibrium orbit (repeating after one sector). This prediction is then tested, and, if satisfactory, the sector is integrated through twice more with z and $p_z \neq 0$. There are determined in this way the values of r and p_r at $\theta = 0$ for the equilibrium orbit of momentum p_0, the revolution time, and $\cos 2\pi\nu_r/N$ and $\cos 2\pi\nu_z/N$, which determine the small-amplitude stability. The momentum value is then advanced by an amount Δp and the process repeated. In this way a detailed table of equilibrium orbit properties for various momenta in a specified field can be prepared for use in design work or as a guide in theoretical nonlinear orbit studies.

In code 244.2, on the other hand, an attempt is made to duplicate conditions in a real accelerator. The error field components are not set to zero but can be given arbitrary amplitudes and frequencies. In addition, both p and p_r can be changed discontinuously whenever accelerating gaps of specified shape and azimuth are crossed. By using this equipment, acceleration through resonances and acceleration by slant gaps can be realistically studied. The standard output is by Brown recorder, as previously described. One Brown recorder plots z, while the other plots $r - \bar{r}(p)$ ($\bar{r} = \beta$, for fixed frequency), both variables being suitably scaled.

Another set of codes is essentially complete and will be designated as the 289 series. In these, the lessons learned from the 244 series are being incorporated with enough flexibility to allow for reasonable shifts in the emphasis of the ORNL accelerator program. In these codes, both the accuracy and convenience of representation of the magnetic field can be altered to obtain either faster or more accurate computation than in series 244. Provision has been made for introducing, in a simple way, forms for $B_0(r)$, $B_1(r)$, and $\zeta(r)$ which are appropriate for a ring magnet with nearly constant ν_r and ν_z, rather than constant orbital frequency, so that machines of the MURA type can be studied.

ANALYTICAL TREATMENT OF ACCELERATION THROUGH RESONANCES

M. M. Gordon[1] T. A. Welton

In conventional accelerators the radial and vertical focusing frequencies are not allowed to satisfy the condition for a so-called resonance. If ν_r and ν_2 are the ratios of the radial and vertical frequencies to the orbital frequency, then a resonance will occur if

$$p\nu_r + q\nu_2 = n \quad , \tag{1}$$

where p, q, and n are integers. Such a resonance is particularly destructive of beam stability if p and q are small integers, the worst cases being $p = 1$, $q = 0$ and $p = 0$, $q = 1$, the *integral* radial and vertical resonances, respectively. The integer n refers to the angular dependence ($\sim \cos n\theta$) of some Fourier component of the guide field, and may be zero, N (the sector number), or some integer less than n. In this last event the resonance is called an *imperfection* resonance, and its effect can be made as small as desired by accurate shimming of the guide field.

The fixed-frequency cyclotron is energy-limited by the fact that ν_r satisfies the following inequality:

$$\nu_r \geqq E \quad , \tag{2}$$

where E is the particle energy (including rest energy) in units of the rest energy. The equality holds closely for $\nu_r \ll N$, so that, if acceleration starts at zero energy, ν_r must start at unity and steadily increase. During this process, assuming ν_z constant, ν_r passes in sequence:

$$\nu_r = \ldots, \frac{6}{5}, \frac{5}{4}, \frac{4}{3}, \frac{3}{2}, \frac{2}{1} \quad , \tag{3}$$

which are radial imperfection resonances of increasing seriousness. It can be shown that with a 5 (or larger number) in the denominator no real instability results, but the others can all cause beam loss, the last being the most serious.

The situation is much improved by the fact that the particle acceleration prevents it from spending a large number of revolutions in exact resonance, and an attempt has been made to derive expressions for the increase in beam amplitude at resonances of various types in terms of the energy gain per turn and the fractional magnetic field error.

Let δ be the energy gain per turn in units of mc^2, a typical value for a cyclotron with an anticipated energy gain of about 1 Mev per turn being $\delta \cong 10^{-3}$. Let ϵ be the fractional field error, or rather the ratio of the undesired Fourier component (amplitude) to the main field. A very precise field might have $\epsilon \cong 10^{-4}$ over a small range of radius, while a fairly easily achievable accuracy would be $\epsilon \cong 10^{-3}$.

For an integral radial imperfection resonance, a fixed radial amplitude is produced by the resonance which adds incoherently to the pre-existing amplitude. This additional amplitude is

$$\delta a = \frac{\pi\epsilon}{n\sqrt{2\delta}} \quad , \tag{4}$$

the δa being in units of the mean orbit radius. If this radius is taken as 10^3 cm, as is reasonable for $n = 2$, then the larger field error ($\epsilon = 10^{-3}$) yields

$$\delta a \cong 50 \text{ cm} \quad , \tag{5}$$

which is probably too large to allow beam transmission. The smaller error ($\epsilon = 10^{-4}$) yields, on the other hand,

$$\delta a \cong 5 \text{ cm} \quad , \tag{6}$$

which is probably quite safe.

By similar methods, the corresponding formulas for the half-integral imperfection resonances ($p = 2$, $q = 0$, $n = 3$, for example) and the integral coupling resonances ($p = 1$, $q = 1$, $n = 2$, for example) have been derived. For the half-integral case, a result similar to Eq. 4 is obtained, but for the fractional *increase* in amplitude

$$\frac{\delta a}{a} = \frac{\pi\epsilon}{n\sqrt{2\delta}} \quad . \tag{7}$$

The result for these resonances will therefore be quite unimportant. With $a = 10$ cm, a reasonable upper limit, and with the larger error ($\epsilon = 10^{-3}$),

$$\delta a \cong 0.3 \text{ cm} \quad , \tag{8}$$

[1]Summer participant, University of Florida.

which can be ignored. Similar but more complicated formulas show that the coupling resonances are also insignificant and that larger values of p and q produce even smaller effects.

The practical consequence is that a fixed-frequency cyclotron with a proton beam energy of 930 Mev ($E \cong 2$) appears to be quite feasible. For a higher energy, one or more integral resonances must be passed. The field accuracy requirement from Eq. 4 does not seem impossible to meet, and work is in progress to study the feasibility of accelerating to $\nu_r = 3$ and 4.

Preliminary numerical results, obtained through the use of the Oracle code 244.2, described in the previous section, indicate that formulas 4 and 7 are quite dependable. It further has become clear from the numerical work what factor sets the limit on radial amplitude for stability. As the radial amplitude increases, the vertical motion sees an increasing alternating gradient focusing arising from the radial excursions, coupled with the field gradient. At some amplitude, $2\nu_z = \nu_r$, and the beam becomes vertically unstable. In the one case studied ($N = 12$, $\nu_r = 2$), the limiting radial amplitude was approximately 5 cm, which would be reached for ϵ between 10^{-3} and 10^{-4}. More detailed results will be reported subsequently.

CYCLOTRON MODEL DESIGN STUDY

T. I. Arnette H. G. Blosser[1] H. C. Owens G. T. Trammell

The Physics and the Electronuclear Research Divisions have cooperated during the past few years in studies of high-energy accelerators (see previous semiannual reports for the two divisions). Interest has been mainly focused on the feasibility and desirability of constructing a 1- or 2-bev fixed-frequency, fixed-field, proton cyclotron. Such a machine would not have a fixed operating point, and therefore a question of first importance is how free of "imperfections" must the field be to prevent loss of beam in passage through the various resonances encountered during the course of acceleration. T. A. Welton, who is principally responsible for the theoretical work to date, has done much work devising Oracle codes for a theoretical study of this question, but it was thought desirable to check and augment the theoretical studies with electron model experiments.

The first model is to be a four-sector, straight Thomas-type cyclotron which will accelerate electrons to an equivalent proton energy of about 400 Mev, where they will encounter the first radial integral imperfection resonance ($\nu_r = 2$), which will also be an essential half-integral resonance. By increasing the number of sectors the first integral resonance can be postponed until an energy $\cong$930 Mev is reached. For this reason the first model is not realistic as a model for a full-scale machine. It seems that for a machine designed to go to 1 bev, or somewhat beyond, a minimum of probably eight sectors would be required to prevent a loss of beam at $\nu_r \leqq 2, E \cong 930$ Mev. In addition, a straight-sector machine of this energy would be uneconomical, since the flutter necessary to maintain vertical focusing would necessitate regions of large reversed fields; in an actual machine the vertical focusing without reversed fields would certainly be maintained by the Kerst scheme of spiraled sectors. In spite of the first model not being a realistic mockup of a practical machine (which the second model is intended to be), it will be relatively simple to construct; many of the techniques used in its construction will be applicable to future constructions, and it will make possible the study of resonances experimentally.

This report describes work done this past summer in computing a set of fields for the model, which is now under construction by members of the Electronuclear Research Division.

The first requirement on the fields is that the time for a particle to make a revolution must be independent, within small limits, of the particle energy. The second requirement is that the machine should give vertical focusing, and, to avoid the possibility of losing the beam as a result of vertical imperfection resonances, the vertical focusing frequency should be maintained small.

[1]Electronuclear Research Division.

The first requisite was made definite by requiring that the period not vary by more than $1:10^4$. Thus a particle initially in phase, at the maximum, with the accelerating voltage could make at least 2.5×10^3 revolutions before becoming out of phase. If the energy gain per turn were about $0.4 \times 10^{-3} \times$ output energy, then particles would be accelerated to the output energy. For the second requirement it was decided to make ν_z, the number of vertical oscillations in one turn, less than $\frac{1}{3}$.

If the field in the median plane (assumed to have only a z, vertical, component) is independent of azimuth, then the equilibrium orbits are circles with radii $R^{(1)}$ determined by

$$\frac{R^{(1)}}{p} B_0\left(R^{(1)}\right) = 1 ,$$

where p is the momentum, B_0 is the field, and e and c have been set equal to 1. The "frequencies" (the number of oscillations per revolution) of radial and vertical oscillations about the equilibrium orbit are given by

$$\left(\nu_r^{(1)}\right)^2 = 1 + \frac{R^{(1)}}{B_0\left(R^{(1)}\right)} \frac{\partial B_0\left(R^{(1)}\right)}{\partial R^{(1)}}$$

and

$$\left(\nu_z^{(1)}\right)^2 = - \frac{R^{(1)}}{B_0\left(R^{(1)}\right)} \frac{\partial B_0\left(R^{(1)}\right)}{\partial R^{(1)}} .$$

If the time of revolution is to be independent of p, then B_0 must increase with R, and the z oscillations are not focused.

If the field has a small azimuthal variation, then the equilibrium orbits are still approximately circles, but if we put

$$B(r,\theta) = B_0(r) + B_f(r,\theta) = B_0(r)\,[1 + f(r,\theta)] = B_0(r)\left[1 + \sum_{n=1}^{\infty} f_n(r) \cos MN\theta\right]$$

and if $r(p,\theta) = R[1 + g(p,\theta)]$ denotes the equilibrium orbits with

$$\int_0^{2\pi} g(p,\theta)\, d\theta = 0 ,$$

then

$$g(p,\theta) = \sum_{n=1}^{\infty} \frac{f_n(R) \cos n - N\theta}{n^2 N^2 - \left(\nu_r^{(1)}\right)^2} + o\left(\frac{f^2}{N^4}\right) ,$$

$$\frac{RB_0(R)}{p} = 1 - \tfrac{1}{2}\left[1 + \left(\nu_r^{(1)}\right)^2\right] \sum \frac{f_n^2}{n^2 N^2 - \left(\nu_r^{(1)}\right)^2} - \frac{R^{(1)}}{2} \sum \frac{(\partial f_n/\partial R)\, f_n}{n^2 N^2 \left(\nu_r^{(1)}\right)^2} + o\left(\frac{f^2}{N^4}\right) ,$$

$$\left(\nu_z^{(2)}\right)^2 = \tfrac{1}{2} \sum_{n=1}^{\infty} f_n^2 - \frac{R}{B} \frac{\partial B}{\partial R} + o\left(\frac{f^2}{N^2}\right) .$$

The last term includes the "Thomas term," $\frac{1}{2} \Sigma f_n^2$, which makes it possible to secure isochronism and z-focusing simultaneously.

If T is the time required to traverse the orbit whose average radius is R, then

$$B_0(R) = \frac{2\pi m_0}{T\sqrt{1 - (2\pi R/T)^2}} \left\{ 1 - \tfrac{1}{4}\left[1 + \left(\nu_r^{(1)}\right)^2\right] \sum \frac{f_n^2}{n^2 N^2 - \left(\nu_r^{(1)}\right)^2} - \frac{R}{2} \sum \frac{f_n\ \partial f_n/\partial R}{n^2 N^2 - \left(\nu_r^{(1)}\right)^2} + o\left(\frac{f^2}{N^4}\right) \right\}$$

where m_0 is the rest mass of the particle and to the accuracy warranted:

$$\left(\nu_r^{(1)}\right)^2 \cong 1 + \frac{R}{B} \frac{\partial B}{\partial R} \cong \frac{1}{1 - (2\pi R/T)^2} .$$

If T_0 is the cyclotron period, we set $T/T_0 = t$, adopt $T_0/2\pi$ and m_0 as units, and we have

$$B_0(R,t) \cong \frac{1}{\sqrt{t^2 - R^2}} \left\{ 1 - \frac{1}{4}\left[1 + \frac{1}{1 - R^2/t^2}\right] \sum \frac{f_n^2}{n^2N^2} - \frac{R}{2} \sum \frac{f_n \, \partial f_n/\partial R}{n^2N^2} \right\}$$

$$\nu_z^2 \cong \frac{1}{2} \sum f_n^2 - \frac{R^2}{t^2 - R^2} \quad .$$

The conditions set for the model are that $B_0(R)$ and $f(R,\theta)$ are to be chosen such that

$$t(R) = 1 \pm 0.0001 \ ,$$

$$\frac{1}{3} > \nu_z > 0 \ .$$

In principle the above equations, or rather the complete equations to which these are first approximations, could be used to determine the fields as follows: putting $t = 1$, assume B_f and approximate B_0 to satisfy the ν_z inequality, then solve for $B_0(R,1)$, repeating the procedure if the $B_0(R,1)$ that is found changes appreciably the f_n's first assumed. In practice this procedure is nearly hopeless for the accuracy on t which we require and the small value of N (=4): at $R^2/(1 - R^2) = 1$, that is, $p \sim 1$, $\Sigma f_n^2 = 2$, the second term on the rhs of the $B_0(R,t)$ equation is the $o(0.1)$, the terms neglected are the $o(0.01)$, so many more terms (which get very involved) would have to be kept.

If we put

$$B_0(R,t) = \frac{1}{\sqrt{t^2 - R^2}} \left[1 - \alpha(R,t,B_0,B_n)\right] \ ,$$

then

$$B_0(R,1) = \sqrt{\frac{t^2 - R^2}{1 - R^2}} \cdot \frac{1 - \alpha\left(R,1,B_0(R,1),B_n\right)}{1 - \alpha\left(R,t,B_0(R,t),B_n\right)} \cdot B_0(R,t) \ .$$

If t is near 1 then

$$\sqrt{\frac{t^2 - R^2}{1 - R^2}} \cong 1 + \frac{t - 1}{1 - R^2} \ .$$

If α is small, then the second ratio is

$$\frac{1 - \alpha(1)}{1 - \alpha(t)} \cong 1 + 2(t - 1)\,\alpha(1) \ .$$

Thus, if we define $t^{(0)} = t$ and $t^{(1)}$ by

$$B_0\left(R,t^{(1)}\right) \equiv \sqrt{\frac{(t^{(0)})^2 - R^2}{1 - R^2}}\, B_0\left(R,t^{(0)}\right) \ ,$$

then

$$-B_0\left(R,t^{(1)}\right) + B_0(R,1) \cong 2\left(t^{(0)} - 1\right)\alpha(1)\, B_0(R,1) \cong \frac{t^{(1)} - 1}{1 - R^2} B(R,t) \ ,$$

therefore

$$t^{(1)} - 1 \cong 2(1 - R^2)\,\alpha(1)\left(t^{(0)} - 1\right) \ .$$

If, then, $\alpha(1)$ is small, this is the basis of an effective iteration procedure to obtain from a given $B_0^{(0)}(R)$, for which $t(R)$ is known, a $B_0^{(1)}(R)$ which will have $t(R)$ nearer $t(R) = 1$.

In the model, B_0 is produced by two main circular coils, above and below the median plane, near the outer orbit and 20 pairs (a superfluous number) of other circular coils distributed in toward the center. The B_f is obtained by winding on each half of each of the four sectors 16 coils; the currents in corresponding coils of the two halves flow in the opposite sense, giving a zero average for B_f around any circle in the median plane (which is the definition of B_f).

There are two main Oracle codes which are used. One code calculates the B_f from assumed current distribution in the coils. The other, code No. 272, takes as input an arbitrary $B(r,\theta) \equiv B_0(r) + B_f(r,\theta)$ at a grid of points (r_i,θ_i) and at regular intervals of p finds the equilibrium orbits and calculates (1) maximum radius, (2) average radius, (3) time of revolution, (4) $\cos\sigma_x \equiv \cos(\pi/2)\nu_x$, and

(5) $\cos \sigma_z \equiv \cos (\pi/2)\nu_z$. This latter code is No. 244.1, described in a preceding section ("Nonlinear Accelerator Orbit Codes"), modified to take the above input. This code requires about 1.5 min for each value of p. In addition there is a small code which takes $B_0(r)$ and time of revolution and iterates to get a $B_0(r)$ whose t is nearer unity, as mentioned above.

The first approximate B_f and B_0 were obtained from code No. 265 which takes an orbit of assumed shape $r(p,\theta) = R_{(p)}\,(1 + g(p) \cos N\theta)$, where $g(p)$ is an analytically given function designed to make $\nu_z \cong 0$ and $R_{(p)}$ is calculated to give isochronism, and calculates the B_0 and B_f that would give rise to it. Since the B_f produced by the model deviates fairly widely from a pure sinusoid, a considerable amount of trial and error modification of the B_f from code No. 265 was necessary before a suitable B_f which gave $\frac{1}{3} > \nu_z > 0$ was found. Once a suitable B_f was found, a $B_0(r)$ which would give isochronism was found by the iteration procedure.

Figure 1 gives results of code No. 272 for the orbit times for the successive iterates. Curve (0) gives $T(p)$, with $B_0(R)$ taken from code No. 265; curve (1) is $T(p)$ after the first iteration. For $p < 0.55$, curve (2) does not differ from $T(p) = 1.5708$ enough to show on the graph. After curve (3), the R in the iteration formula,

$$\sqrt{\frac{t^2 - R^2}{1 - R^2}}\,,$$

was changed from the average R for the p in question to the maximum R, and subsequent iterations by this procedure are denoted by primes.

Figure 2 shows $\cos \sigma_z \equiv \cos (\pi/2)\nu_z$. It is only after the first iteration that $\frac{1}{3} > \nu_z$. Figure 3 shows $\cos \sigma_x$. It is seen that $\nu_x = 2$ occurs at $p = 0.95\ m_0c$. Figure 4 shows $B_0^{(n)}$. Figure 5 shows $r_m \equiv r_{max}$ and $\bar{r} \equiv \frac{1}{2}(r_{max} + r_{min})$ as a function of p. It is seen from this figure why the the simple iteration scheme is not very good at large p: a change of $B_0(R)$ at $R = 0.66$ will affect the timing of all orbits from $p \cong 0.8$ to $p \cong 1.0$.

Finally, preliminary results of H. Blosser and H. M. Mosely indicate that the field $B_0^{10'}(R)$ can be fitted to the desired accuracy with a current distribution in 5 of the 21 pairs of circular coils.

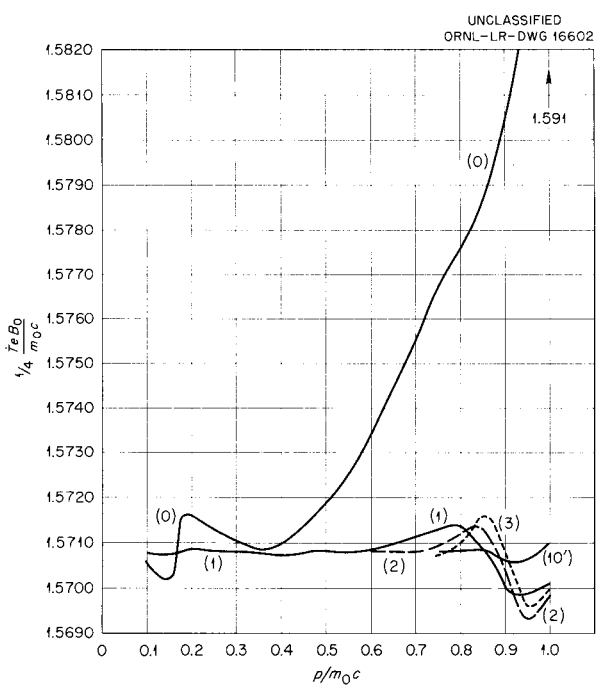

Fig. 1. Orbit Times as a Function of p for Various $B_0(R)$'s Obtained One from the Other by an Iteration Explained in the Text.

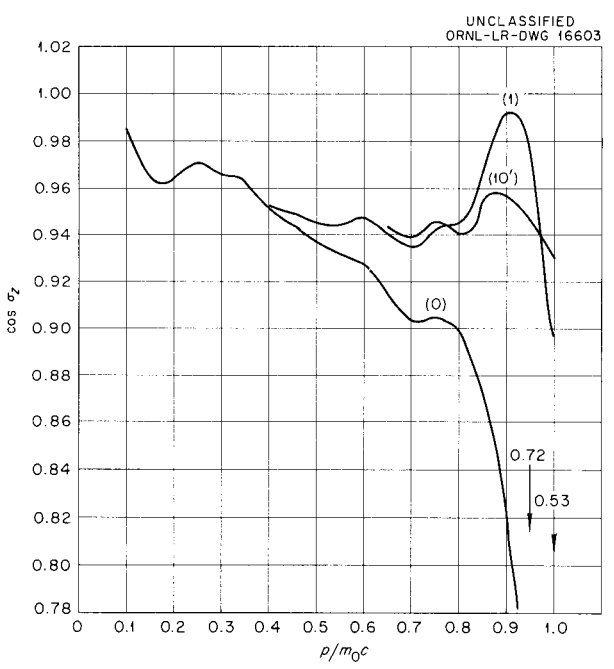

Fig. 2. Cos $\sigma_z \equiv \cos (\pi/2)\ \nu_z$ as a Function of p for the Various $B_0(R)$'s.

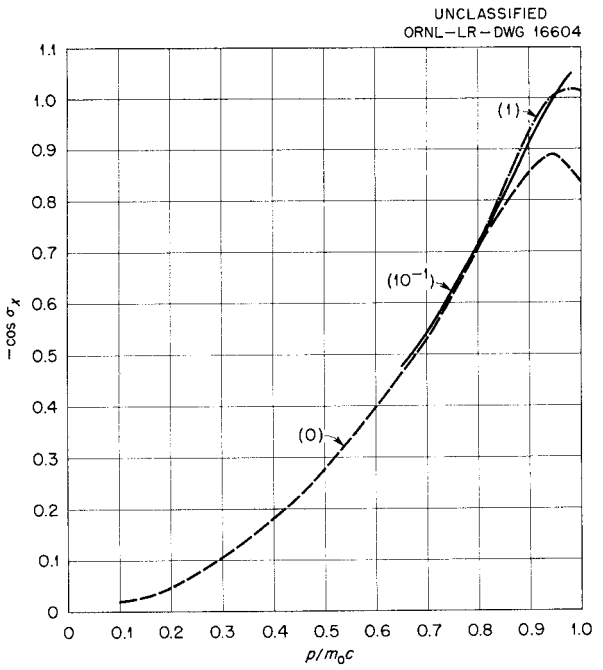

Fig. 3. Cos $\sigma_x \equiv \cos(\pi/2)\,\nu_x$ as a Function of p.

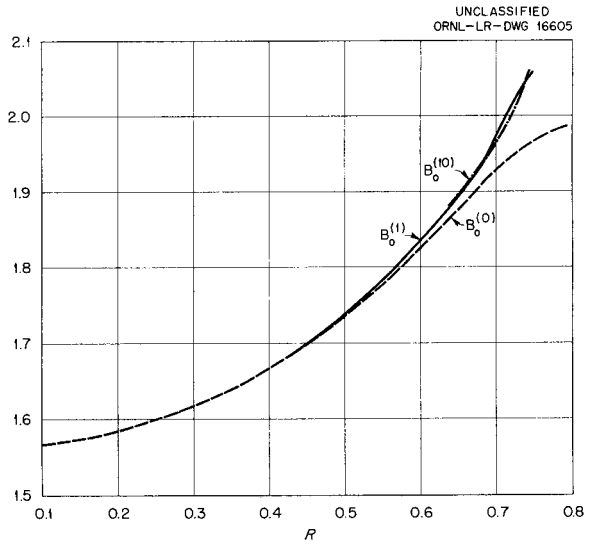

Fig. 4. Gross Differences in the $B_0(R)$'s as a Function of R. The $B_0(R)$'s are in arbitrary units; R is measured in cyclotron units, $T_0c/2\pi$.

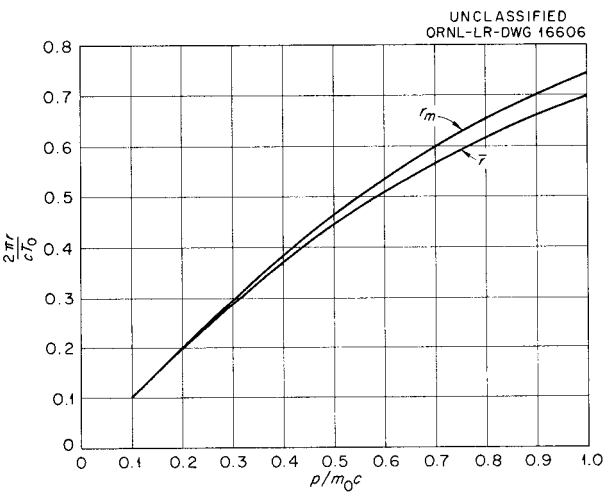

Fig. 5. Maximum and "Average" r as a Function of p. $r_m \equiv r_{max}(p)$, $\bar{r} \equiv \frac{1}{2}\left(r_{max}(p) + r_{min}(p)\right)$.

ANGULAR DISTRIBUTIONS AND POLARIZATION OF GAMMA RAYS FROM COULOMB EXCITATION

F. K. McGowan P. H. Stelson

We have previously reported experiments[1] undertaken to test the calculations[2] of the particle parameters, a_ν, that enter in the angular distribution of gamma rays following coulomb excitation. Within the accuracy of the experiments (± 2 to 5% for the particle parameter a_2) there is agreement with the numerical results from the quantum mechanical treatment. In the same range of interest the semiclassical results are 10 to 20% smaller than the exact results.

For odd-A nuclei an angular distribution measurement gives information on the spins of the excited states produced by coulomb excitation. That is, one measures $A_\nu a_\nu$ and uses the known particle parameters to determine the A_ν which depend on the spins of the levels and the multipole order of the radiation. Coulomb excitation of levels in odd-A nuclei frequently results in the emission of mixed $E2 + M1$ gamma rays. An angular-distribution measurement gives information on the ratio $(E2/M1)1/2$, and this, combined with the cross section for excitation, yields the reduced transition probability for the magnetic dipole transition. However, several cases have been encountered in which the angular distribution was equally well fitted either by two rather different values of $E2/M1$ or by two different spins for the excited state. The ambiguity for five transitions of the type $3/2(E2 + M1)1/2$ has been removed by polarization-direction correlation measurements.[3]

A polarimeter based on the Compton scattering mechanism, whose effectiveness was determined by measurements of the known polarization of gamma rays from excitation of 2+ levels in even-even nuclei, has been described previously.[4] The values obtained for the asymmetry ratio, R, or the effectiveness of the polarimeter, at E_γ = 330 and 358 kev seemed to be smaller than those expected. We attributed part of this to our choice of window widths used in the scintillation spectrometers. We have recalibrated the polarimeter and also extended the calibration to lower energies (E_γ = 200 kev). The results are shown in Fig. 1. The shape of R_{exp} as a function of E_γ is now reasonable.

Angular distributions and polarization-direction correlations have been measured for the gamma rays following coulomb excitation in Tl^{205}, Tl^{203}, Au^{197}, Ir^{193}, Ir^{191}, Os^{188}, $Os^{190,192}$, Ag^{109}, Ag^{107}, and Mo^{95}. A summary of the results is given in Tables 1 and 2. The discrepancy between $(A_2)_{exp}$ and $(A_2)_{\gamma\gamma}$ for Os^{188} might possibly be attributed to the influence of extranuclear fields, because the half life of the intermediate state is 6.5×10^{-10} sec. Another possible explanation is that the 155-kev transition is not entirely due to Os^{188}. The measurements were made with a target of normal osmium, and we have not attributed any of the gamma radiation to Os^{189} (16.1%).

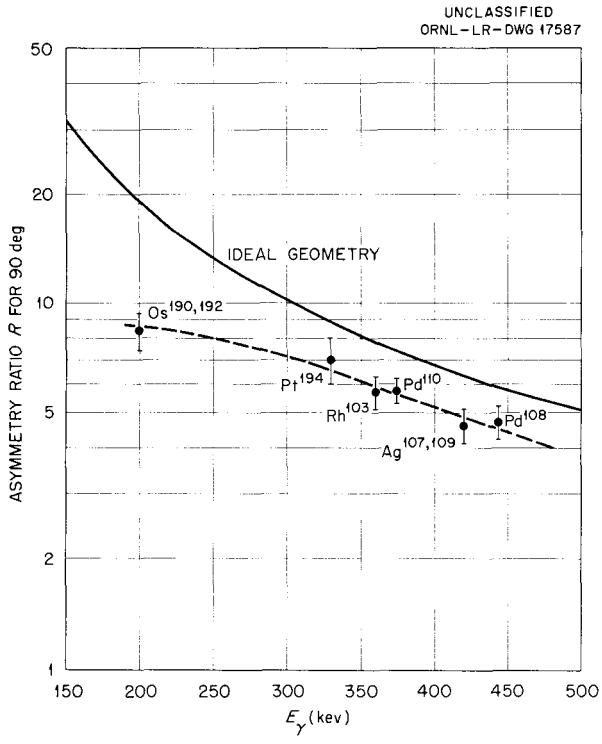

Fig. 1. Asymmetry Ratio R as a Function of E_γ for Both Ideal and Finite Geometry.

[1] F. K. McGowan, P. H. Stelson, and M. M. Bretscher, *Bull. Am. Phys. Soc.* 1(II), 164 (1956).

[2] L. C. Biedenharn, *Phys. Rev.* **101**, 662 (1956); K. Alder and A. Winther, *Kgl. Danske Videnskab. Selskab Mat. Fys. Medd.* **29**, No. 19 (1955).

[3] F. K. McGowan and P. H. Stelson, *Bull. Am. Phys. Soc.* 1(II), 164 (1956).

[4] F. K. McGowan and P. H. Stelson, *Phys. Semiann. Prog. Rep. March 20, 1956*, ORNL-2076, p 12.

A summary of the information obtained for some odd-A nuclei is given in Table 3; $B(E2)_{ex}$ and $B(E2)_d$ are the reduced electric quadrupole transition probabilities for excitation and decay, respectively, in units of cm^4; $B(M1)_d$ is the reduced magnetic dipole transition probability for decay and is actually the quantity $B(M1)/(e\hbar/2Mc)^2$; $B(E2)_{sp}$ is the reduced transition probability expected for a transition between states of the independent particle model.

Table 1. Proton-Gamma Angular-Distribution Coefficients of the Terms in the Expansion of the Correlation Function in Legendre Polynomials for a Thick Target

Nucleus	E_p (Mev)	E_γ (kev)	Spin Sequence	$(A_2)_{\gamma\gamma}$	$(a_2G_2A_2)_{exp}$	$(a_2G_2)_t$	$(A_2)_{exp}$	$\delta = (E2/M1)1/2$	$(a_4G_4A_4)_{exp}$
Tl^{205}	3.0	205	1/2(E2) 3/2(E2 + M1)1/2		0.315 ± 0.009	0.587	0.537 ± 0.015	1.7 ± 0.3	−(0.068 ± 0.012)
	4.5	410	1/2(E2) 5/2(E2 + M1)3/2		−(0.18 ± 0.02)	0.808	−(0.22 ± 0.02)	≲−0.05	−(0.02 ± 0.01)
Tl^{203}	3.0	279	1/2(E2) 3/2(E2 + M1)1/2		0.310 ± 0.013	0.715	0.434 ± 0.018	1.0 to 3.9	−(0.015 ± 0.017)
	4.5	403	1/2(E2) 5/2(E2 + M1)3/2		−(0.14 ± 0.02)	0.848	−(0.17 ± 0.02)	≲0.05	−(0.03 ± 0.02)
Au^{197}	3.0	277	3/2(E2) 5/2(E2 + M1)3/2		−(0.128 ± 0.004)	0.704	−(0.182 ± 0.005)	−(0.41 ± 0.03)	−(0.006 ± 0.005)
Ir^{193}	1.9	140	3/2(E2) 5/2(E2 + M1)3/2		−(0.143 ± 0.014)	0.68	−(0.210 ± 0.020)		0.0135 ± 0.017
	2.4	140	3/2(E2) 5/2(E2 + M1)3/2		−(0.117 ± 0.008)	0.57	−(0.204 ± 0.014)	−(0.75 ± 0.25)	−(0.038 ± 0.010)
	2.7	140	3/2(E2) 5/2(E2 + M1)3/2		−(0.097 ± 0.006)	0.51	−(0.189 ± 0.011)		−(0.001 ± 0.007)
	3.6	217	3/2(E2) 7/2(E2 + M1)5/2		−(0.239 ± 0.019)	0.700	−(0.341 ± 0.027)	−0.22 or −2.2	−(0.069 ± 0.024)
	4.0	217	3/2(E2) 7/2(E2 + M1)5/2		−(0.205 ± 0.004)	0.650	−(0.316 ± 0.010)		−(0.011 ± 0.004)
	3.6	357	3/2(E2) 7/2(E2)3/2	0.2186	0.157 ± 0.005	0.700	0.225 ± 0.007	∞	0.010 ± 0.006
	4.0	357	3/2(E2) 7/2(E2)3/2	0.2186	0.139 ± 0.005	0.650	0.213 ± 0.008		0.010 ± 0.007
Ir^{191}	3.6	348	3/2(E2) 7/2(E2)3/2	0.2186	0.150 ± 0.009	0.690	0.217 ± 0.013	∞	−(0.019 ± 0.012)
	4.0	348	3/2(E2) 7/2(E2)3/2	0.2186	0.111 ± 0.007	0.640	0.173 ± 0.010		−(0.011 ± 0.008)
Ag^{109}	2.7	309	1/2(E2) 3/2(E2 + M1)1/2		−(0.268 ± 0.004)	0.690	−(0.388 ± 0.006)	−(0.19 ± 0.01) or −1.15	0.010 ± 0.005
Ag^{107}	2.7	324	1/2(E2) 3/2(E2 + M1)1/2		−(0.284 ± 0.003)	0.705	−(0.403 ± 0.004)	−(0.21 ± 0.01) or −1.10	0.010 ± 0.003
Os^{188}	3.0	155	0(E2) 2(E2)0	0.3571	0.102 ± 0.004	0.480	0.213 ± 0.008	∞	0.029 ± 0.054
$Os^{190,192}$	3.0	186	0(E2) 2(E2)0	0.3571	0.190 ± 0.003	0.575	0.330 ± 0.005	∞	−(0.0005 ± 0.003)
		206	0(E2) 2(E2)0						

Table 2. Summary of Transitions for Which a Polarization Measurement Has Resolved the Ambiguity for Either the Value of (E2/M1)1/2 or the Spin of the Excited State

Nucleus	E_p (Mev)	E_γ (kev)	Transition	$[P(\theta = \pi/2)]_{exp}$	$\delta = (E2/M1)1/2$
Tl^{205}	3.0	205	3/2 → 1/2	0.91 ± 0.06	1.46 ± 0.16
Tl^{203}	3.0	279	3/2 → 1/2	0.91 ± 0.04	1.50 ± 0.08
Au^{197}	3.0	277	5/2 → 3/2	1.006 ± 0.015	−(0.55 ± 0.06)
Ag^{109}	2.7	309	3/2 → 1/2	0.73 ± 0.03	−(0.20 ± 0.04)
Ag^{107}	2.7	324	3/2 → 1/2	0.78 ± 0.03	−(0.29 ± 0.04)
Mo^{95}	2.7	203	3/2 → 5/2	1.17 ± 0.04	−(0.58 ± 0.20)

Table 3. Summary of Quantities Obtained from $B(E2)_{ex}$ for Some Odd-A Nuclei

Nucleus	E (kev)	$B(E2)_{ex} \times 10^{48}$ (cm^4)	Transition	$B(E2)_d \times 10^{48}$ (cm^4)	Cascade / Crossover	$(E2/M1)1/2$	$T_{1/2}$ (sec)	$B(M1)_d$	$B(E2)_d / B(E2)_{sp}$
Tl^{205}	205	0.100	3/2 → 1/2	0.050		1.46	1.34×10^{-9}	6.9×10^{-4}	7.0
	410		5/2 → 3/2	≤ 0.006		≤ -0.05		2.7×10^{-1}	0.8
	615	0.114	5/2 → 1/2	0.038	9	∞	1.66×10^{-12}		5.3
Tl^{203}	279	0.124	3/2 → 1/2	0.062		1.50	3.00×10^{-10}	1.5×10^{-3}	8.7
	403		5/2 → 3/2	≤ 0.013		≤ 0.05		5.8×10^{-1}	1.8
	682	0.210	5/2 → 1/2	0.070	6		0.77×10^{-12}		9.9
Ir^{193}	140	0.697	5/2 → 3/2	0.465		−0.75	2.95×10^{-10}	1.14×10^{-2}	70
	217		7/2 → 5/2	0.097		−0.22		6.67×10^{-2}	15
	357	0.597	7/2 → 3/2	0.299	0.88	∞	1.64×10^{-11}		45
Cd^{113}	300	0.110	3/2 → 1/2	0.055		0.29	3.20×10^{-11}	4.14×10^{-2}	18
	582	0.304	5/2 → 1/2	0.101	0.02	∞	9.05×10^{-12}		31
	675	0.09	? → 1/2		0.19				
Cd^{111}	342	0.110	3/2 → 1/2	0.055	0.026	0.39	2.72×10^{-11}	2.99×10^{-2}	18
	610	0.143	5/2 → 1/2	0.048	0.29	∞	1.08×10^{-11}		15
Ag^{109}	309	0.249	3/2 → 1/2	0.125		−0.19	5.65×10^{-12}	2.25×10^{-1}	41
	107		5/2 → 3/2			~0		4.6×10^{-2}	
	416	0.377	5/2 → 1/2	0.126	0.07	∞	3.33×10^{-11}		41
Ag^{107}	324	0.219	3/2 → 1/2	0.110		−0.21	5.93×10^{-12}	1.85×10^{-1}	36
	99		5/2 → 3/2			~0		7.7×10^{-2}	
	423	0.334	5/2 → 1/2	0.111	0.10	∞	3.38×10^{-11}		36
Rh^{103}	298	0.209	3/2 → 1/2	0.105		−0.18	6.96×10^{-12}	2.05×10^{-1}	35
	62		5/2 → 3/2			~0		2.1×10^{-1}	
	360	0.393	5/2 → 1/2	0.131	0.19	∞	5.90×10^{-11}		45
Mo^{95}	203	0.035	3/2 → 5/2	0.053		−0.6	7.64×10^{-10}	4.4×10^{-3}	21

THE REACTION $N^{14}(p,p'\gamma)N^{14}$

J. K. Bair
H. O. Cohn
J. D. Kington
H. B. Willard

The yield of the 2.31-Mev gamma rays resulting from the inelastic scattering of protons by the first excited state of N^{14} has been measured for bombarding energies ranging from 2.5 to 5.1 Mev.

A thin, stable target of nitrogen was produced by bombarding a disk of clean, 7-mil tantalum with the 100-kev molecular nitrogen beam from the ORNL heavy-ion Cockcroft-Walton accelerator. This target had a total of about 10^{19} atoms of nitrogen distributed over an area of somewhat less than 1 cm^2. Target thickness is estimated to be less than 3 kev at a 3.0-Mev proton energy.

The target was bombarded with protons from the ORNL 5.5-Mv Van de Graaff and analyzed with a 90-deg magnet giving less than 0.1% energy resolution. Energy calibration is believed to be accurate to ±0.2% relative to the $Li^7(p,n)Be^7$ threshold.[1]

The gamma rays were detected by means of a 3-in.-dia by 3-in.-high NaI(Tl) crystal mounted on a 3-in. photomultiplier tube of the DuMont-type K1197. Pulses from the photomultiplier tube were recorded with a 20-channel, pulse-height analyzer, adjusted to cover only the region of the full energy peak. The datum plotted for the yield curve is the reading of the peak channel, while for the angular distributions the highest three channels in the peak were used.

Figure 1 shows the yield of the 2.31-Mev gamma ray taken with the detector at 90 deg to the proton beam. The triangle points indicate background measured by bombarding the reverse side of the target. Spectra taken at proton energies below and above the two highest resonances show that the general rise upon which the two resonances are superimposed does consist of the same radiation as the resonances themselves. A yield curve (not shown) taken at 0 deg to the target differed in no essential feature from the 90-deg yield. The inserts on Fig. 1 show the angular distribution of the gamma rays at the four resonances. The four levels found are at energies of excitation in the compound nucleus O^{15} of 11.00, 11.08, 11.83, and 11.91 Mev, with experimental widths of 90, 25, 80, and 70 kev, respectively. Angular distributions of the gamma rays taken at the resonances were isotropic, in agreement with the previous assignment of spin 0 to the 2.31-Mev state in N^{14}.

A gas target was used to measure the absolute cross section for production of the 2.31-Mev gamma rays at the 3.91-Mev resonance. Measurements were made for both air and nitrogen and for pressures ranging from 0.2 to 0.7 atm. Corrections were made for the target resolution. For each determination, the integrated number of counts in the full energy peak of the spectrum was used, together with the crystal efficiency curves of Lazar *et al.*,[2] to obtain the gamma-ray source strength. The differential cross section so determined was 3.90 ± 0.6 mb/steradian at 90 deg.

[1] J. D. Kington *et al.*, *Phys. Rev.* 99, 1393 (1955).

[2] N. H. Lazar, R. C. Davis, and P. R. Bell, *Nucleonics* 14(4), 52 (1956).

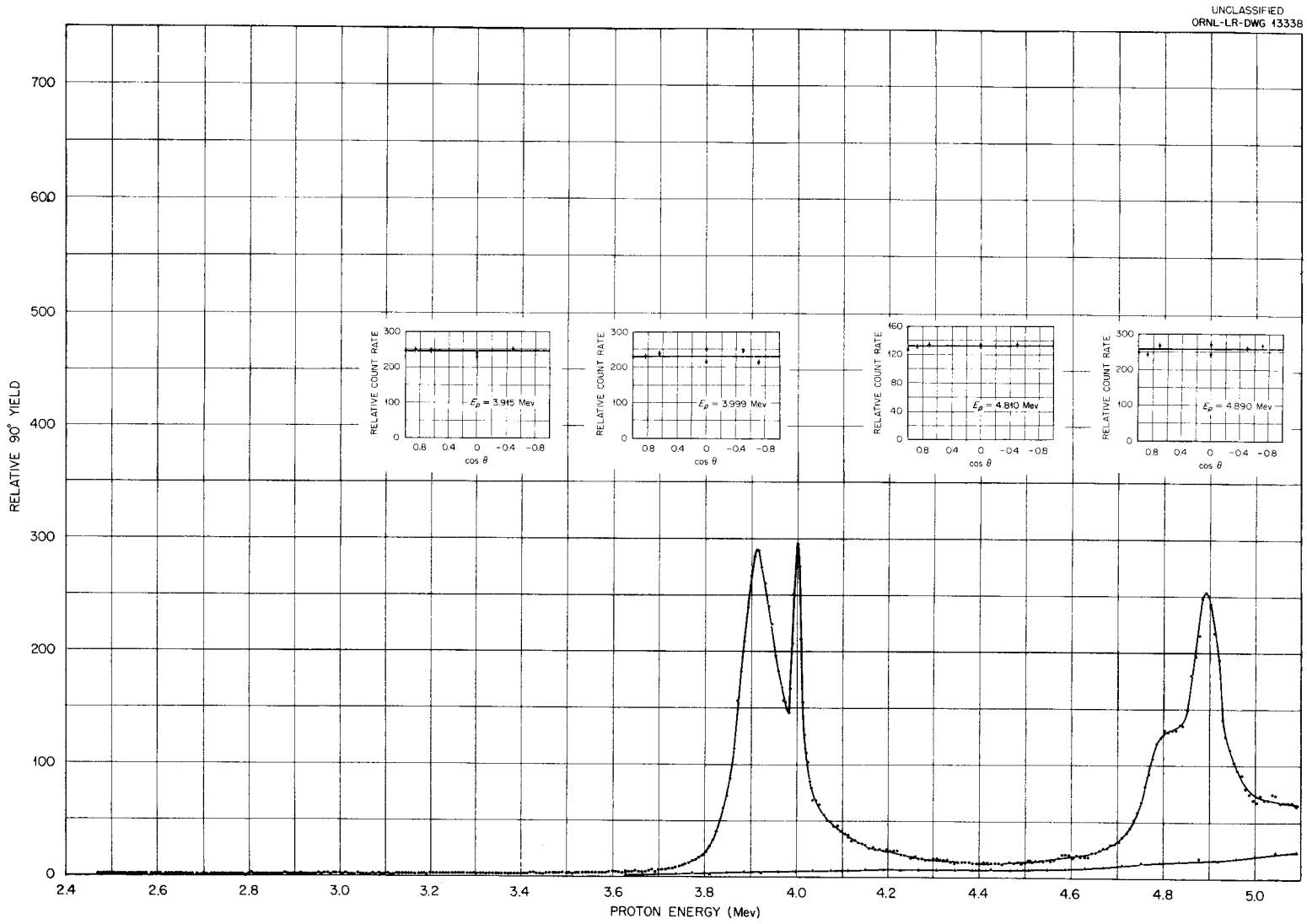

Fig. 1. Yield Curve of the 2.31-Mev Gamma Ray. The triangles represent background as measured by bombarding the tantalum target backing. The inserts show the angular distribution of the gamma rays on or near the four resonances.

THE $C^{13}(p,\gamma)N^{14}$ REACTION

H. B. Willard J. K. Bair H. O. Cohn

Attempts were made to reduce the contamination (B^{11}, F^{19}, and Si^{28}) of C^{13} targets prepared by cracking methyl iodide vapor on machined platinum disks. Proton capture gamma rays were detected by means of a 3 × 3 in. NaI crystal located at $\theta = 90$ deg and $h = 5.0$ cm (distance from target to front face of crystal). The spectrum of gamma rays at the 3.11-Mev resonance[1] is shown in Fig. 1. The data have been resolved into three gamma rays, 10.43, 6.42, and 4.03 Mev, by using the shapes of spectra of "monoenergetic" gamma rays previously measured.[2] It can be seen that the 10.43-Mev level in N^{14} decays predominantly to the ground state with about a 10% cascade through the 6.42-Mev level. Below the pulse height of 20, the rapid rise is due to the still-present contaminating reactions $B^{11}(p,p'\gamma_{2.14\ Mev})$ and $Si^{28}(p,p'\gamma_{1.78\ Mev})$. The measured width of this resonance is 30 ± 3 kev, and the peak cross section for the ground-state transition is 0.70 ± 0.14 mb. The 10.43-Mev level in N^{14} is assigned the values $J = 2^-$ and $T = 1$ from the observed ground-state angular correlation

$$W(\theta) = 1 - (0.40 \pm 0.02)\, P_2\,(\cos\theta)$$

and the large radiation width of 17 ev. That is, the level is formed by d-wave proton capture followed mainly by electric dipole radiation to the ground state of N^{14}.

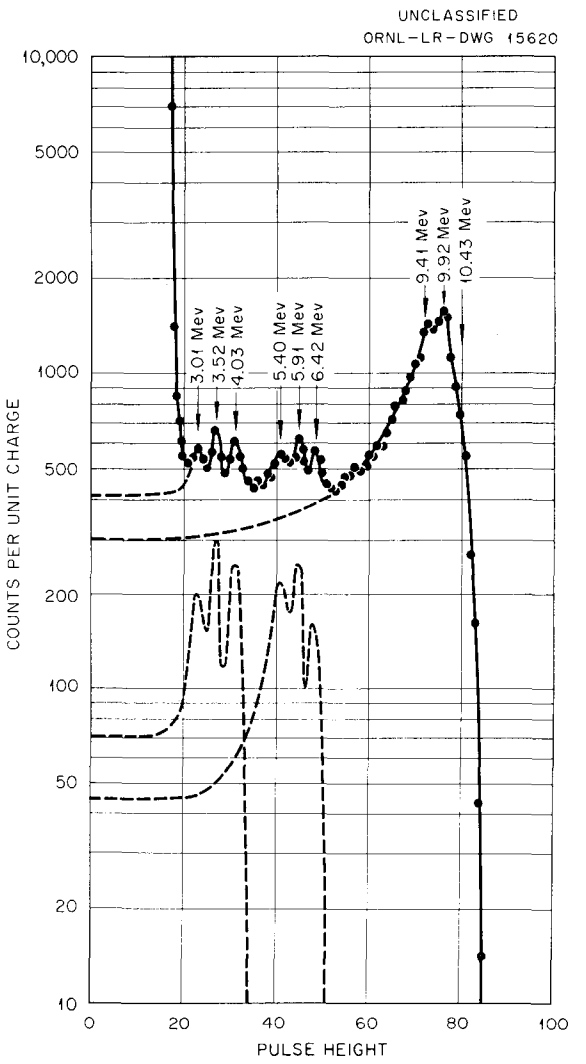

Fig. 1. Differential Pulse-Height Spectrum of Gamma Rays from C^{13} Proton Capture Taken at the 3.11-Mev Resonance.

[1] H. B. Willard, J. D. Kington, and J. K. Bair, *Phys. Rev.* **98**, 1184 (1955).

[2] N. H. Lazar and H. B. Willard, *Phys. Semiann. Prog. Rep. March 10, 1956*, ORNL-2076, p 55.

PRELIMINARY YIELD OF THE REACTION $C^{13}(p,p'\gamma)C^{13}$

H. O. Cohn J. K. Bair H. B. Willard

The level structure of the compound nucleus N^{14} between the 11- and 12-Mev excitation energy has been previously investigated by means of C^{12}-plus-deuteron reactions and by the reaction $C^{13}(p,n)N^{13}$, with results summarized by Ajzenberg and Lauritsen.[1] The present work reports a preliminary investigation of this region of excitation in which the yield of the gamma rays was measured from the 3.68- and 3.09-Mev levels in C^{13} following excitation by inelastic proton scattering.

Target and bombarding techniques were essentially those described for the $C^{13}(p,n)N^{13}$ experiment.[2] All data were taken with a target 5 kev thick for 1.75-Mev protons. Points were taken at intervals of about 5 to 8 kev in proton energy.

Since the energy threshold for excitation of even the lowest level in C^{13} is above the threshold for the (p,n) reaction, it is necessary to measure the gamma radiation in the presence of this neutron background. In this particular case the relative intensities were such that it was found possible to suitably reduce the neutron intensity by means of shielding without seriously affecting the spectrum of the (fortunately relatively high energy) gamma rays as measured with a 3-in.-dia by 3-in.-high NaI(Tl) crystal. The shield used to take the data presented here consisted, in order, of 11 cm of lithiated paraffin, 3½ cm of boral, 4½ cm of lithiated paraffin, and 0.6 cm of lead, with the lead nearest the detector. Figure 1 shows the gamma-ray spectrum taken with this arrangement at a bombarding proton energy of 4.75 Mev. Peak V is the full energy peak for the 3.68-Mev radiation, while peak IV consists of the full-energy 3.09-Mev radiation plus a contribution from the single escape peak of the 3.68-Mev gamma ray. Peak III consists of the two escape peaks of the higher energy and the single escape peak of the lower-energy gamma ray. Peak II is the two escape peaks for the 3.09-Mev gamma ray. Peak I is due to annihilation radiation.

Figure 2 shows the yield curves obtained with the detector located at 0 deg with respect to the incoming proton beam and at a distance of about 25 cm from the target. The data plotted are the readings of the highest channel in the full-energy peaks. The open points represent the yield of the 3.68-Mev radiation. Below about 4.3-Mev proton energy, the high-energy gamma ray makes essentially no contribution to the 3.09-Mev gamma-ray data (solid points). Above 4.3 Mev the solid points must be corrected for the presence of the single escape peak of the 3.68-Mev radiation. By fitting a semiempirical curve of a "pure" 3.68-Mev gamma ray to the experimental spectrum, it can be shown that this correction to the yield can be made with reasonable accuracy by subtracting from the height of peak IV the height of peak V. Thus above 4.3 Mev the true yield of the 3.09-Mev gamma ray can be represented by the difference between the solid and open points.

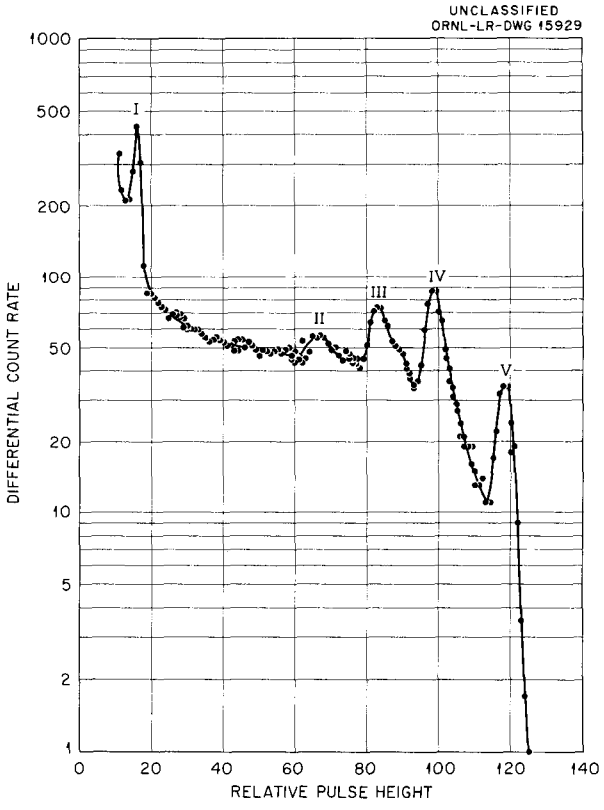

Fig. 1. Spectrum of Gamma Rays from $C^{13}(p,p'\gamma)$ Taken at $E_p = 4.75$ Mev.

[1] F. Ajzenberg and T. Lauritsen, *Revs. Mod. Phys.* 27, 77 (1955).

[2] J. K. Bair, J. D. Kington, and H. B. Willard, *Phys. Rev.* 90, 575 (1953).

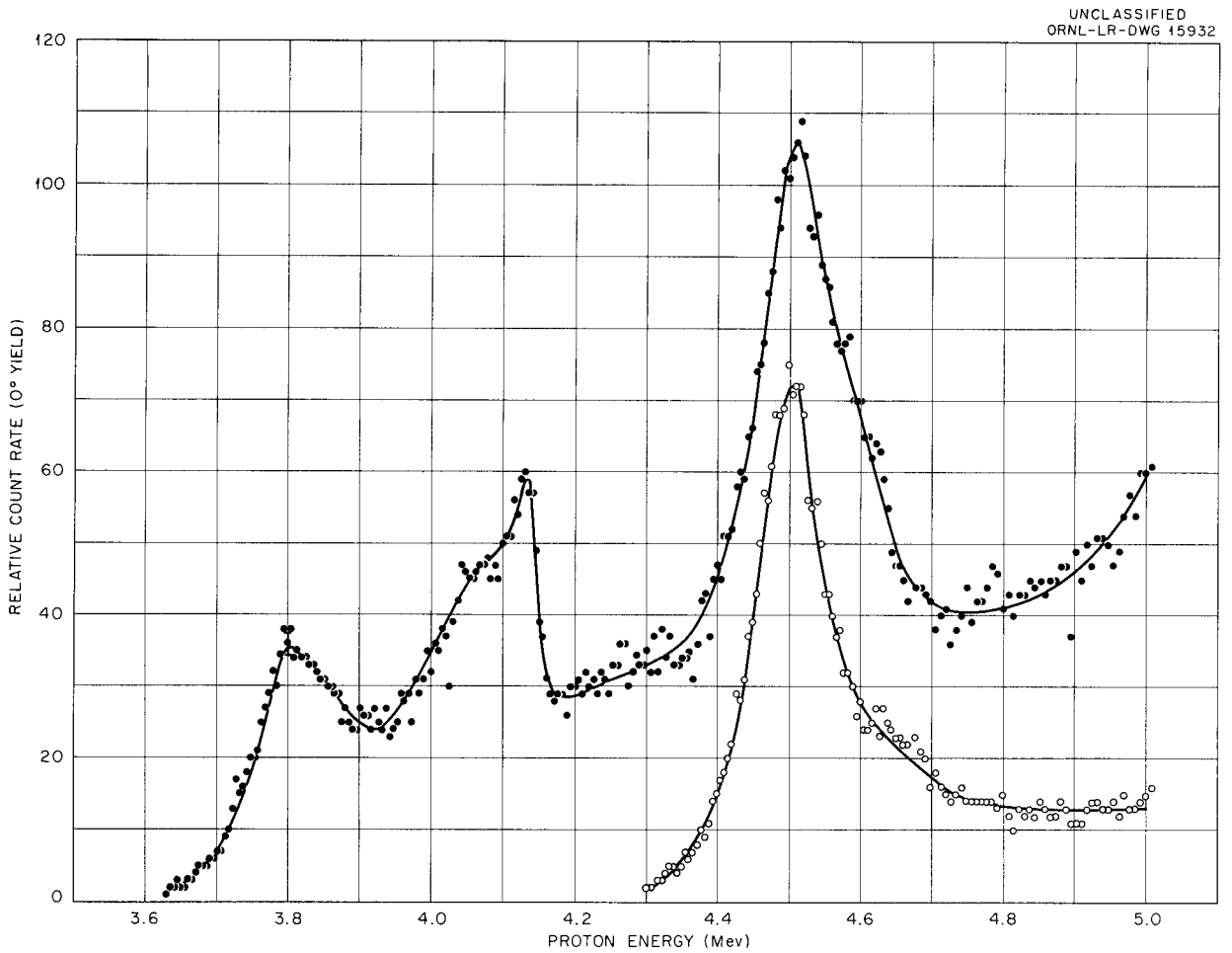

Fig. 2. The 0-deg Yields of the 3.09- and 3.68-Mev Gamma Rays from $C^{13}(p,p'\gamma)$.

THRESHOLDS AND CROSS SECTIONS FOR (p,n) REACTIONS IN INTERMEDIATE NUCLEI

C. H. Johnson A. Galonsky J. Ulrich[1]

The statistical theory formulated by Hauser and Feshbach[2] specifically for inelastic scattering of neutrons is also applicable to (p,n) reactions. Measurements of the relative yields of (p,n) reactions for ten target nuclei with intermediate atomic weight were previously reported.[3] These measurements showed relative agreement with the theory within experimental error, that is, within a factor of 2. The present measurements give absolute rather than relative cross sections to ±15%.

Protons from the 3-Mv Van de Graaff were used to bombard approximately 20-kev-thick targets on platinum blanks. Neutrons were detected by means of BF_3 counters embedded in a paraffin cube, 40 cm on a side, surrounding the target. The relative efficiency of this counter assembly was obtained by comparison with the activity produced in a 50-liter $MnSO_4$ solution which replaced the assembly around the target. Absolute calibration was made by activating the solution with an Sb-Be source calibrated at the Bureau of Standards. The counter efficiency decreased from 9.3% at 10 kev to 6.0% at 700 kev neutron energy.

Figures 1 through 5 present cross sections for target nuclei Ti^{49}, V^{51}, Mn^{55}, Ga^{71}, and As^{75}. Each curve has been corrected for the background observed with a platinum-blank target. Measurements have been completed for Cl^{37}, Cr^{53}, Co^{59}, Cu^{65}, Se^{77}, Se^{82}, and a thick-target yield for Nb^{93}. An attempt will be made to describe the complete set by the theory of Hauser and Feshbach.

Thresholds not previously reported in this group are Se^{77} (2176 ± 4 kev), Se^{82} (≦970 kev), and Nb^{93} (≦1310 kev). The threshold for $Nb^{93}(p,n)Mo^{93}$ is much lower than the value 2683 ± 18 kev observed by Willard, Bair, and Kington.[4] Their higher value may be for neutrons leaving Mo^{93} in an excited state.

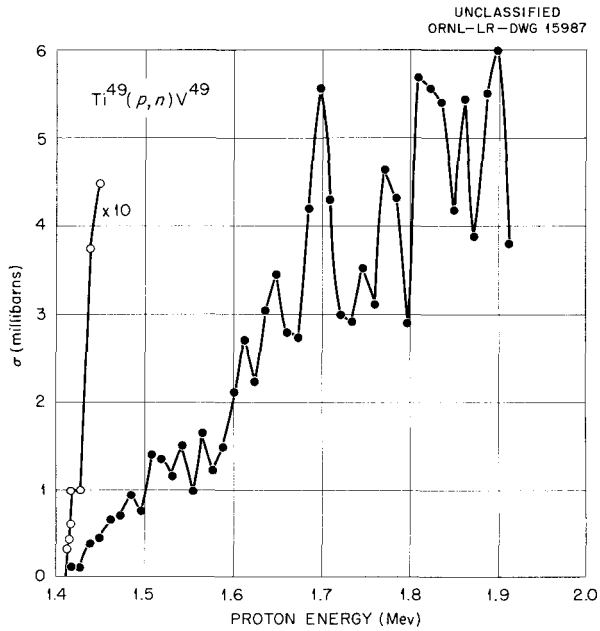

Fig. 1. Cross Section for the $Ti^{49}(p,n)V^{49}$ Reaction.

[1]ORNL summer employee from the University of Michigan.

[2]W. Hauser and H. Feshbach, *Phys. Rev.* 87, 366 (1952).

[3]C. H. Johnson and C. C. Trail, *Phys. Semiann. Prog. Rep. Sept. 10, 1953*, ORNL-1620, p 3.

[4]H. B. Willard, J. K. Bair, and J. D. Kington, *Phys. Quar. Prog. Rep. Dec. 20, 1951*, ORNL-1278, p 5.

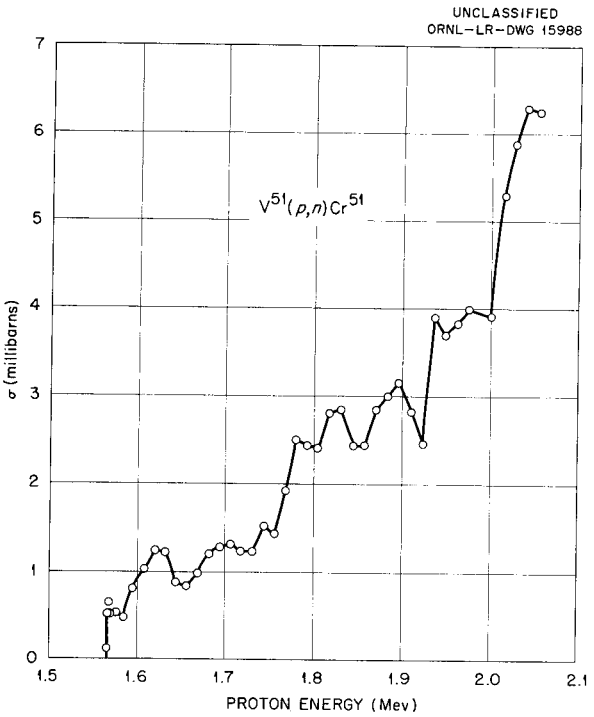

Fig. 2. Cross Section for the $V^{51}(p,n)Cr^{51}$ Reaction.

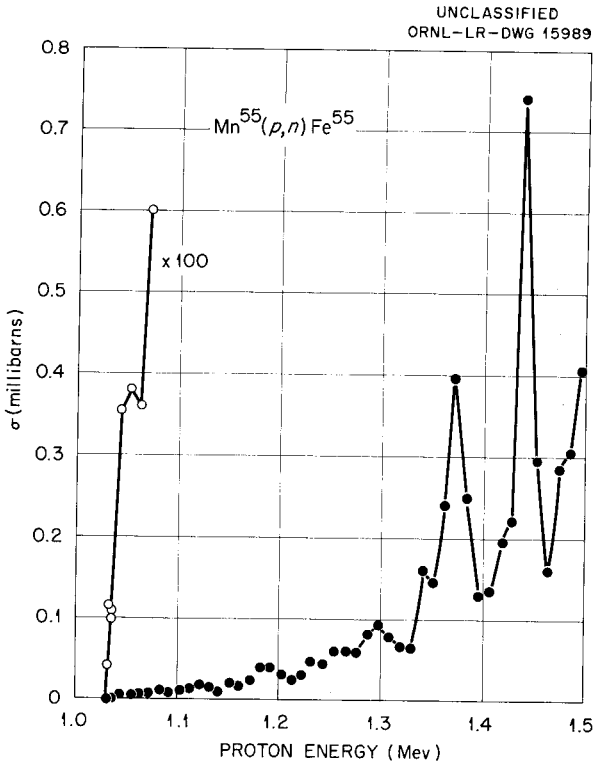

Fig. 3. Cross Section for the $Mn^{55}(p,n)Fe^{55}$ Reaction.

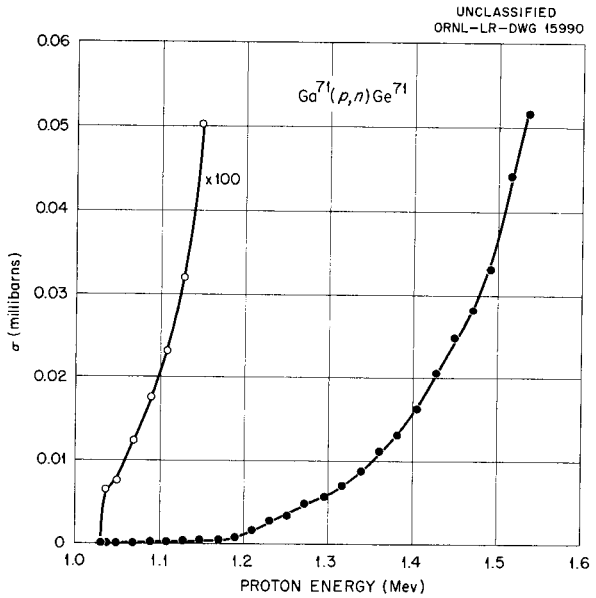

Fig. 4. Cross Section for the $Ga^{71}(p,n)Ge^{71}$ Reaction.

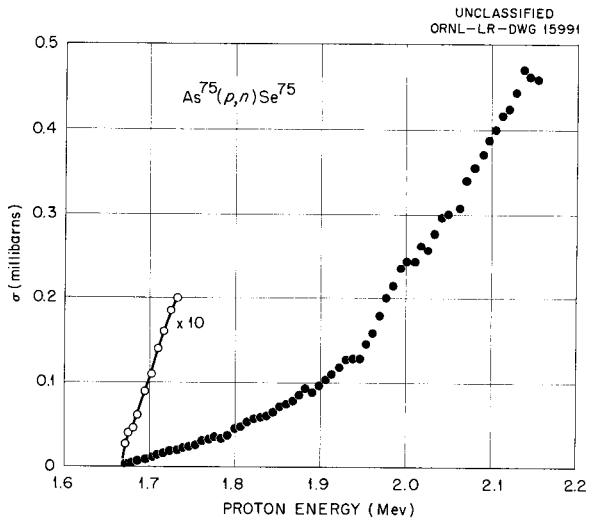

Fig. 5. Cross Section for the $As^{75}(p,n)Se^{75}$ Reaction.

THE 2.07-Mev RESONANCE IN THE NEUTRON TOTAL CROSS SECTION OF C^{12}

H. B. Willard J. K. Bair H. O. Cohn

Previous work[1] on the total cross section of $C^{12} + n$ indicated that the 2.07-Mev resonance had an observed width of 11 kev and a spin of 3/2. Elastic-scattering angular distributions[1] showed that this level in C^{13} at the 6.86-Mev excitation is due to d waves. More recent work[2] on the reaction $C^{12} + p$ assigns unambiguously the value of $D_{5/2}$ to what is presumed to be the mirror level in N^{13}. Accordingly, it was felt worthwhile to reinvestigate the total cross section of C^{12} in the region of this resonance.

Neutrons produced by the $Li^7(p,n)Be^7$ reaction, from a thin metallic layer of the metal evaporated in place, were detected by a propane recoil counter (1 in. in diameter, 4 in. in sensitive length) located a mean distance of 11.5 in. in the forward direction. Transmissions of C^{12} (high-purity graphite) samples, 1.125 in. in diameter and located 4 in. from the target, were measured in the conventional manner. Sample thicknesses were changed to keep the transmission ~0.6. The data thus obtained are plotted in Fig. 1.

The J value of a resonance produced by pure elastic scattering can be deduced from the maximum height of the total cross section above the average potential scattering (or tails of distant levels). There are, however, a number of factors which can reduce the experimentally observed maximum:

1. Pure elastic scattering may not be the only mode of interaction. In the case of 2.1-Mev neutrons on C^{12}, capture is also possible. However, the thermal capture cross section[3] is 4.7 mb, and it is estimated that the effect on the total cross section at 2.1 Mev will be negligible.

2. The background of neutrons not originating directly at the target, as well as those scattered from equipment, walls, and floors, must be subtracted. An 8-in.-long Lucite shadow cone placed between the target and the detector gave a background value 2.2% of the direct beam. This value may be slightly high because of forward diffusion of the neutrons in the shadow cone. The machine background with a clean piece of tantalum in place of the target is about 2.4% of the direct beam for the thinnest target used. All data points have been corrected for the above backgrounds.

3. Some of the neutrons traversing the graphite samples are scattered into the detector. This "in-scattering" correction is a function of the geometry, sample thickness, and angular distribution of first-scattered neutrons. Since both $D_{3/2}$ and $D_{5/2}$ levels give large forward scattering, the theoretical angular distributions were used for the correction. In view of the final result, the $D_{5/2}$ distributions were used to correct the data points. This correction was 3.8% of the direct beam at the peak of the resonance.

4. If the sample and detector are not properly aligned, the observed cross section will be low. The location of the beam was determined by placing paraffin on the outside of the tantalum-backed target, and the heat of the beam melted the paraffin, defining the beam spot (~$^3/_{16}$ in. in diameter). The sample and counter were then aligned geometrically.

5. If the energy resolution used is comparable with the observed width of the level, the total cross section will be reduced. The resolution is

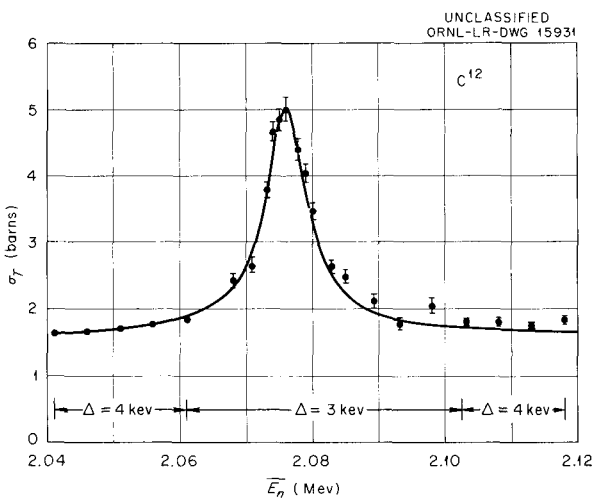

Fig. 1. Total Cross Section of C^{12} in the Region of the 2.076-Mev Resonance.

[1] J. E. Wills, Jr., *Phys. Semiann. Prog. Rep. March 10, 1956*, ORNL-2076, p 22.

[2] G. C. Phillips, private communication.

[3] K. Way, *Natl. Bur. Standards (U. S.) Cir.* 499 (Sept. 1, 1950).

taken to be the rms value of machine energy resolution, target thickness, and neutron energy variation with angle. The machine resolution was checked by the narrow (p,γ) resonances in Al^{27} at 933.3 kev (ref 4) and in C^{13} at 1746.9 kev (ref 5), giving a value of 0.06%. This is equivalent to 2.3 kev at the 2.07-Mev resonance (proton energy 3.75 Mev) in C^{12}. The target thickness can be obtained from the geometric peak at the threshold of the $Li^7(p,n)$ reaction. However, for thin targets ($\leq$5 kev) this method is not reliable, and a check on the over-all resolution was obtained by measuring the narrow resonance in the total neutron cross section of S^{32} at 585 kev (ref 6). Figure 2 shows this total cross section measured before and after the run on C^{12} with the thinnest target obtained. The observed width is 3.6 kev, the natural width 1.5 kev, the machine resolution 1.4 kev, and the angular resolution 0.2 kev; hence the target thickness is 3.1 kev at this proton-bombarding energy. Accordingly, the target thickness at E_p = 3.75 Mev is about 2.3 kev, and the total resolution is 3.3 kev. The observed width of the 2.07-Mev level with this target is 8 kev; hence the natural width is 7 kev, and the resonant contribution to the total cross section will be reduced to the value

$$\left(\frac{\Gamma_n}{\Delta}\tan^{-1}\frac{\Delta}{\Gamma_n}\right)\sigma^{res}_{theo} = 0.93\sigma^{res}_{theo} .$$

Thus, if the resonance is $D_{3/2}$, the observed cross section will be 0.21 barn low, whereas from a $D_{5/2}$ level it would be 0.31 barn low. The data in Fig. 1 have not been corrected for resolution.

6. The $Li^7(p,n)$ reaction is not monoenergetic. At the 3.75-Mev bombarding proton energy, there is a lower energy (1.61 Mev) group of neutrons which is about 10% of the main group[7] (2.07 Mev). Since the total cross section of C^{12} for 1.61-Mev neutrons is 2.00 barns (ref 8), the total cross section at resonance will be reduced by 0.25 barn if it is $D_{3/2}$ and by 0.40 barn if it is $D_{5/2}$. The nonresonant cross section will be raised by 0.04 barn. The assumption is made that the detector has the same efficiency for both groups of neutrons, which was the case for the bias setting employed. The data points have *not* been corrected for this effect.

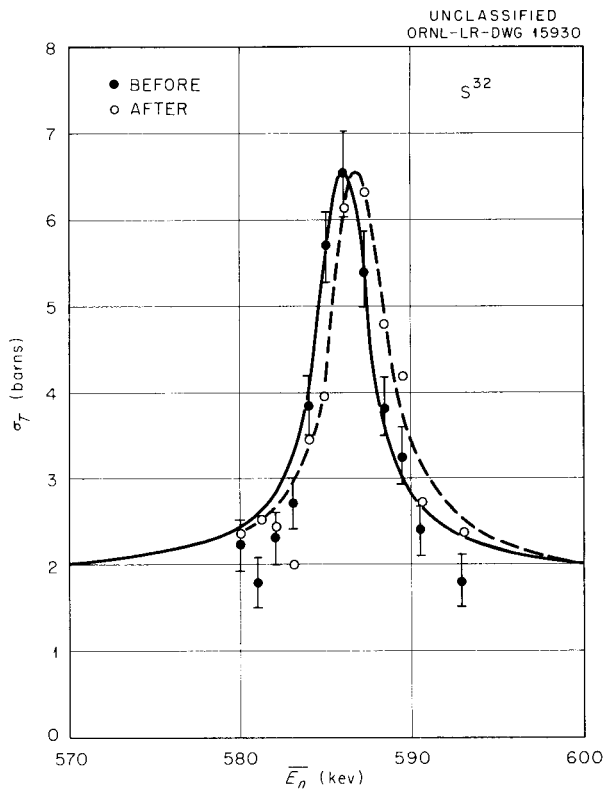

Fig. 2. Total Cross Section of S^{32} in the Region of the 585-kev Resonance.

The data in Fig. 1, after a consideration of factors 1 through 4, give a peak cross section of 5.01 ± 0.20 barns (standard deviation). This value is higher than the theoretical maximum for a J = 3/2 resonance (4.54 barns), and hence applying the $D_{5/2}$ factors 5 and 6 one obtains 5.7 ± 0.2 barns, which is in good agreement with the theoretical value of 6.01 barns for a J = 5/2 resonance.

Further work is planned in an attempt to reduce the size of the above corrections. However, the present data show that the resonance occurs at 2.076 ± 0.008 Mev with a natural width of 8 kev and is $D_{5/2}$.

[4] R. G. Herb, S. C. Snowdon, and O. Sala, *Phys. Rev.* 75, 246 (1949).

[5] J. B. Marion and F. B. Hagedorn, *Phys. Rev.* (to be published).

[6] R. E. Peterson, H. H. Barschall, and C. K. Bockelman, *Phys. Rev.* 79, 593 (1950).

[7] L. Cranberg, *$Li^7(p,n)Be^7$ Reaction Study by Time-of-Flight*, LA-1654 (April 12, 1954).

[8] C. K. Bockelman, *Phys. Rev.* 84, 69 (1951).

It is felt that the earlier work[1] did not consider the above corrections in enough detail. Furthermore, the target thickness used by Wills was 1.7 kev as measured by the geometric peak. The actual thickness may have been somewhat greater; hence the actual resolution was 3 kev at best.

ELASTIC NEUTRON SCATTERING DIFFERENTIAL CROSS SECTIONS FOR OXYGEN AND BERYLLIUM

H. O. Cohn J. L. Fowler

The differential elastic neutron scattering cross section was measured for scattering of 1.5- and 0.73-Mev neutrons from oxygen and beryllium by the method described by Willard *et al.*[1] A tritium gas target bombarded with protons from the 5.5-Mv Van de Graaff served as the neutron source with an energy resolution of ~50 kev. A propane recoil counter biased to give a flat response for the scattered neutron energies served as the detector. The samples were a $\frac{5}{8}$-in.-dia × $4\frac{1}{2}$-in.-long BeO cylinder and a metallic beryllium cylinder of the same length and having the same number of beryllium nuclei as the BeO sample. The resulting angular distributions are shown in Figs. 1 and 2. All values are in the C.M. system. The errors shown represent the counting statistical errors only. These curves have not been corrected for angular resolution or for multiple scattering.

[1]H. B. Willard, J. K. Bair, and J. D. Kington, *Phys. Rev.* 98, 669 (1955).

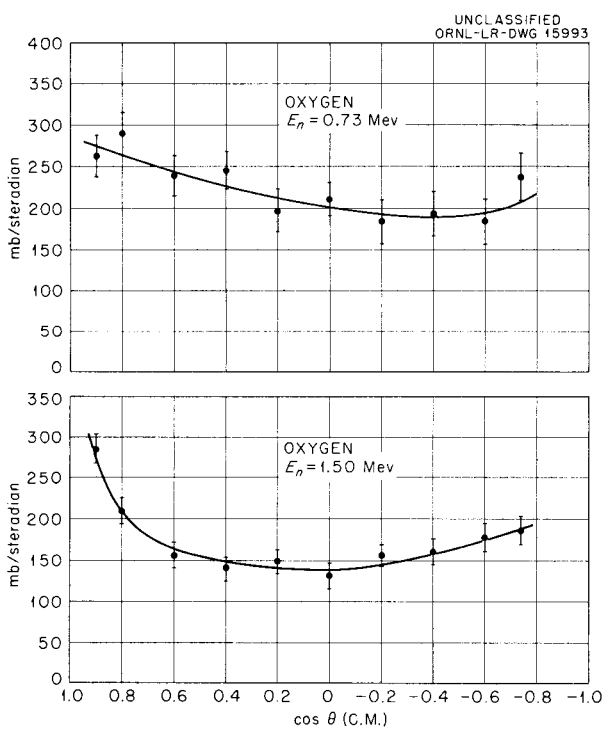

Fig. 1. Elastic Neutron Scattering Differential Cross Section for Oxygen at E_n = 0.73 and 1.50 Mev.

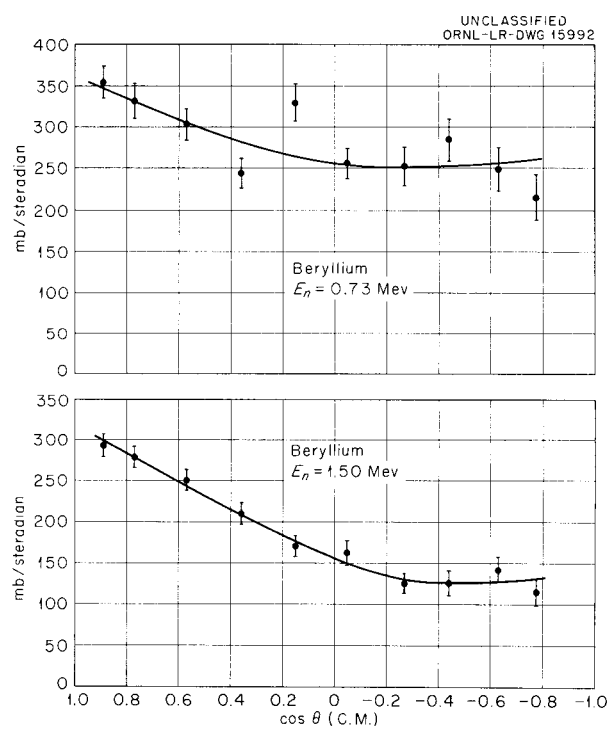

Fig. 2. Elastic Neutron Scattering Differential Cross Section for Beryllium at E_n = 0.73 and 1.50 Mev.

NEUTRON RESONANCE PARAMETERS OF Eu^{151} AND Eu^{153}

J. A. Harvey R. C. Block

The total neutron cross sections of samples of Eu^{151} (enriched to 91.9%) and Eu^{153} (enriched to 95.0%) have been measured with the ORNL fast chopper. The transmission curves have been analyzed from 1 to 10 ev to obtain the parameters of the resonances. The resonances[1] which have been reported previously at 1.76, 3.35, 3.84, 4.83, 7.47, and 8.90 ev are shown to be two resonances, with a resonance in each isotope, as given in Table 1. In this energy range 11 resonances were observed in Eu^{151}, and eight resonances were observed in Eu^{153}. The average level spacing per spin state is 2.3 ± 0.6 ev in Eu^{153} and 1.3 ± 0.2 ev in Eu^{151} (including the three Eu^{151} resonances[1] below 1 ev). From the resonance parameters up to 10 ev, the strength functions (the ratio, $\overline{\Gamma_n^0}/D$) of Eu^{151} and Eu^{153} are $(3.4 \pm 0.9) \times 10^{-4}$ and $(1.8 \pm 0.6) \times 10^{-4}$, respectively.

[1] D. J. Hughes and J. A. Harvey, *Neutron Cross Sections*, BNL-325 (July 1, 1955).

Table 1. Resonance Parameters

E_0	$\sigma_0\Gamma$ (bev)	$2g\Gamma_n$ (mv)	$2g\Gamma_n^0$ (mv)
		Eu^{151}	
1.055	330 ± 60	0.27 ± 0.05	0.26 ± 0.05
1.84 ± 0.02	25 ± 3	0.035 ± 0.004	0.026 ± 0.003
2.73	130 ± 30	0.27 ± 0.06	0.16 ± 0.04
3.35	1300 ± 300	3.4 ± 0.8	1.9 ± 0.4
3.72	210 ± 100	0.6 ± 0.3	0.31 ± 0.15
4.85 ± 0.05	23 ± 14	0.09 ± 0.05	0.04 ± 0.02
5.47	60 ± 20	0.25 ± 0.07	0.11 ± 0.03
6.05	100 ± 30	0.47 ± 0.15	0.19 ± 0.06
7.24	320 ± 100	1.8 ± 0.6	0.7 ± 0.2
7.47	370 ± 110	2.1 ± 0.7	0.8 ± 0.3
9.00 ± 0.10	120 ± 50	0.8 ± 0.3	0.27 ± 0.10
		Eu^{153}	
1.76	48 ± 4	0.065 ± 0.006	0.049 ± 0.005
2.46	510 ± 100	0.96 ± 0.20	0.61 ± 0.13
3.28 ± 0.03	230 ± 50	0.58 ± 0.12	0.32 ± 0.07
3.94	280 ± 60	0.85 ± 0.18	0.43 ± 0.09
4.88 ± 0.05	14 ± 8	0.05 ± 0.03	0.023 ± 0.014
6.25	160 ± 40	0.8 ± 0.2	0.32 ± 0.08
7.60 ± 0.10	28 ± 17	0.16 ± 0.10	0.06 ± 0.04
8.90	650 ± 200	4.4 ± 1.4	1.5 ± 0.5

MEASUREMENT OF THERMAL-NEUTRON RELAXATION TIMES IN SUBCRITICAL SYSTEMS

E. C. Campbell P. H. Stelson

Further measurements of the relaxation time of thermal neutrons in cylindrical $U^{235}O_2F_2$-H_2O solutions have been made by the method previously described.[1] The measurements have been extended with a solution containing 26.5 g of U^{235} per liter to systems from 11 in. to 3 in. in diameter, in most cases with the cylinder height equal to the diameter. Additional measurements were also made with the original 53.0-g/liter solution before dilution.

On the basis of simple theory,[1] one expects the dependence of decay constant on geometrical buckling of the fundamental mode B^2 to be given by the expression

$$(1) \quad \lambda = v\Sigma_a + DB^2 + v\Sigma_{25}[1 - \eta\bar{P}(B^2)] \ .$$

Figure 1 is a schematic diagram showing the meaning of the separate terms. Experimentally determined values of all terms in the equation, with the exception of the nonescape probability $\bar{P}(B^2)$, were inserted in Eq. 1, and several different simple expressions for $\bar{P}(B^2)$ were tried in order to obtain a good fit of the data. No one expression gave a good fit over the whole buckling range. However, for $B^2 < 0.14$ cm^{-2}, the expression $\bar{P}(B^2) = (1 + \tau B^2)^{-1}$ gave an excellent fit, with $\tau = 21.2$ cm^2 for the data on both concentrations. The data, as well as the theoretical curves, are shown in Fig. 2.

It is possible that for the systems of 3, 4, and 5 in. in diameter the geometric buckling is not a suitable parameter to use in describing the nonescape leakage for the following reason. In order for a fission neutron emitted inside a small system to be thermalized, it must suffer a hard collision (large energy loss) with hydrogen on the way out of the system, and the smaller the system, in general, the harder must be the collision. One might expect, therefore, that the effective mean free path for such first collisions should be very much greater than the dimensions of the system.

[1] E. C. Campbell and P. H. Stelson, *Phys. Semiann. Prog. Rep. March 10, 1956*, ORNL-2076, p 37.

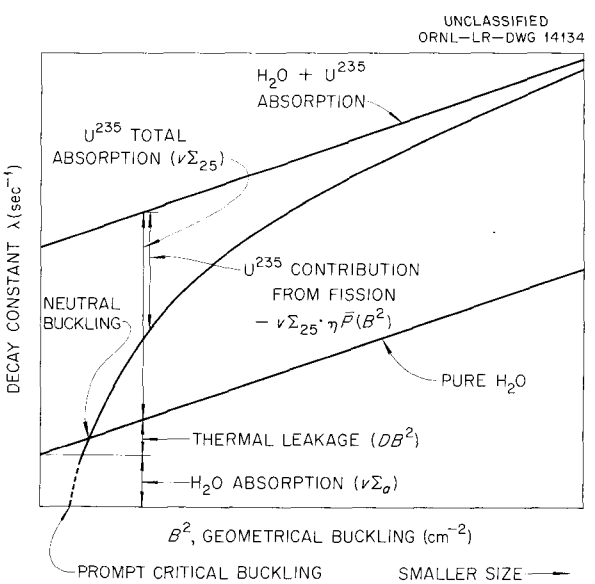

Fig. 1. Illustration of Theoretical Dependence of Decay Constant of U^{235}-H_2O System on Size as Given by Geometrical Buckling. The contribution from the individual terms of Eq. 1 is indicated.

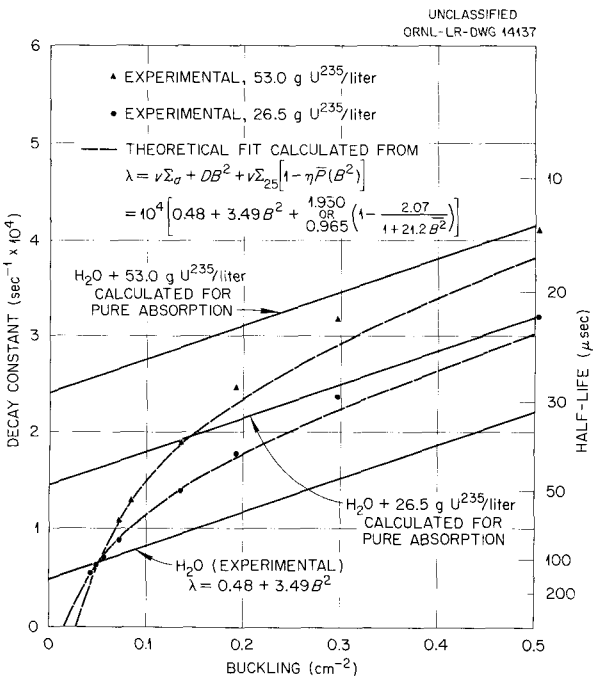

Fig. 2. Decay Constant of U^{235}-H_2O System as a Function of Geometrical Buckling. The solid curved lines are calculated from Eq. 1 with the indicated constants.

If this qualitative picture is accepted, then the nonescape probability is not simply a function of B^2 but depends in some other way on the dimensions and shape of the system. This interpretation is supported by the observation that the decay constant of the 53.0-g/liter U^{235} system with a height of 2 in. and a diameter of 4 in. was considerably smaller than was the decay constant of the 3 × 3 in. cylinder, although the calculated geometrical bucklings were almost the same. A Monte Carlo calculation of this effect would be of interest.

One difficulty in the interpretation of these measurements is in calculating the geometrical buckling from the dimensions of the system, since there is some uncertainty as to what extrapolation length to assume. In order to reduce this uncertainty, as well as to make certain that we are dealing with the fundamental mode, flux distribution measurements were undertaken. A schematic diagram of the apparatus is shown in Fig. 3. The detector was an $Li^6I(Eu)$ scintillation crystal 1.2 mm thick and 4 mm in diameter, optically connected to a 6199 photomultiplier by a Lucite rod and contained in a thin stainless steel tube. This tube was 8 in. long and $^3/_{16}$ in. in diameter and was supported from a rigid rod attached to a rigidly supported optical bench, as shown in the diagram. The results of radial and axial traverse measurements in an 8 × 8 in. H_2O cylinder are shown in Figs. 4 and 5, respectively, together with the best fit of the fundamental diffusion mode functions to the data. The plotted experimental points represent the ratio between the number of Li^6I detector counts (collected between 200 and 300 μsec following the end of 1000-μsec bursts) and the number of neutron counts recorded on a long counter placed

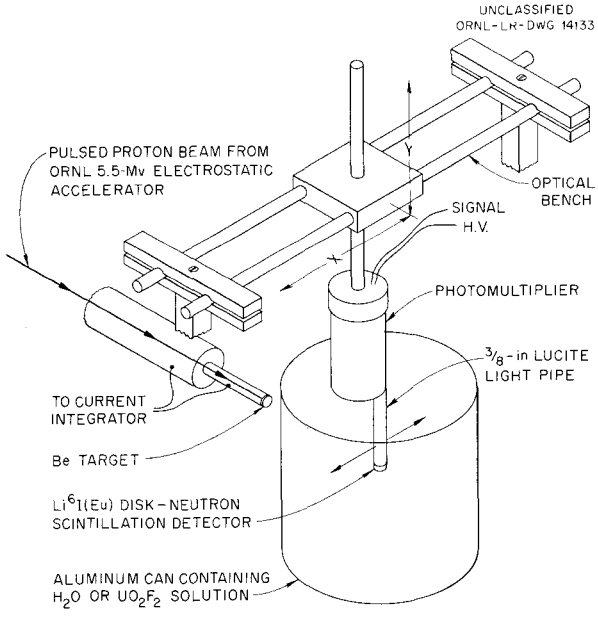

Fig. 3. Schematic Diagram of Apparatus for Measuring Fundamental Mode Thermal-Neutron Flux Distributions Inside Liquid Systems. Not shown is long-counter neutron monitor.

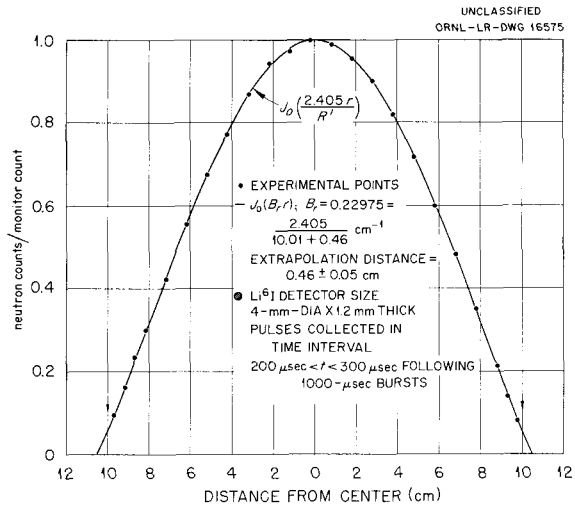

Fig. 4. Radial Thermal-Neutron Flux Distribution in Small H_2O Cylinder.

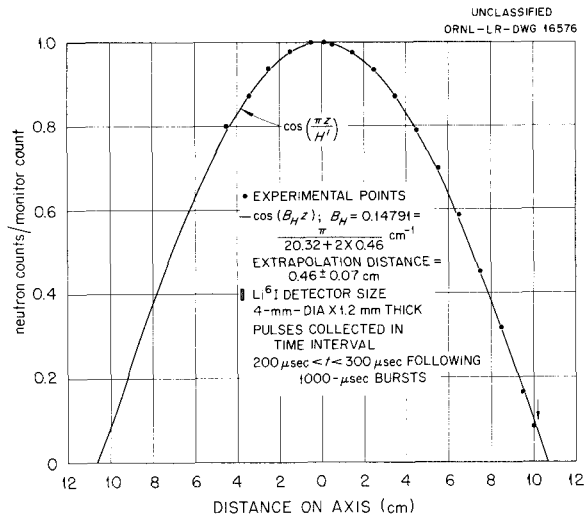

Fig. 5. Axial Thermal-Neutron Flux Distribution in Small H_2O Cylinder.

about 3 m from the pulsed source. About 10^4 detector counts were recorded at each position of the detector.

In fitting the data of Fig. 4 it was noticed that slightly different values of the extrapolation distance were obtained, depending on whether one took the best linear representation of the data near the boundary, or whether one selected the best fit of J_0 to the data. Since our interest was primarily in determining the proper buckling, the over-all fit seemed most appropriate. The extrapolation distance measured in this way is 0.46 ± 0.05 cm. The straight linear fit gives 0.37 ± 0.05 cm. The reason for the discrepancy lies in the slight curvature of $J_0(x)$ from its point of inflection at 1.84 to its zero at 2.405.

With the same apparatus, similar data were taken for the radial traverse in UO_2F_2 solution and for the radial flux distribution with a central cadmium control rod. These data are now being analyzed. The extrapolation distance in the uranium solution appears to be considerably greater than in H_2O. Since the original data were plotted (Fig. 2) with a geometrical buckling calculated with an assumed constant extrapolation length of 0.32 cm, a slight revision of Fig. 2 may be needed to take account of the new experimental information.

The effective multiplication constant k_{eff} can be introduced into Eq. 1 to obtain

$$\lambda = \lambda_0(B^2)(1 - k_{eff}) \ , \tag{2}$$

where

$$\lambda_0(B^2) = v\Sigma_a + DB^2 + v\Sigma_{25}$$

is the equation of the straight line labeled "pure absorption" in Fig. 2. On the basis of Eq. 2, the k_{eff} for the lowest experimental point in Fig. 2 is 0.655. It appears that with additional enriched material the decay constant could be followed safely to about 10% of the smallest value yet determined. If Eq. 1 is to be relied upon, one should expect that for $k_{eff} = 0.95$ the system would decay with a half life of 1 msec. By setting $\lambda = 0$ in Eq. 1, one can determine the buckling corresponding to prompt critical. For dilute systems these calculations show good agreement with critical data obtained at the Laboratory by A. D. Callihan and his associates.

ENERGY LOSS OF PROTONS IN SILVER AND GOLD

P. H. Stelson F. K. McGowan

One of the sources of error in the determination of electric quadrupole transition rates from coulomb excitation measurements is the uncertainty in the energy loss of the exciting projectiles in the target materials. In the limit of very thin targets the error caused by the uncertainty in energy loss is eliminated. However, it has been impractical to construct thin targets of accurately known thickness from the normally limited amounts of enriched isotopes available. Therefore most of the measurements were made with metallic foils which were thick to the incident projectiles (protons of several Mev energy). In order to correct these thick-target experiments for errors in the energy loss of protons, measurements were made with thick and thin targets of silver ($z = 47$) and gold ($z = 79$), since for these two elements one can make stable, uniform thin targets of accurately known thickness.

The number of gamma rays detected, I, when bombarding a target with N particles is

$$I = \epsilon N \int_{E_f}^{E_i} \frac{\sigma(E)\, dE}{S(E)} \ , \tag{1}$$

where

$$E_f = E_i - \int_0^x S\, dx \ ,$$

$\sigma(E)$ is the cross section, $S(E)$ is the energy loss, ϵ is the over-all detection efficiency, and x is the target thickness. The shape of the cross-section curve as a function of energy for coulomb excitation has been accurately calculated and has been experimentally confirmed. The absolute value depends on an unknown constant, the reduced electric quadrupole transition probability, B. One

has that $\sigma(E) = B \cdot Y(E)$, where $Y(E)$ is known; we therefore have that

$$(2) \qquad B = \frac{1}{\epsilon}\frac{I}{N}\frac{1}{\int_{E_f}^{E_i} Y(E)\, dE/S(E)} .$$

From a measurement of I/N and from the knowledge of ϵ, $Y(E)$, $S(E)$, and x, one deduces the quantity B. Now, for a thick target ($E_f = 0$) one sees that if $S(E)$ is, for example, uniformly 10% too large then B will be in error by 10%. On the other hand, if the target is sufficiently thin, then the error introduced in the integrand of

$$\int_{E_f}^{E_i} \frac{Y(E)\, dE}{S(E)}$$

is just counteracted by the change in the limit E_f. So, from thin-target measurements on silver and gold, one can get good values of B, even with an error in the value taken for $S(E)$. We then compared these values with those obtained by bombarding thick targets with protons of various incident energies. From this comparison one can deduce the error in $S(E)$ and alter $S(E)$ until the yields from thick and thin targets give consistent values for B. It is not necessary to know the overall efficiency, ϵ, to high accuracy, since it drops out in the comparison of thick and thin targets. However, it is necessary to know quite accurately the thickness x of the thin target, since this enters into the determination of B for these targets.

The thin foils were chosen to be only moderately thin because we wanted sufficient coulomb excitation yield to make the yield of the proton bremsstrahlung (from foil and foil backing) small in comparison.

Gold and silver foils in 6 × 6 in. squares were obtained from Baker & Co., Inc. These were successively cut into smaller squares in order to study the macroscopic uniformity. In this way profiles of the thickness of the original large foils were obtained. Small foils for the experiment were chosen from those sections showing the greatest uniformity. It is judged that the thickness of the foils used is known to 0.5% for the gold foils (thickness ~10 mg/cm^2) and to 1.0% for the silver foils (thickness ~6 mg/cm^2). The silver foils were mounted on tin backings of approximately 80 mg/cm^2 thickness, and the gold foils were mounted on bismuth backings of approximately 120 mg/cm^2 thickness. Both the tin and bismuth backings were prepared by electrodeposition onto 5-mil nickel foils. Three thin targets each of silver and gold were prepared to check the reproducibility of the measurements.

Since the foils are only moderately thin, one expects that the values obtained for B are not completely independent of the values taken for $S(E)$. We have studied this problem in the following way: We assumed that the shape of $S(E)$ was known. We then changed the absolute values by a certain percentage, for example, 10%, and carried out numerical integration to find the resultant change in the thin-target B value for various incident proton energies and for the foil thicknesses used. The ratio of the percentage change in B to the percentage change in $S(E)$ was 0.35 for the worst case (3-Mev protons on gold foil) and 0.08 for the best case (5-Mev protons on gold foil). This ratio is then useful in the determination of the values of $S(E)$ which will give the same B values for thick and thin targets.

Measurements were made at proton energies of 3.0, 3.5, 4.0, 4.5, and 5 Mev for gold and at 2.4, 2.7, 3.0, and 3.3 Mev for silver. Coulomb excitation of the states at 550 and 277 kev in gold and at 415 and 313 kev in silver was studied.

Two small corrections were applied. First, one must take into account the fact that angular distribution of the gamma rays from coulomb excitation varies (slowly) with the incident proton energy. The angular distributions are known for silver and gold.[1] Appropriate averages over target thickness have been determined and applied to measurements. Second, allowance was made for the fact that the multiple small-angle Rutherford scattering makes the effective path length in the foil somewhat larger than the foil thickness. This increase can be calculated by the use of the theory of Goudsmit and Saunderson.[2] For our cases it was found that the largest correction for this effect was 1% (3-Mev protons on the gold foil).

Our best values for $S(E)$ for silver and gold are given in Table 1. These measurements are of an integral type and are useful in obtaining accurate

[1] F. K. McGowan and P. H. Stelson, *Phys. Rev.* 99, 127 (1955).

[2] S. Goudsmit and J. L. Saunderson, *Phys. Rev.* 57, 24 (1940).

values of B from coulomb excitation with thick targets. However, they are not suited for a detailed examination of the shape of $S(E)$. Rather, one must assume that he knows the shape of $S(E)$ and then determine whether the experiments are consistent with the assumed shape. Our shape for $S(E)$ for silver is of the form $S(E) \propto E^{-1/2}$, and that for gold is very nearly of this shape. Theoretical consideration and experimental results[3] suggest this energy dependence for $S(E)$. If one accepts the fact that the shapes for $S(E)$ are correct (and the experiments are consistent with these shapes), then it is felt that the absolute values of $S(E)$ are determined to within ±4% (standard deviation).

[3] A. Winther, private communication.

Table 1. $dE/d\rho x$ for Protons in Gold and Silver

Gold		Silver	
E_p (Mev)	$(dE/d\rho x)_p$ [kev/(mg/cm^2)]	E_p (Mev)	$(dE/d\rho x)_p$ [kev/(mg/cm^2)]
5.0	27.8	3.3	50.7
4.8	28.5	3.2	51.6
4.6	29.2	3.1	52.4
4.4	30.0	3.0	53.4
4.2	30.8	2.9	54.3
4.0	31.6	2.8	55.4
3.8	32.7	2.7	56.4
3.6	33.7	2.6	57.5
3.4	34.9	2.5	58.6
3.2	36.1	2.4	59.7
3.0	37.3	2.3	61.0
2.8	38.7	2.2	62.3
2.6	40.3	2.1	63.7
2.4	42.2	2.0	65.2
2.2	44.4	1.9	66.8
2.0	46.7	1.8	68.5
1.8	49.3	1.7	70.5
1.6	52.3	1.6	72.7
1.4	55.9	1.5	75.1
1.2	60.1	1.4	77.8
1.0	65.1	1.3	80.8
0.8	71.3	1.2	84.1
		1.1	87.9
		1.0	92.5
		0.9	98.0
		0.8	104.0

CROSS SECTIONS FOR ELECTRON LOSS BY HYDROGEN ATOMS AND EQUILIBRIUM CHARGE DISTRIBUTIONS OF A HYDROGEN BEAM

C. F. Barnett H. K. Reynolds[1] R. G. Reinhardt

Previous reports[2] have included descriptions and results of a number of experiments in which were investigated the cross sections for the electron capture and loss of fast hydrogen atoms and ions in gases. The particle energy ranged from 3 to 200 kev. Present results include measurements of the electron-loss cross sections of fast hydrogen atoms in various gases. Also included are the equilibrium charge distributions of a hydrogen beam after it has been passed through a thick gas target. From these two measurements the electron capture cross sections may be computed. The particle energy interval was 250 kev to 1 Mev for target gases of hydrogen, helium, nitrogen, and argon.

The apparatus used for these measurements consisted of two charge-exchange chambers shown schematically in Fig. 1. The ion beam from the 3-Mv Van de Graaff accelerator was incident upon the first differentially pumped gas cell, designated as the neutralizer. Since the Van de Graaff does not operate stably below 500 kev, it was necessary in the energy region of 250 to 500 kev to accelerate molecular hydrogen ions at higher energies and dissociate them in the neutralizer by impact with gas molecules, resulting in particles of half energy. For higher energies, protons were accelerated, and a small fraction was converted into neutral particles in the neutralizer by charge exchange. The electrostatic deflection plates (electrostatic analyzer No. 1) removed all ions from the emergent beam, so that only neutral particles were incident on the second gas cell. Ions formed by electron-loss collisions in this second gas cell are removed from the beam by the applied transverse electric field. The geometrical path length was determined by measuring the attenuation of the neutral beam, with voltage applied to all four analyzers and then only to the center two. Beam intensity was measured by use of secondary electron emission from a brass target and was corrected for the effect of the relative secondary-electron emission for hydrogen ions and atoms. This correction was determined by measuring with a thermocouple the rise in temperature of the target with only ions or atoms impinging. The ratio of the relative secondary-electron emission for hydrogen atoms to ions increased from 1.36 at 250 kev to 1.59 at 1 Mev.

The ratio of the electron-loss cross section to the electron-capture cross section (σ_{01}/σ_{10}) was determined by observing the charge distribution in the particle beam after it passed through a gas target which was thick enough for equilibrium to be established between competing capture and loss processes. This equilibrium is independent of the initial charge state. For higher energies (500 kev to 1 Mev) the equilibrium charge distribution was determined for a proton beam incident on the first gas cell (the neutralizer). For lower

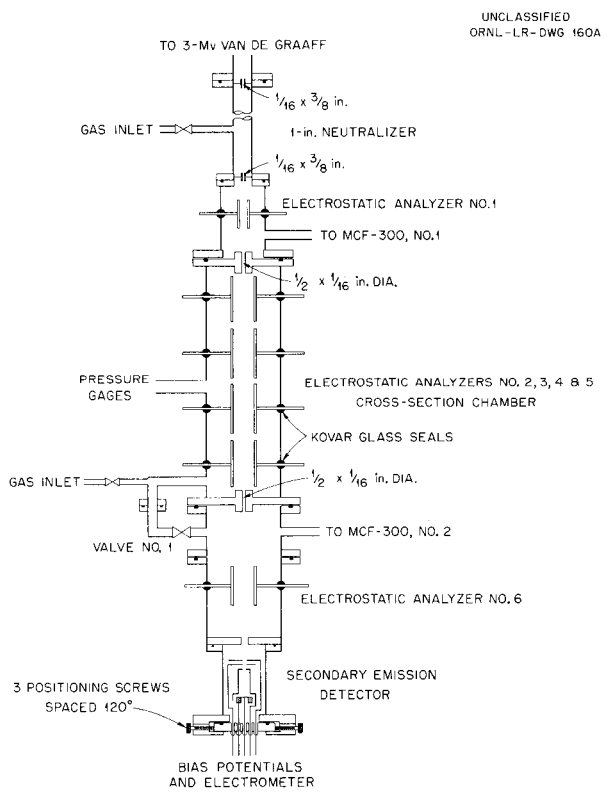

Fig. 1. Apparatus for Electron-Loss Cross Sections.

[1] Summer employee from the University of Houston.

[2] P. M. Stier *et al.*, *Phys. Semiann. Prog. Rep. Sept. 10, 1954*, ORNL-1798, p 64; also, P. M. Stier and C. F. Barnett, *Phys. Semiann. Prog. Rep. March 20, 1955*, ORNL-1879, p 39.

energies (250 to 500 kev) the charge distribution was determined by first dissociating H_2^+ in the first gas cell, then removing all emergent ions by means of the electrostatic deflecting plates so that only neutral atoms were incident on the second cell. This is necessary to eliminate any H_2^+ ions not dissociated in the neutralizer, although the presence of H^+ would not have altered the charge distribution. The measurements of equilibrium charge distribution with a 500-kev proton beam or a 1-Mev molecular ion beam, which is dissociated, yield results which are identical to within the accuracy of the experiment. To obtain the sufficiently thick gas target it was necessary to increase the pressure in the appropriate gas cell until no further change was noticed in the ion-to-atom ratio.

From the measurements of electron-loss cross sections (σ_{01}) and the equilibrium charge distribution ($n_1/n_0 = \sigma_{01}/\sigma_{10}$), the electron-capture cross sections may be readily computed. Shown in Figs. 2, 3, 4, and 5 are the experimental determinations of the electron-loss cross sections and the computed electron-capture cross sections as a function of energy or velocity. The present results agree well with those obtained with the Cockcroft-Walton accelerator in the adjoining region, and for completeness these results are plotted for energies less than 250 kev.

For the case of hydrogen target gas we can compare our result with theoretical predictions. Plotted in Fig. 2 are the theoretical results of Dalgarno and Griffing[3] and of Jackson and Schiff.[4]

[3] A. Dalgarno and G. W. Griffing, *Proc. Royal Soc. (London)* A232, 423 (1955).

[4] J. D. Jackson and H. Schiff, *Phys. Rev.* **89**, 359 (1953).

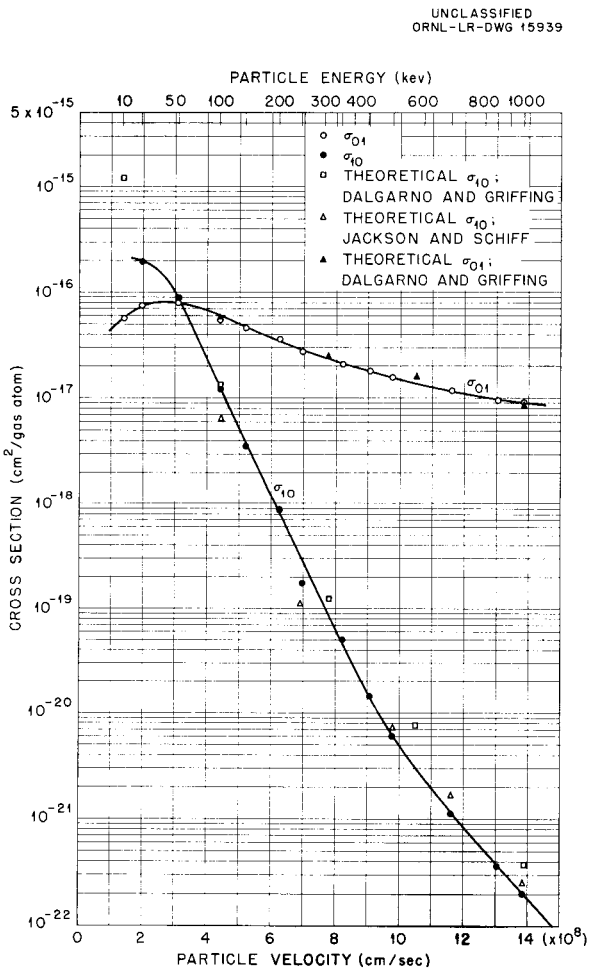

Fig. 2. Charge Transfer Cross Section per Atom of Gas Traversed as a Function of Particle Velocity and Energy. Hydrogen atoms and ions in hydrogen gas.

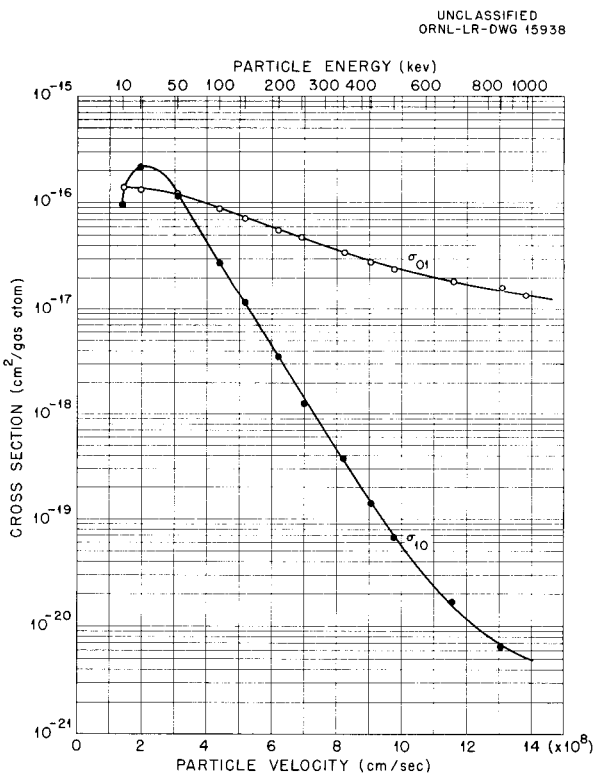

Fig. 3. Charge Transfer Cross Section per Atom of Gas Traversed as a Function of Particle Velocity and Energy. Hydrogen atoms and ions in helium gas.

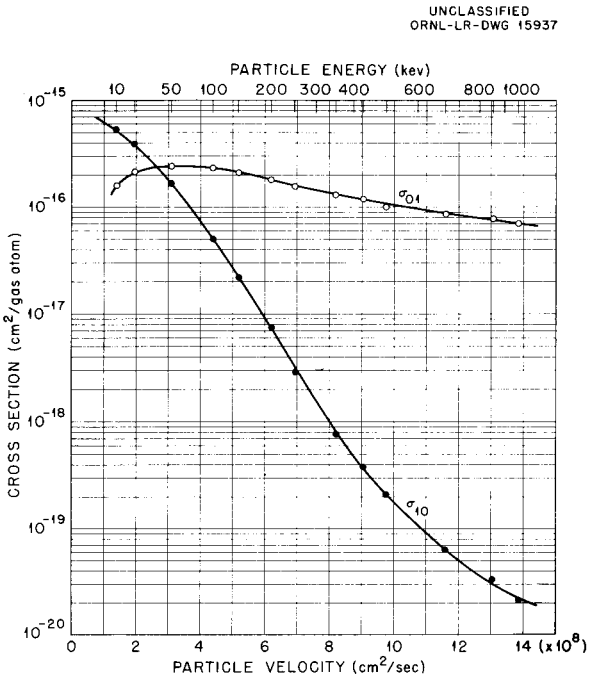

Fig. 4. Charge Transfer Cross Section per Atom of Gas Traversed as a Function of Particle Velocity and Energy. Hydrogen atoms and ions in nitrogen gas.

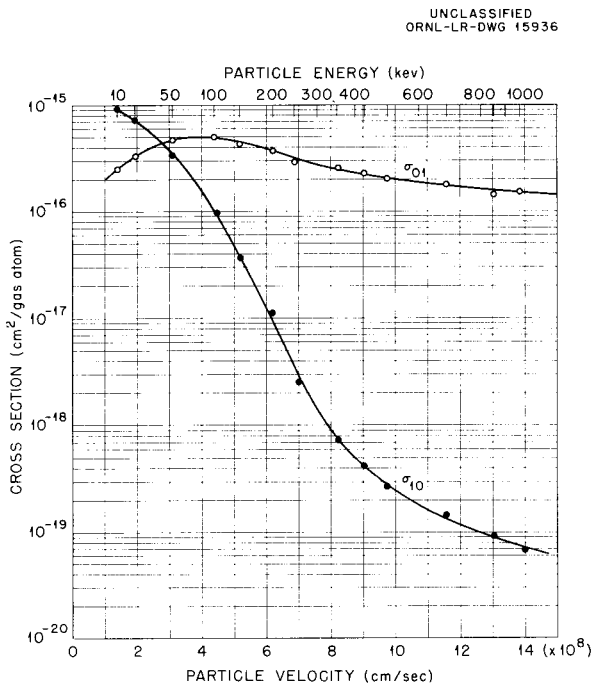

Fig. 5. Charge Transfer Cross Section per Atom of Gas Traversed as a Function of Particle Velocity and Energy. Hydrogen atoms and ions in argon gas.

The capture cross sections reported are the computed cross sections for the transition to the ground state only. If transitions to excited states are considered, then the cross section will be larger. The value of the theoretical electron-capture cross section deviates from the experimental points at higher energies. It had been expected from theoretical predictions that the calculated cross sections should agree closely to the measured values at the higher energies. On the other hand, the theoretical electron-loss cross sections of Dalgarno and Griffing[3] agree with the present experimental values to within 10% throughout the energy range.

At the present time the theoretical calculations for cross sections of hydrogen atoms and ions in gases heavier than hydrogen are not satisfactory. This arises from the strong dependence of the cross sections on the effective charge of the target atom. Therefore we cannot adequately compare the predicted values with the present measurements.

For the case of argon it is to be noted that the slope of the capture cross section is rapidly decreasing in the energy range 300 kev to 1 Mev. In contrast, the electron-loss cross sections decrease less than an order of magnitude throughout the high energy range.

MOLECULAR BREAKUP FOLLOWING BETA DECAY OF TRITIUM HYDRIDE

A. H. Snell F. Pleasonton H. E. Leming[1]

When the HT molecule undergoes beta decay, the tritium atom turns into He^3, and two possible courses appear to be open:

1. The nuclear charge change shakes off one of the electrons, leaving $(HHe^3)^{++}$, which should certainly break up, either into $(He^3)^{++}$ and H, or into $(He^3)^+$ and H^+ within about one vibration time of the molecule, namely, 10^{-12} sec. This shake-off process is well known theoretically and experimentally for atoms, where for the K shell the probability of occurrence is $0.3/Z^2_{eff}$, so that for an isolated tritium atom the process should be frequent. Little is known about how the probability will be modified in molecular combination; Schwartz[2] and Cantwell[3] have given the matter theoretical consideration, in particular, for HT, but no experimental information heretofore has existed for any molecule.

2. The nuclear charge change fails to shake off an electron. The immediate product is then $(He^3H)^+$, which has been observed in mass spectrometry to be stable[4] and for which several theoretical treatments[5-8] have indicated a dissociation energy ranging from 0.6 to 2.1 ev relative to He and H^+ (the most recent estimate[8] lying between 1.75 and 2.05 ev) and 3.6 ev relative to He^+ and H (refs 6, 9). The recoil of the He^3 atom from the beta-neutrino emission has a maximum (and most common) value of 3.3 ev, and this will produce molecular vibration, rotation, and center-of-mass motion.

Our apparatus is adapted to investigation of the HT breakup by magnetic analysis of the fragments. An H-T sample of rather uncertain composition, but containing somewhat more than 50% of T, was prepared and allowed to equilibrate as to molecular composition under the action of its own beta radiation. When it was introduced into the analyzer, the following e/m peaks were observed with the indicated relative intensities:

e/m	Ion	Measured Relative Intensity
1	H^+	0.0064
1/2	H_2^+	0.0023
1/3	T^+, $(He^3)^+$ (unresolved)	0.058
2/3	$(He^3)^{++}$	0.0014
1/4	$(He^3H)^+$	0.408
1/6	$(He^3T)^+$	0.523

First, we must analyze these results to obtain the composition of the gas. Suppose that the concentration of the H_2 molecules in the source volume is designated by $[H_2]$, that of the T_2 molecules by $[T_2]$, and that of the TH molecules by [TH]. Then

$$[H_2] + [T_2] + [TH] = 1 \quad . \tag{1}$$

Now we assume that the breakup of $(He^3T)^+$ and the breakup of $(He^3H)^+$ are equally probable as the gas undergoes beta decay, and we neglect the small amount of secondary ionization caused by the beta particles, as exemplified by the intensity of the mass 2 peak. Under these assumptions the relative intensities of the mass 6 and mass 4 peaks give the relative concentrations of T_2 and TH:

$$\frac{[T_2]}{[TH]} = \frac{0.523}{0.408 \times 2} \quad , \tag{2}$$

where the factor 2 allows for the fact that T_2 is twice as likely to undergo radioactive decay as is TH.

Finally, we assume that the equilibrium constant of Dorfman and Mattraw[10] holds in the storage vessel and that this equilibrium has not been disturbed as the gas entered the spectrometer source volume through an adjustable leak. This gives

$$\frac{[TH]^2}{[H_2]\,[T_2]} = 2.87 \quad . \tag{3}$$

[1] Summer employee from the University of Arkansas.

[2] H. M. Schwartz, *J. Chem. Phys.* **21**, 45 (1953).

[3] M. Cantwell, *Phys. Rev.* **101**, 1747 (1956).

[4] K. T. Bainbridge, *Phys. Rev.* **44**, 59 (1933).

[5] J. Y. Beach, *J. Chem. Phys.* **4**, 353 (1936).

[6] C. A. Coulson and W. E. Duncanson, *Proc. Roy. Soc. (London)* **A165**, 90 (1938).

[7] S. Toh, *Proc. Phys. Math. Soc. Japan* **22**, 119 (1940).

[8] A. A. Evett, *J. Chem. Phys.* **24**, 150 (1956).

[9] G. Gloekler, D. L. Fuller, and C. P. Roe, *J. Chem. Phys.* **1**, 886 (1933).

[10] L. M. Dorfman and H. C. Mattraw, *J. Phys. Chem.* **57**, 723 (1953).

Solution of Eqs. 1, 2, and 3 then gives the composition of the gas: $[HT] = 0.46$, $[T_2] = 0.29$, $[H_2] = 0.25$.

With this knowledge of the composition, the main features of the breakup can be appreciated. The probability that the $(He^3H)^+$ ion will hold together is high, and, when there is dissociation, the chances favor the formation of $(He^3)^+$ as against that of H^+; that is, the electrons prefer to go one with the helium nucleus and one with the hydrogen nucleus.

For closer analysis we note first of all that the presence of the H_2^+ peak indicates a small amount of ionization of the gas by the beta particles; this must be contributing slightly to the mass 4 peak (HT) and to the mass 6 peak (T_2). Assuming that the cross sections for impact ionization are the same for H_2, HT, and T_2, we weight the numbers of impacts according to the concentrations of H_2, HT, and T_2, and subtract the impact ionization from the HT and T_2 intensities, which yields, for the decay ionization alone,

Ion	Relative Decay Intensities
$(He^3H)^+$	0.404
$(He^3T)^+$	0.519

Now let us assume a probability P that the molecule dissociates, with or without electron shake-off, as the result of the beta decay. Since all decays lead to ionized fragments,

$$(4)\quad P_{HT} = \frac{(\text{fragments})}{(\text{fragments}) + (He^3H)^+} = \frac{(H)^+ + (He^3)^+_{HT} + (He^3)^{++}_{HT}}{(H)^+ + (He^3)^+_{HT} + (He^3)^{++}_{HT} + (He^3H)^+},$$

where the bracketed symbols refer to the relative counting rates and where $(He^3)^+_{HT}$ refers to that fraction of the $(He^3)^+$ ions that results from HT decay, as opposed to the fraction $(He^3)^+_{TT}$ that results from T_2 decay. In evaluating P_{HT}, the numbers for H^+ and for $(He^3H)^+$ can be written in directly from above. To evaluate $(He^3)^+_{HT}$, we note that

$$(5)\quad (He^3)^+_{HT} + (He^3)^+_{TT} + (T)^+ = 0.058 \quad ,$$

and we again assume that the HT and T_2 molecules dissociate equivalently; that is, we neglect the difference in the vibration level structures of the two kinds of molecule. Under this assumption

$$(6)\quad \begin{aligned} (T)^+ &= (H)^+ \frac{(He^3T)^+}{(He^3H)^+} = 0.0064\left(\frac{0.519}{0.404}\right), \\ (He^3)^+_{TT} &= (He^3)^+_{HT}\,\frac{0.519}{0.404}\ ; \end{aligned}$$

hence $T = 0.0082$, $(He^3)^+_{HT} = 0.022$, and $(He^3)^+_{TT} = 0.028$.

Under equivalent assumptions,

$$(7)\quad \begin{aligned} (He^3)^{++}_{HT} + (He^3)^{++}_{TT} &= 0.0014 \quad , \\ (He^3)^{++}_{TT} &= (He^3)^{++}_{HT}\left(\frac{0.519}{0.404}\right)\ ; \end{aligned}$$

hence $(He^3)^{++}_{HT} = 0.00062$, and $(He^3)^{++}_{TT} = 0.00078$.

We now have all the numbers needed to evaluate P_{HT}, and the result is

$$(8)\quad P_{HT} = 0.067 \ .$$

Thus 6.7% of the HT molecules dissociate under beta decay, and 93.3% remain bound as the $(He^3H)^+$ ion. This immediately sets an upper limit of 6.7% to the extent of the electron shake-off, but this limit can be restricted much further. The shake-off dissociation process would have the alternate courses

$$(9)\quad (HT) \begin{cases} \nearrow (He^3)^{++} + H + \beta + e \ , \\ \searrow (He^3)^+ + H^+ + \beta + e \ , \end{cases}$$

of which the former is measured by the intensity of $(He^3)^{++}$ to occur in only 0.14% of the decays, and the latter by the intensity of H^+ to occur at most in 1.5% of the decays. Thus the upper limit of shake-off is 1.6%. The remaining 5.1% of the dissociations would result from vibration, and all would go by the process

$$(10)\quad HT \longrightarrow (He^3)^+ + H + \beta \ .$$

On the other hand, if there were no electron shake-off at all, the courses of dissociation would be

$$(11)\quad HT \begin{cases} \nearrow (He^3)^{++} + H^- + \beta, \text{ intensity } 0.14\% \ , \\ \rightarrow (He^3) + H^+ + \beta, \text{ intensity } 1.5\% \ , \\ \searrow (He^3)^+ + H + \beta, \text{ intensity } 5.1\% \ . \end{cases}$$

The balance between the two extremes, that is, the actual extent of shake-off, could in principle be determined by comparing the intensity of H^- with that of $(He^3)^{++}$, but we did not attempt to look for the H^- because the reversed polarities lead to an awkward situation with regard to the voltages applied to our detector, an electron multiplier.

The preference of the $(He^3)^+$ dissociation branch over that of H^+ is surprising on the basis of atomic ionization potentials, for the former requires 24.46 − 13.53 = 10.93 ev more energy. As noted previously, it is expected to require also a greater energy (by 1.6 ev) for molecular dissociation.

The foregoing results and analysis depend upon two main assumptions, both of which are being given further consideration and study. The first is the equivalence assumed between the HT and T_2 breakup mechanisms, in the face of the difference in the inertial state of affairs, when the He^3 recoils relative to a mass 1 partner in one case and a mass 3 partner in the other. The second assumption is that all particles are equally efficiently collected into the magnetic analyzer, despite the fact that the kinetic energies will vary with the mode of breakup. One can see qualitatively the effect of failure of this assumption. The highest energy recoils (3.3 ev) will be the He^3's that are unbound because of electron shake-off. These will be least efficiently collected, and therefore the measured extent of shake-off may be too low. In the vibrational breakup, on the other hand, the $(He^3H)^+$ ion will recoil as a whole with an energy of 2.4 ev, but fragments will have less kinetic energy because a large part of the initial energy of recoil must be used for dissociation. Therefore the measured intensity of $(He^3H)^+$ may also be too low relative to the intensity of the fragments.

This was a one-shot experiment, and hindsight shows some respects in which it could have been improved. A repeated experiment using dilute T in H, and with the extension to DT and pure TT gases has much appeal. However, the contamination produced in the apparatus was so severe that the work will not be undertaken lightly.

NEUTRON DIFFRACTION BY RARE-EARTH COMPOUNDS

W. C. Koehler
E. O. Wollan
M. K. Wilkinson
J. W. Cable

In a previous publication the paramagnetic scattering of rare-earth sesquioxides[1] at temperatures above 20.4°K has been reported. Recently the study of rare-earth sesquioxides has been extended to lower temperatures, and evidence has been obtained for antiferromagnetic ordering transitions in the liquid-helium temperature region. Our previous studies of perovskite-like compounds[2] have been extended to the rare-earth orthoferrites $AFeO_3$, in which both the rare-earth and iron ions are magnetically active. We discuss here preliminary results for $ErFeO_3$ and Er_2O_3.

ERBIUM ORTHOFERRITE

Erbium orthoferrite is one of a large class of compounds which crystallizes in the orthorhombic $GdFeO_3$ modification[3] of the perovskite structure. In the ideal ABO_3 structure the A- and B-site cations form simple cubic lattices, and, ideally, each B-site ion is surrounded by an octahedral array of oxygen ions. In a large number of compounds in which the B-site ions are magnetically active, magnetic ordering transitions have been observed at relatively high temperatures.

In an earlier paper a neutron-diffraction investigation of the series of perovskite-type mixed oxides $(La,Ca)(Mn^{3+},Mn^{4+})O_3$ was reported[2] in which ferromagnetic and antiferromagnetic configurations were found which depended upon the relative concentrations of trivalent and tetravalent manganese. Four simple structure types, among others, were found, and these will be described briefly because of their pertinence to the present report.

[1] W. C. Koehler and E. O. Wollan, *Phys. Rev.* 92, 1380 (1953).

[2] E. O. Wollan and W. C. Koehler, *Phys. Rev.* 100, 545 (1955).

[3] S. Geller, *J. Chem. Phys.* 24, 1236 (1956).

The structure types are all discussed for convenience relative to a cubic magnetic cell of edge twice that of the ideal (cubic) chemical cell, although smaller cells can be chosen. The type *A* configuration may be considered to be formed of ferromagnetic sheets with the spin direction changing sign from layer to layer. In this arrangement each ion has four ferromagnetic and two antiferromagnetic nearest neighbors. The type *B* configuration is truly ferromagnetic: all spins have the same direction. For the *C*-type structure each ion has two ferromagnetic and four antiferromagnetic nearest neighbors, and the structure may be considered as chains of like spins, each of which is surrounded by four chains with opposite spin direction. Finally, in the *G*-type structure each ion has six antiferromagnetic nearest neighbors, and the structure may be envisaged as two interpenetrating face-centered cubic lattices on each of which the spins are parallel but have opposite spin orientations from each other. Each of these structure types gives rise to a characteristic set of absences in its neutron-diffraction pattern. For type *A*, only reflections which have one odd and two even indices are allowed. Similarly, for type *B*, all indices are even; for *C*, two odd and one even; for *G*, all odd. It is thus a matter of inspection to decide which of the above four magnetic structure types may be present.

Of the perovskite-type compounds which have hitherto been investigated,[4] only two magnetic structure types have been observed in those cases in which the B sites are occupied by a single ionic species: the type *A* antiferromagnetic structure for $LaMnO_3$ and the type *G* antiferromagnetic structure for $CaMnO_3$, $LaCrO_3$, and $LaFeO_3$. In each of the last three compounds the B-site ions very closely form a simple cubic lattice. There are, however, significant distortions from ideal locations of the A-site and oxygen ions.

The distortions in the rare-earth orthoferrites $AFeO_3$, among which we also include $LaFeO_3$, are now fairly well known as a result of the recent work of Geller,[3] Geller and Wood,[5] and Gilleo.[6] The iron ions remain, within the limits of detection by x-ray diffraction, on special positions in the orthorhombic cell, but the rare-earth ions and one set of oxygen ions are progressively less ideal as the atomic number of the rare-earth ion increases. Of the orthoferrites studied so far, $LaFeO_3$ is the least distorted and $ErFeO_3$ is the most distorted. Although the erbium ions, say, in $ErFeO_3$ are approximately still on a simple cubic lattice, the deviations are important for an understanding of the neutron-diffraction experiments.

Neutron-diffraction data have been obtained for $ErFeO_3$ at temperatures ranging from 682°C to 1.25°K, and the results are conveniently described for the three intervals 682 to 360°C, 360°C to 4.2°K, and 4.2 to 1.25°K. In the high-temperature range the coherent reflections can be satisfactorily interpreted in terms of the $GdFeO_3$ modification of the perovskite structure, although it must be emphasized that the present resolution of our neutron data is not adequate for a definitive structure determination. The background scattering is that characteristic of a paramagnetic substance. In this case the paramagnetic scattering cross section is quite large because of the high magnetic moment of trivalent erbium.

Below about 360°C new coherent reflections appear in the pattern at positions corresponding to the cubic cell indices which are all odd, and simultaneously there is a characteristic drop in the background scattering level. With decreasing temperature the intensities of these reflections increase until at 77°K they are apparently temperature-saturated. The magnitudes and angular positions of these new reflections are characteristic of a *G*-type ordering of the iron ions. The erbium ions are, however, still randomly oriented, as evidenced by the very sizable paramagnetic scattering background. These observations are illustrated in Fig. 1, in which are shown portions of the diffraction patterns which were obtained at room temperature and at 682°C. The transition temperature for the ordering of the iron ions was measured by following the intensity of the (111) magnetic reflection as a function of temperature, and it was found to be 360°C.

At liquid-helium temperatures some additional phenomena were observed from which one infers the onset of magnetic ordering in the erbium ion lattice. In Fig. 2 are shown portions of diffraction patterns for $ErFeO_3$ at room temperature, at 4.2°K, and at 1.5°K. One notes from these patterns that new reflections have developed at the lower temperatures which are characteristic

[4] W. C. Koehler and E. O. Wollan, *Phys. Semiann. Prog. Rep. Sept. 10, 1954*, ORNL-1798, p 41.

[5] S. Geller and E. Wood, *Acta Cryst.* (to be published).

[6] M. A. Gilleo, *Acta Cryst.* (to be published).

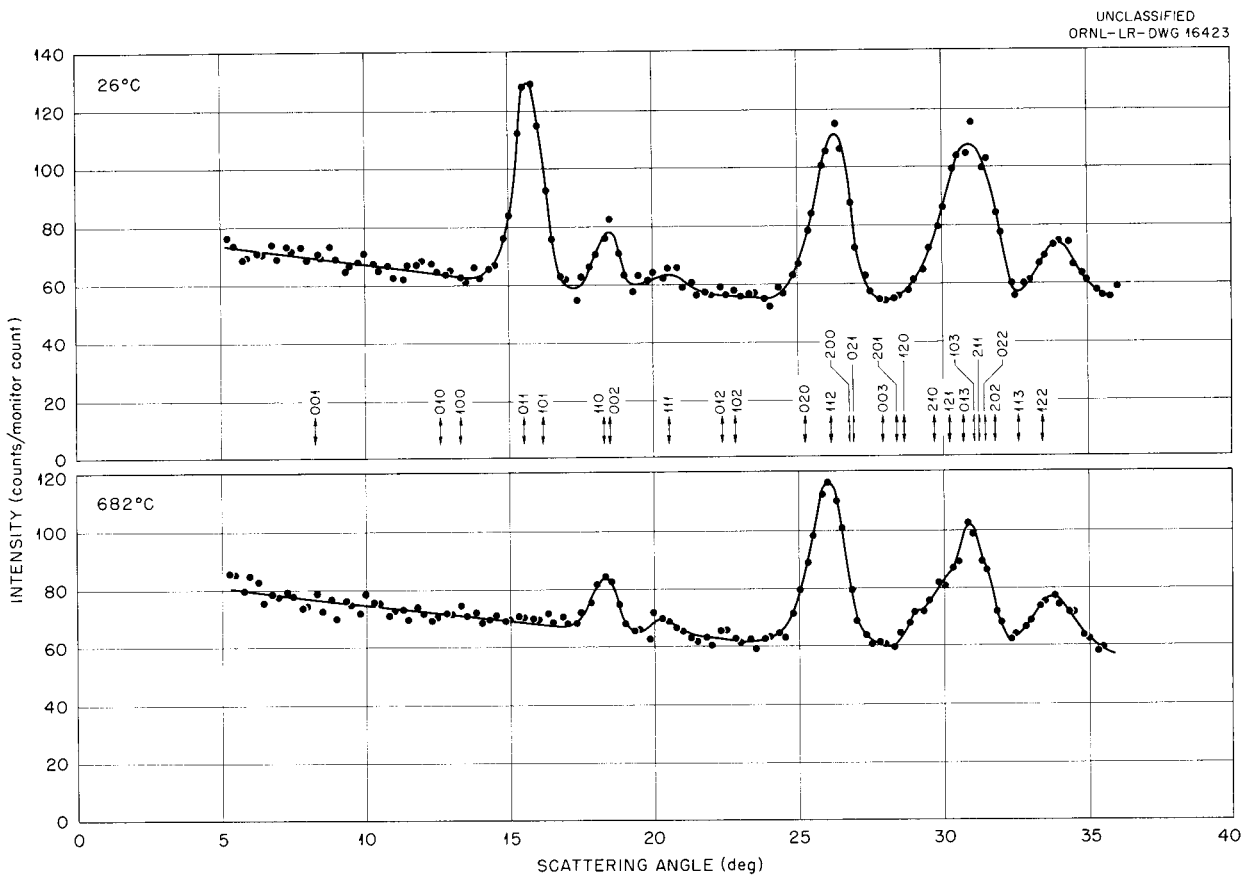

Fig. 1. Neutron-Diffraction Patterns of $ErFeO_3$. The room-temperature and high-temperature patterns illustrate the development of magnetic ordering in the iron sublattice.

of a *C*-type antiferromagnetic arrangement. The magnitudes of the new reflections are such that they can be due only to erbium ion ordering, and this inference is further substantiated by the decrease, at these low temperatures, of the diffuse scattering. The relative intensities of the new reflections suggest that the erbium ion moments must have at least a large component in the direction of the unique (ferromagnetic) direction of the *C*-type configuration.

However, in addition to these strong intensities at new positions, a growth in intensity of the (111) reflection can be observed which is attributed to the magnetic scattering from the ordered erbium ion system for the following reasons:

1. The iron ion spin system is temperature-saturated at much higher temperatures and is already scattering as much as it can into the (111) reflection.

2. The temperature dependence of the (111) reflection below 4.2°K is similar to that of the (110), which must be due to the erbium ion moments.

3. Crystallographic transformations between 4.2 and 1.5°K are improbable.

4. The absolute intensities of the new magnetic reflections appear to be too small when compared with those expected for an ideal *C*-type arrangement in which the erbium ion moments have their maximum value of 9.0 Bohr magnetons.

An unambiguous interpretation of these results has not yet been achieved and, indeed, may not be possible from powder diffraction data alone. Nevertheless, some qualitative inferences may be made at this time.

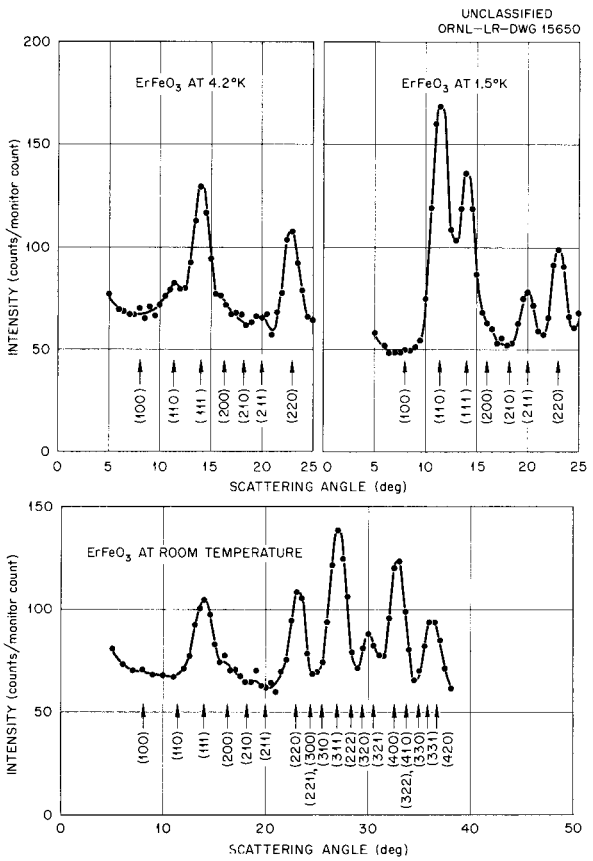

Fig. 2. Neutron-Diffraction Patterns of $ErFeO_3$. The low-temperature patterns demonstrate the ordering of the erbium ions.

It is known that the erbium ion positions in erbium orthoferrite are at least as badly distorted from ideal as Gd^{+++} in $GdFeO_3$, for which the parameters have been measured.[3] If one assumes these parameters to be applicable to $ErFeO_3$, then the erbium ion moments will indeed contribute to the (111) reflection, and the (110) reflection will be reduced from what one would expect if there were no distortion. The extent of this contribution will depend also upon the relative orientations of the directions of magnetization of the iron and erbium sublattices. It is possible, in addition, that the erbium ion sublattice itself does not have a single axis of magnetization, in which case, even for an undistorted crystal, a (111) contribution could be obtained.

The neutron data at the present time cannot rule out the possibility of more than one magnetization direction, and there is good reason to believe that this system is indeed complex. The low transition temperature, 4.5°K, for the erbium ion moment system is not too high for dipole-dipole interactions among the erbium ions to be appreciable, and the approximate *C*-type arrangement which they take is a highly probable one for magnetic dipole arrays.[7] As a result of the erbium and oxygen parameters, the interactions of the iron ions among themselves and with the erbium ions will not be equivalent in the three cube-edge directions. Indeed, Gilleo[8] has observed complicated anisotropy of the magnetic susceptibility and parasitic magnetization in single-crystal $GdFeO_3$ at 77°K and above, including a rotation of the direction of magnetization of the iron ion lattice. We observe, too, that if exchange forces play a role in the ordering of the erbium ions these also will probably be anisotropic. Finally, the not-negligible parasitic ferromagnetization[9] of $ErFeO_3$ at 1.3°K suggests uncompensated antiferromagnetism. One mechanism by which such uncompensation can be produced is the existence of angles between magnetization directions.

ERBIUM SESQUIOXIDE

Erbium sesquioxide, Er_2O_3, has the body-centered cubic bixbyite structure. To a first approximation, however, the metal ions can be considered to be on a face-centered cubic lattice, and the structure to be intermediate between the face-centered cubic fluorite and sphalerite structures.

Antiferromagnetic ordering of transition element ions on face-centered cubic lattices has been described for rock-salt-type oxides, for example, MnO (ref 10) and for the sphalerite modification of MnS (ref 11). Neutron-diffraction data for Er_2O_3 at low temperatures show evidence for antiferromagnetic ordering in the bixbyite structure.

At temperatures above 20.4°K the neutron-diffraction data for Er_2O_3 are characteristic of a paramagnetic substance. Below about 5°K, however, there are observed strong coherent magnetic

[7] J. M. Luttinger and L. Tisza, *Phys. Rev.* **70**, 954 (1946).

[8] M. A. Gilleo, *J. Chem. Phys.* **24**, 1239 (1956).

[9] R. Bozorth, private communication.

[10] C. G. Shull, W. A. Strauser, and E. O. Wollan, *Phys. Rev.* **83**, 333 (1951).

[11] L. M. Corliss, J. M. Hastings, and N. Elliott, *Bull. Am. Phys. Soc.* 1(II), 190 (1956).

reflections caused by ordering of the erbium ion moments. In Fig. 3 are shown portions of difference patterns for Er_2O_3 between room temperature and 4.2°K and between room temperature and 1.5°K. In these difference patterns the nuclear contributions to the pattern have been essentially subtracted out. At 4.2°K there is observed a broad maximum, characteristic of short-range magnetic ordering, which, as the temperature is reduced, develops into a series of sharp, coherent, magnetic reflections. As in the previously discussed $ErFeO_3$ case, the data have not yet yielded to an unambiguous interpretation, but again some striking qualitative observations can be made.

One notes certain regularities in the indices of the observed magnetic reflections. Only reflections with one even and two odd indices are present, and one recalls that this is the same condition which was required for a *C*-type structure in the simple cubic lattice of erbium ions in $ErFeO_3$. In the course of analyzing these data some interesting general conclusions for antiferromagnetic ordering on face-centered cubic lattices were reached.

A face-centered cubic lattice may be considered to be subdivided into four interpenetrating simple cubic lattices, and this subdivision is illustrated in Fig. 4. The simplest type of antiferromagnetic ordering which one might consider would be one in which two of the sublattices have their spins parallel, while the other two are antiparallel. Such an arrangement has been classified by Van Vleck[12] as ordering of the first kind. In this arrangement two-thirds of the nearest neighbors of a given ion have antiparallel spin, and there is no net correlation among next nearest neighbors. Anderson[13] noted that this situation could be improved by an ordering arrangement which has become known as improved ordering of the first kind, in which the same relationships among nearest neighbors remain, but now one-third of the next nearest neighbors are also antiparallel. Anderson also noted that for very strong second nearest neighbor interactions a third structure, called ordering of the second kind, was favored in which all the next nearest neighbors of a given ion are antiparallel, but there is no net correlation among nearest neighbors. Now, we noticed that ordering of the first kind could be obtained if *B*-type lattices were properly assigned to the four sublattices, improved

[12] J. H. Van Vleck, *J. phys. radium* **12**, 262 (1951).

[13] P. W. Anderson, *Phys. Rev.* **79**, 350 (1950); P. W. Anderson, *Phys. Rev.* **79**, 705 (1950).

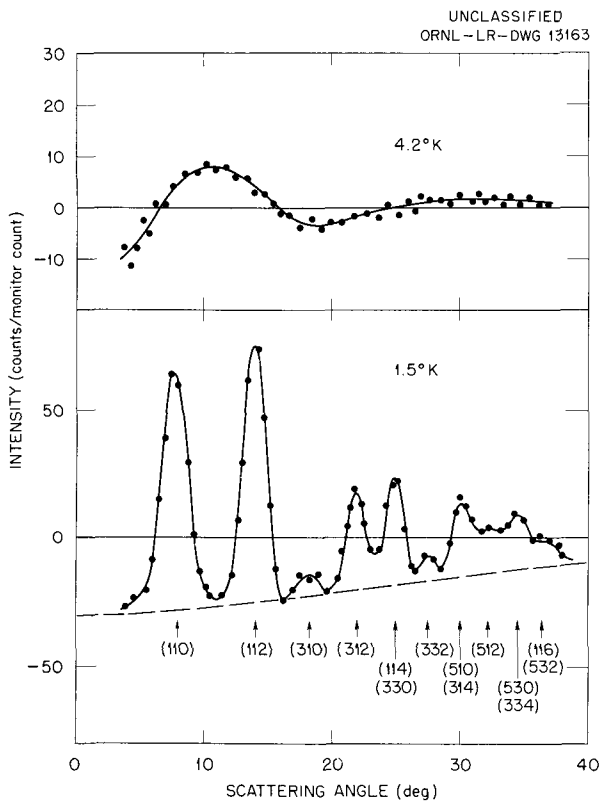

Fig. 3. Neutron-Diffraction Patterns of Er_2O_3.

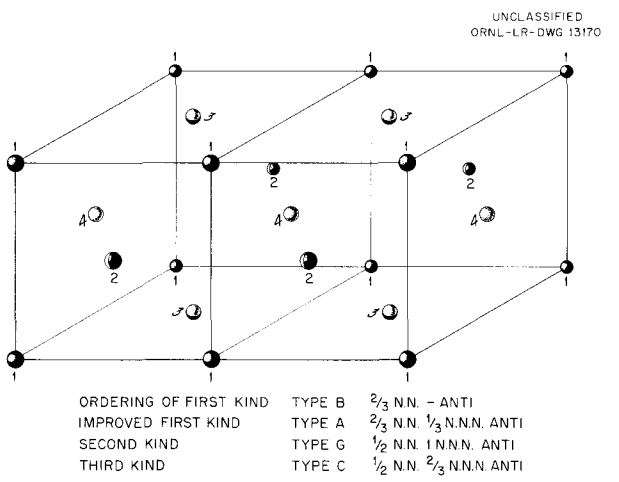

Fig. 4. Possible Ordering Arrangements on a Face-centered Cubic Lattice.

ordering of the first kind if each sublattice was type *A*, and ordering of the second kind if each sublattice was type *G*. It was natural, then, to inquire as to the configuration which results when *C*-type lattices are used. An ordering of the third kind is obtained in which only two-thirds of the next nearest neighbors are antiparallel, and again there is no net correlation among nearest neighbors.

One of the interesting properties of the simple cubic lattice types *A*, *B*, *C*, and *G* is that every ion in these structures has the same number of parallel and antiparallel first, second, ... , *n*th nearest neighbors as any other ion. This property is also carried over to the face-centered cubic case when the four sublattices, types *A*, *B*, *C*, and *G*, are properly oriented. Again for these cases there are special requirements on the indices of the observed magnetic reflections, and these are identical to those described above for $ErFeO_3$. Thus it appears that the magnetic structure of Er_2O_3 is approximately one in which the four sublattices are type *C*.

There are a large number of detailed magnetic structures which fall within the above restriction, and the analysis is complicated by the following effects, which are similar to those described above: (1) the structure is not really face-centered cubic, and the ions are distorted from ideal positions; (2) there are at least four interacting sublattices, all of which may not have the same magnetization directions.

We observe also that the transition temperatures of Er_2O_3 and $ErFeO_3$ are very close, in spite of the very much different structures of the two systems, and that the same type of configuration favored by dipole-dipole interactions is observed in the two systems. Finally, it has been shown[14] that the *C* sublattice model is not energetically stable for isotropic interactions.

We wish to express our appreciation to H. R. Child for his assistance with the collection and processing of the neutron-diffraction data.

[14]H. A. Gersch, private communication.

METHOD FOR SINGLE-CRYSTAL MAGNETIC NEUTRON-DIFFRACTION STUDIES AT LOW TEMPERATURES

E. O. Wollan
W. C. Koehler
M. K. Wilkinson
J. W. Cable

Up to the present time the magnetic neutron-diffraction studies carried out in the region of liquid-helium temperatures have involved the use of powder-crystal techniques only. For elements or compounds which develop complicated antiferromagnetic structures the information obtained by the powder technique may be insufficient to permit a determination of the magnetic structure. A number of substances which have been studied at the Laboratory fall in this category. In the case of the rare-earth metals erbium and neodymium and the compounds $MnBr_2$ and $MnCl_2$, it has not been possible to determine the antiferromagnetic structures from the powder data. For this reason the low-temperature cryostat associated with the neutron spectrometer has been modified to permit studies with single crystals. In the case of $MnBr_2$ and $MnCl_2$, the Neel temperatures are 2.16 and ~1.9°K (see the following section), so it is necessary to operate the cryostat at pumped-helium temperatures.

The design of the single-crystal goniometer which has been installed in the cryostat system is shown in Fig. 1. This drawing represents the inner helium-containing chamber of the cryostat, which is located on the center of the crystal table of the spectrometer, and, as previously described,[1] there is also associated with the spectrometer a magnet which allows a magnetic field of up to about 17 kilogauss to be applied to the sample. The lower part of the inner chamber represented in Fig. 1 consists of a thin-walled aluminum unit sealed to the brass can of the main helium container by metal-to-metal contact maintained by the flange shown. Within this aluminum shell is located the goniometer, which consists of a longitudinal section of aluminum rod which can be turned about a vertical axis by a thin-walled tube

[1]E. O. Wollan and W. C. Koehler, *Phys. Semiann. Prog. Rep. Sept. 10, 1954*, ORNL-1798, p 45.

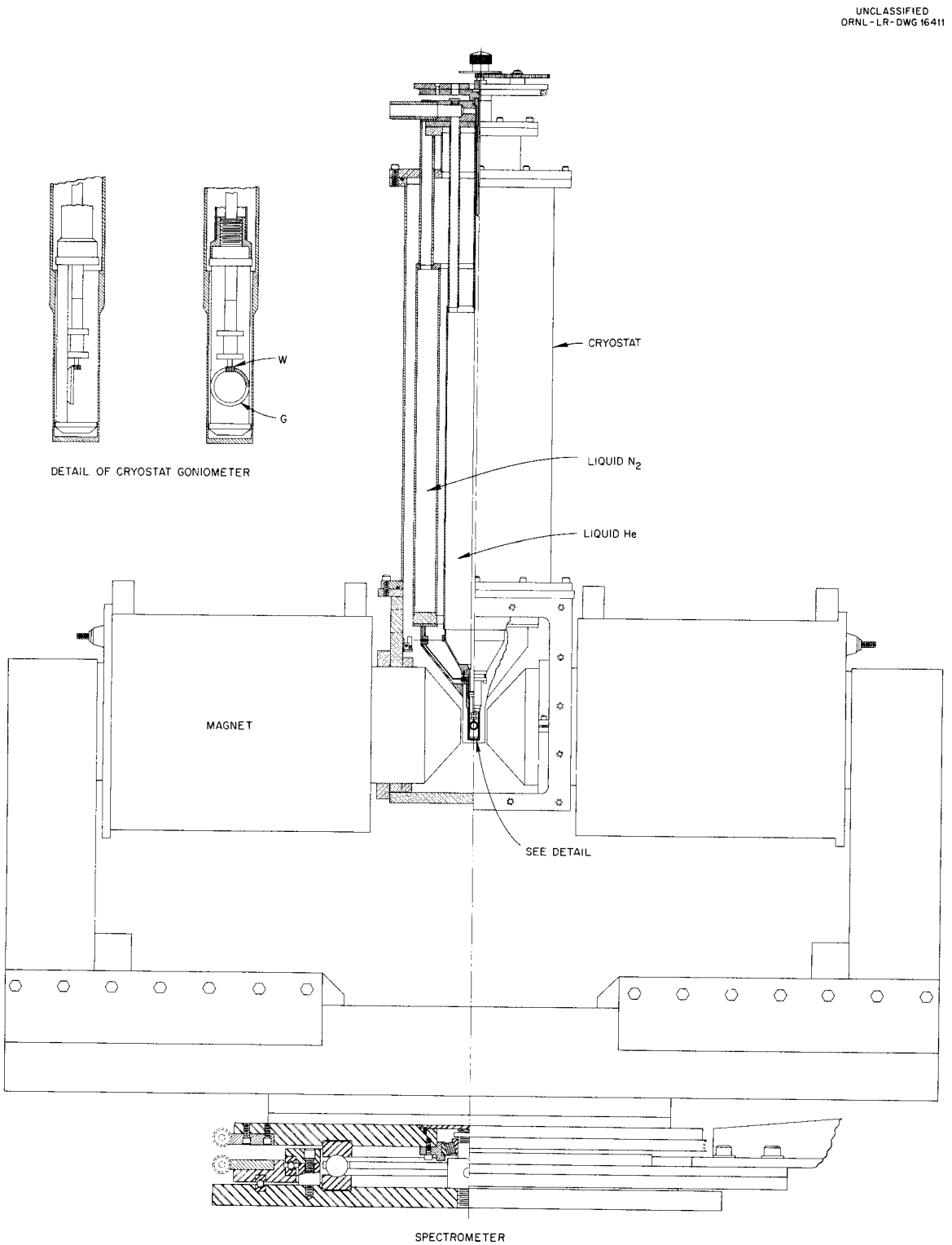

Fig. 1. Neutron-Diffraction Spectrometer with Magnet, Cryostat, and Single-Crystal Goniometer.

which passes up through the helium container and out of the top of the cryostat through an O-ring seal to a graduated circle driven by a worm and worm gear. Concentric with this tube is a smaller inner tube also sealed at the top with an O-ring. This tube is attached at the top to another but smaller graduated circle and at the bottom to a small spur gear G, which drives the small ($\frac{3}{8}$-in.-dia) gear wheel W about an axis perpendicular to the wheel. The single crystal to be studied is cemented to the center of the gear wheel, and, since the above-described driving mechanism allows rotation of the crystal about two perpendicular axes, any set of planes in the crystal can be oriented into a position for Bragg reflection of the incident neutron beam. A hexagonal type of crystal is most conveniently mounted, with the c axis perpendicular to the gear wheel. Planes (hkl) with sixfold symmetry are then successively brought into positions to reflect by one turn of the upper dial, which in this equipment is made to turn the gear wheel 60 deg about the horizontal axis.

Single-crystal studies are now being made on $MnBr_2$ and $MnCl_2$, but the magnetic structures have not yet been determined. The $MnBr_2$ was thought to order in a magnetic layer structure, with the spins oppositely directed in adjacent hexagonal layers, because of the presence of a strong magnetic reflection in the powder pattern at $2\theta \cong 5$ deg, which could be indexed as (00l). The single-crystal studies, however, showed no magnetic intensity for these planes and showed the reflection in question to be of an (hkl) type.

With the present spectrometer, which is equipped with goniometer, cryostat, and associated magnetic field equipment, the effects of magnetic fields on individual single-crystal reflections are being studied at sample temperatures down to about 1.4°K.

ANTIFERROMAGNETISM IN $MnCl_2$

M. K. Wilkinson
J. W. Cable
E. O. Wollan
W. C. Koehler

Recent experimental investigations at this Laboratory of the cryomagnetic properties of anhydrous $MnCl_2$ have shown that both specific heat[1] and magnetic susceptibility[2] exhibit unusual behaviors at low temperatures. Specific-heat measurements show two sharp λ-type anomalies at 1.81 and 1.96°K, while the polycrystalline magnetic susceptibility passed through a plateau between 2 and 1.5°K and was rising again at 1.1°K, which was the lowest temperature obtained during the measurements. These results have been interpreted as an indication that there is a double transition in the electron-spin system of the divalent manganese ions and that both transitions involve antiferromagnetic ordering. Presumably, the specific-heat maximum at 1.96°K would represent a transition from the paramagnetic state to a first type of antiferromagnetic ordering, while the maximum at 1.81°K would result from a reorientation to a second type of antiferromagnetic structure.

Preliminary neutron-diffraction experiments[3] were performed on both polycrystalline and single-crystal samples at temperatures in the vicinity of the specific-heat anomalies. There was a definite indication of an antiferromagnetic transition in this temperature region, but the experimental conditions did not permit a complete investigation of the structure or a detailed study of the two possible transitions. It is unlikely that the sample temperatures obtained were much lower than the transition points, and there was no goniometer available to allow proper single-crystal studies at low temperatures.

Since these preliminary measurements, techniques have been improved so that powdered samples can be investigated at temperatures down to about 1.2°K, and a goniometer has been designed and constructed[4] for single-crystal measurements at temperatures down to 1.4°K. Both

[1] R. B. Murray, *Phys. Rev.* 100, 1071 (1955).

[2] R. B. Murray and L. D. Roberts, *Phys. Rev.* 100, 1067 (1955).

[3] M. K. Wilkinson, R. B. Murray, and C. G. Shull, *Phys. Semiann. Prog. Rep. March 20, 1955*, ORNL-1879, p 27.

[4] M. K. Wilkinson, J. W. Cable, E. O. Wollan, and W. C. Koehler (preceding paper).

methods have been used in the present investigations on new samples of $MnCl_2$, and both show definite antiferromagnetic reflections at the lowest temperatures. Although the powder patterns show strong magnetic reflections, the magnetic structure is sufficiently complex that it has been impossible to determine the structure from the small number of reflections which appeared.

The single-crystal measurements are now in progress, and, while the magnetic structure is still not known, these measurements confirm the specific-heat data, which indicate two transition temperatures. The intensities of some of the magnetic reflections have been studied as a function of temperature, and two Néel points are definitely indicated. Figure 1 shows the intensities of two of the reflections as the temperature was varied, and it is seen that these intensities follow partial Brillouin curves to two different transition temperatures. Furthermore, the temperatures of 1.83 and 1.98°K agree quite well with those found for the two λ-type anomalies in the specific-heat data. The neutron measurements were obtained for both increasing and decreasing temperatures, and, as shown by the open and closed points, they were quite reproducible. An interesting feature of the two transition curves is that the intensity of reflection 1 shows no anomaly at the temperature at which reflection 2 begins. This indicates that the scattering interaction which causes reflection 1 is unaffected by that causing reflection 2, which suggests that the two reflections originate from independent structures. In order to determine whether both reflections were of magnetic origin, the intensities were studied with the sample at 1.4°K as an external magnetic field was applied parallel to the scattering vector. The intensities of both reflections were found to be field-sensitive,

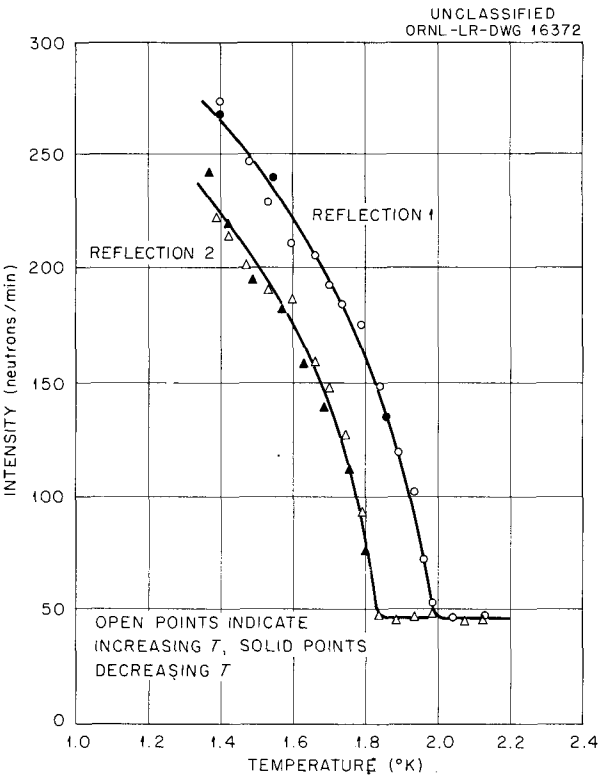

Fig. 1. Temperature Variation of Single-Crystal Antiferromagnetic Reflections from $MnCl_2$.

but they were not affected in the same manner. In an external field of 10 kilogauss, the intensity of reflection 1 had doubled its zero field value, while the intensity of reflection 2 was reduced to background. Until more is known about the antiferromagnetic structures, it is not possible to discuss these field effects except to state that they show that both reflections originate from magnetic structures.

MAGNETIC NEUTRON SCATTERING FROM $CoCl_2$ AND $FeCl_2$

M. K. Wilkinson J. W. Cable

Magnetic measurements made on anhydrous $CoCl_2$ and $FeCl_2$ by Starr, Bitter, and Kaufmann[1] have shown that these materials possess some rather unusual properties. The variation of the inverse susceptibilities with temperature exhibits a minimum in the same temperature region where specific-heat data[2] show λ-type anomalies: 24°K for $FeCl_2$ and 25°K for $CoCl_2$. These measurements therefore suggest that antiferromagnetic ordering of the atomic magnetic moments occurs in both materials at these temperatures. However, the paramagnetic Curie temperature, θ, obtained by applying the Curie-Weiss law, $\chi = C/(T - \theta)$, to measurements of the susceptibility at higher temperatures is positive. According to the Curie-Weiss law, the positive θ is indicative of ferromagnetic coupling between the atomic moments. Furthermore, measurements of the magnetization[1] below the indicated transition temperatures are inconsistent with the normal behavior of antiferromagnetic materials. For both compounds, magnetic fields of only about 20,000 oersteds are required to attain a large fraction of the saturation magnetizations, whereas the exchange field to be expected in antiferromagnetic materials with a Néel temperature near 25°K is over 100,000 oersteds.

Both $CoCl_2$ and $FeCl_2$ crystallize in the rhombohedral or pseudohexagonal structure characteristic of $CdCl_2$, so that they are actually hexagonal layer structures in which the layers of metal atoms are separated by two layers of chlorine atoms. To explain the magnetic measurements, suggestions have been given for several types of magnetic structures at low temperatures. In 1933 Landau[3] suggested that the compounds might have parallel coupling of the magnetic moments within each metal layer and that the adjacent moment layers would be aligned antiparallel. This model has not been completely accepted, however, and the most recent criticism was by Leech and Manuel,[4] who suggested that the materials actually represent two-dimensional ferromagnetism. Each metal layer would be a strong ferromagnetic domain, and there would be no interaction between layers.

As has been previously reported,[5] the neutron-diffraction data show that there is ordering of the atomic magnetic moments at low temperatures in the manner suggested by Landau. There is one important difference in the magnetic structures for the two compounds, however, since the direction in which the atomic moments are oriented is not the same. In $CoCl_2$ the moments are within or nearly within the layers, whereas in $FeCl_2$ the moments are oriented parallel to the c axis of the hexagonal unit cell.

After the magnetic structures were known, molecular-field calculations were made in an effort to explain the magnetic susceptibility measurements. These measurements are consistent with the structure obtained from neutron diffraction if the strength of the ferromagnetic interaction between atoms within a layer is considerably larger than that of the antiferromagnetic interactions between atoms in adjacent layers. Specifically, the ferromagnetic coupling should be about three times larger than the antiferromagnetic coupling. Since the relative strengths of the interactions can be determined from neutron scattering[6] at temperatures near the transition point by an examination of the diffuse scattering, it was of interest to obtain an experimental check on the molecular-field calculations. For a predominant ferromagnetic interaction, ferromagnetic short-range order would be present, which would enhance the small-angle scattering above the paramagnetic level. Conversely, for a predominant antiferromagnetic interaction, the intensity of small-angle scattering would be less than the paramagnetic value.

Both the incident and reflected neutron beams were severely collimated to allow investigations into the small-angle region, and the sample was enclosed in a flat aluminum cell. Scattering data

[1] C. Starr, F. Bitter, and A. R. Kaufmann, *Phys. Rev.* 58, 977 (1940).

[2] O. N. Trapeznikowa and L. V. Schubnikov, *Physik. Z. Sowjetunion* 7, 66 (1935); O. N. Trapeznikowa, L. V. Schubnikov, and G. Miliutin, *Physik. Z. Sowjetunion* 9, 237 (1936).

[3] L. Landau, *Physik. Z. Sowjetunion* 4, 675 (1933).

[4] J. W. Leech and A. J. Manuel, *Proc. Phys. Soc. (London)* 69B, 210 (1956); J. W. Leech and A. J. Manuel, *Proc. Phys. Soc. (London)* 69B, 220 (1956).

[5] M. K. Wilkinson and J. W. Cable, *Phys. Semiann. Prog. Rep. March 10, 1956*, ORNL-2076, p 44.

[6] M. Slotnick, *Phys. Rev.* 83, 1226 (1951).

at small angles were obtained as the sample temperature was varied near the Néel transition, and Fig. 1*a* shows the results from $FeCl_2$. The curves plotted in this figure represent the scattered intensity at the various indicated temperatures in excess of that at 4.2°K. Since it can be assumed that the magnetic lattice is ordered almost completely at 4.2°K, these curves represent the magnetic scattering resulting from the disruption of the long-range magnetic structure at the various temperatures. At 295°K the magnetic lattice is completely disordered, and the scattering is representative of that from a purely paramagnetic material. The absolute magnitude of this scattering, as shown by the cross-section scale at the right, agrees very well with that predicted for the magnetic moment of the Fe^{++} ion resulting only from its spin. Specifically, the magnetic scattering cross section in the forward direction on this type of plot should be 0.774 barn for ions with $S = 2$, whereas the experimental value is 0.73 barn. As the sample temperature was lowered, increased small-angle scattering was present at a sample temperature of 78°K, showing that ferromagnetic short-range order is present at temperatures well above the Néel transition. The intensity of the small-angle scattering increased as the sample temperature approached the transition point and reached a maximum in the vicinity of this temperature. This is more apparent in Fig. 1*b*, where the intensity at the 2-deg scattering angle in excess of that at the 16-deg scattering angle is plotted as a function of temperature.

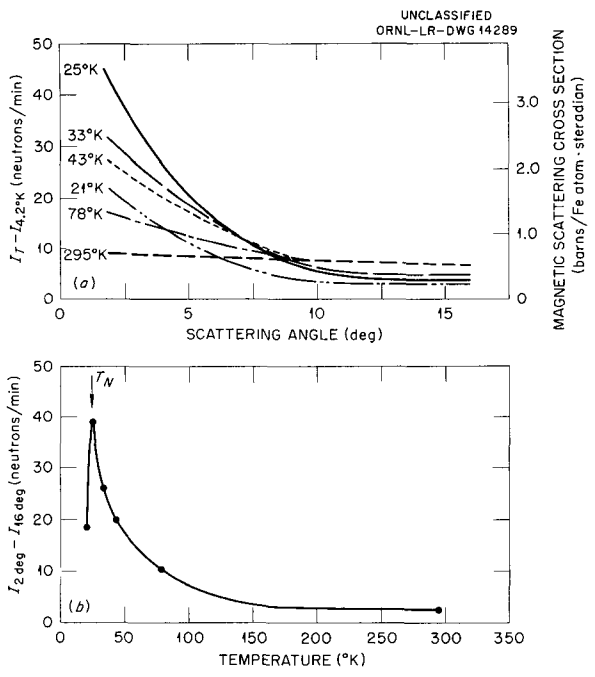

Fig. 1. (*a*) Small-Angle Scattering from $FeCl_2$. (*b*) Temperature Variation of the Small-Angle Scattering from $FeCl_2$.

A theoretical treatment of the neutron scattering from ferromagnetic materials near their Curie transitions has recently been given by Van Hove,[7] and the scattering has been termed critical magnetic scattering. This type of scattering has been observed[8] at small angles from iron near its Curie temperature and has been analyzed[9] according to the Van Hove treatment. For ferromagnetic materials, a maximum in the intensity of the small-angle scattering is expected at the Curie temperature, since the short-range correlations between atomic moments reach a maximum at this temperature. While the details of the analysis are probably different for $FeCl_2$ than for ferromagnetic materials, the maximum in the small-angle scattering at the Néel temperature is undoubtedly associated with a maximum in the range over which the short-range order exists. A rough value for the size of the regions of ferromagnetic short-range order can be determined by applying small-angle scattering theory to the angular distribution of the scattered intensity. This analysis indicates that at 25°K the regions in which the magnetic moments are clustered vary in size between 5 and 10 Å.

Similar small-angle scattering experiments were also performed on $CoCl_2$. While these experiments were somewhat more difficult to analyze because of large magnetic reflections which occurred at small angles below the Néel temperature, the small-angle diffuse scattering was also indicative of ferromagnetic short-range order.

The magnetic scattering of neutrons from $FeCl_2$ and $CoCl_2$ has therefore shown experimentally that the ferromagnetic interaction between atomic moments within a layer is larger than the antiferromagnetic interaction between atoms in adjacent layers. These measurements are consistent with

[7] L. Van Hove, *Phys. Rev.* **95**, 1374 (1954).

[8] M. K. Wilkinson and C. G. Shull, *Phys. Rev.* **103**, 516 (1956).

[9] H. A. Gersch, C. G. Shull, and M. K. Wilkinson, *Phys. Rev.* **103**, 525 (1956).

the magnetic susceptibility data, which show a positive θ. Of course, the weak antiferromagnetic coupling between layers may not be caused by exchange interactions but may be the result of dipole-dipole forces between layers. Since the antiferromagnetic interaction is weak, the magnetization data[1] can be explained by the assumption that an external magnetic field merely breaks down the interaction between layers and rotates the moments of each layer into the direction of the field. Such a rotation should easily be seen in the coherent scattering from the magnetic lattice. This experiment was attempted with the use of powdered samples in external fields up to about 15,000 oersteds, but the results were not conclusive, since the intensities of the magnetic reflections available were very small. It is planned to repeat these experiments with single-crystal specimens.

THE A-8 LINEAR AMPLIFIER

G. G. Kelley

The need for improved overload performance in linear amplifiers has become more and more pressing. More specifically, however, the acquisition of NaI scintillation crystals of the order of 100 lb and the construction of two 120-channel analyzers were responsible for the development of the A-8. This amplifier has extremely high overload tolerance, very good stability and linearity, fast pulse response, and high gain. At the same time it offers economy in cost and power consumption.

Over-all maximum gain is 13,500, 40,000, or 135,000, depending on a choice of feedback factor in the preamplifier. At the highest gain the noise figure is about as good as in the A-1D in the wide band condition, and the gain is comparable. A step attenuator reduces the gain by factors of 2 to a maximum reduction of a factor of 64.

There are no positive excursions of the base line following overload signals and no effect lasting more than 5 or 6 μsec so long as the preamplifier is not allowed to overload. This preamplifier consists of a feedback group which is capable of driving a long 100-ohm cable to about 18 v before saturation, and, since the group terminates this cable at its input, unless the cable is many hundreds of feet in length, serious overload does not occur until the signal is more than 80 v in amplitude. About 0.5 v is required at this point to produce full output at maximum gain.

The output is a double differentiated-shaped pulse with greater than 100 v maximum amplitude (each sign) into a 1000-ohm load. Because of the small d-c component in this type of signal there is very little base-line shift through an RC coupling circuit at high counting rates. Rise time of this pulse is about 0.18 μsec.

Long-term checks of stability and careful checks of linearity have not been made, but preliminary tests indicate that the amplifier is at least adequate in these respects. The integral linearity is within 0.2% (it is apparently much better), and the variation in gain with line voltage is 0.9% for a 10% change and 3.6% for a change from 90 to 130 v. Because of the large amounts of feedback used, no trouble is to be expected.

The pulse-height selector is of a new type which is considerably faster than previous designs and has a very good linearity to zero pulse height. Hysteresis is less than 0.3 v.

A circuit diagram of the amplifier is given in Fig. 1. Complete construction details will be made available in the literature as soon as possible.

UNCLASSIFIED
2-01-077-AB-1A

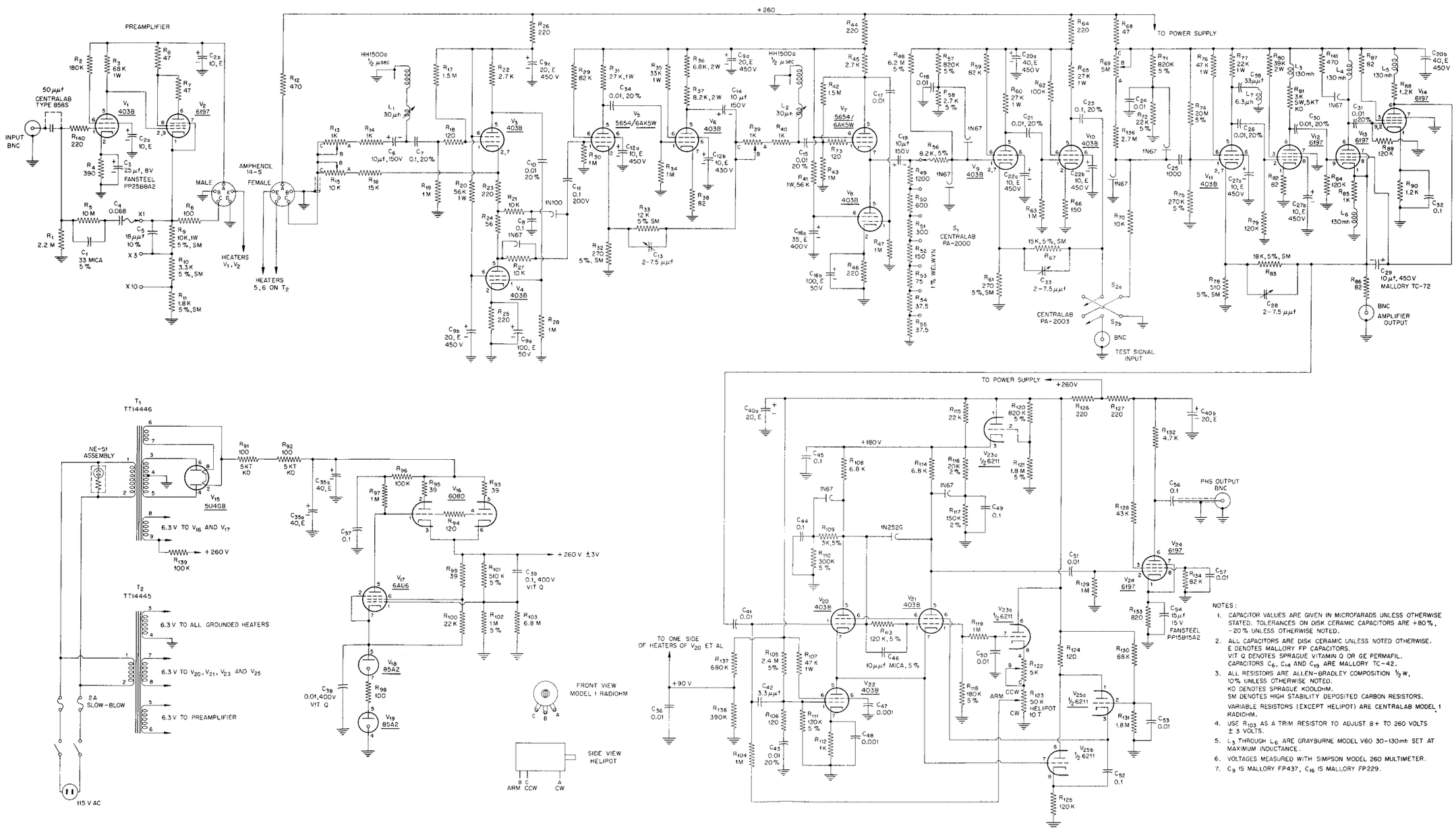

NOTES:

1. CAPACITOR VALUES ARE GIVEN IN MICROFARADS UNLESS OTHERWISE STATED. TOLERANCES ON DISK CERAMIC CAPACITORS ARE +80%, −20% UNLESS OTHERWISE NOTED.
2. ALL CAPACITORS ARE DISK CERAMIC UNLESS NOTED OTHERWISE.
   E DENOTES MALLORY FP CAPACITORS.
   VIT Q DENOTES SPRAGUE VITAMIN Q OR GE PERMAFIL.
   CAPACITORS C_6, C_{14} AND C_{19} ARE MALLORY TC-42.
3. ALL RESISTORS ARE ALLEN-BRADLEY COMPOSITION ½ W, 10% UNLESS OTHERWISE NOTED.
   KO DENOTES SPRAGUE KOOLOHM.
   SM DENOTES HIGH STABILITY DEPOSITED CARBON RESISTORS.
   VARIABLE RESISTORS (EXCEPT HELIPOT) ARE CENTRALAB MODEL 1 RADIOHM.
4. USE R_{103} AS A TRIM RESISTOR TO ADJUST B+ TO 260 VOLTS ± 3 VOLTS.
5. L_3 THROUGH L_6 ARE GRAYBURNE MODEL V60 30-130mh SET AT MAXIMUM INDUCTANCE.
6. VOLTAGES MEASURED WITH SIMPSON MODEL 260 MULTIMETER.
7. C_9 IS MALLORY FP437, C_{16} IS MALLORY FP229.

Fig. 1. Circuit Diagram of A-8 Linear Amplifier.

VARIATION OF NaI(Tl) DETECTION EFFICIENCIES WITH CRYSTAL SIZE AND GEOMETRY FOR MEDICAL RESEARCH

J. E. Francis C. C. Harris J. I. Trombka

The medical profession is often confronted by the problem that there is a maximum permissible dose which can be given to a patient and that there is a high dilution of this dose by body fluids. This is coupled with the fact that only a finite length of time can be used to make a measurement if a large number of patients are to be treated. One specific problem is the diagnosis of pernicious anemia by means of cobalt-labeled vitamin B_{12}. Two methods are used: one involves measuring the amount of Co^{60} in a 20-ml sample of blood plasma 24 hr after the dose is given; the second involves measuring the amount of Co^{60} in the urine which is excreted in the 24-hr period following administration of the dose.

In order to find the best method for determining the amount of Co^{60} for both procedures, the measurements shown in Table 1 were made. As might be expected, the 3 × 3 in. well crystal gives the highest counting rate per microcurie both for peak efficiency and for total efficiency. Although the counting rate is higher when measuring the total number of counts, it is still better to use the spectrometry method for these determinations, since the background is reduced by a factor of 16.5, while the counting rate is reduced only by a factor of 2.5. This means that it takes a source strength of only 0.5×10^{-4} μc to give a counting rate equal to the background for the spectrometry method, while it takes a source strength of 3.21×10^{-4} μc to give a counting rate equal to the background for the integral method.

Although measurements were made on 3 × 3 in. crystals having wells whose volumes were only 1.75 and 4.5 ml, the volume of the well can be increased to 20 ml with little loss of efficiency. The major difficulty in using a well crystal and a blood sample is the low source strength of approximately 0.4×10^{-4} μc.

For sample volumes much larger than 20 ml, placing the source in a beaker directly on top of the crystal seems to be the best solution to the problem. It is noted that, although the sensitivity per microcurie decreases, the counting rate for a given specific activity increases as the volume is increased. The major difficulty with this method is in being sure that the entire 24-hr urine output is obtained.

As an additional part of this experiment, the intrinsic peak efficiency of various sizes of crystals was measured for several different energies. The results of these measurements are shown in Fig. 1. This curve shows the percentage of the gamma rays falling on the crystal which are detected in the full energy peak as a function of the energy of the gamma ray. The source was placed at 9.3 cm from the face of the crystal for the solid crystals and in the bottom of the well for the well crystals.

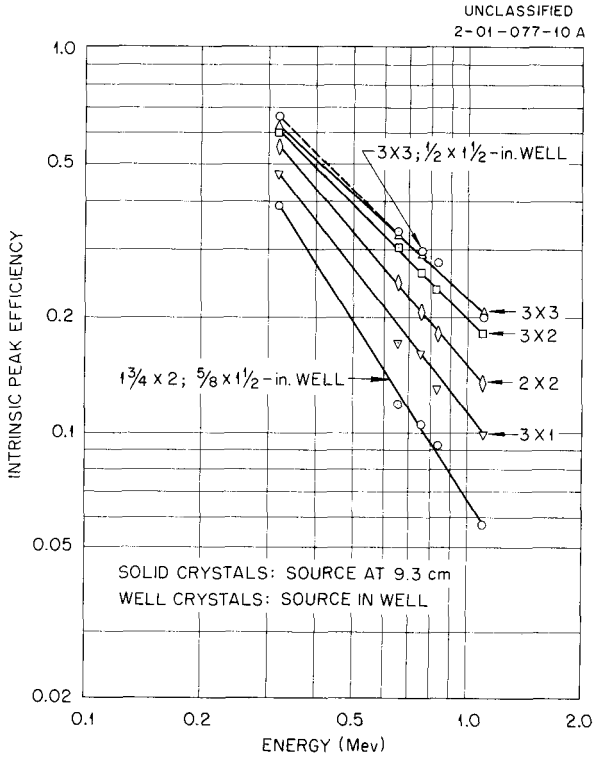

Fig. 1. Intrinsic Peak Efficiency vs Energy.

Table 1. Detection Efficiency for Co^{60} as a Function of Crystal Size and Source Geometry

Crystal Size (in.)	Source Volume (ml)	Volume (ml)		Source Position	Peak Efficiency (counts/sec/μc)	Total Efficiency (counts/sec/μc)	Peak Efficiency / Total Efficiency	Background in Peak (counts/sec)	Total Background (counts/sec)	Source Strength Equal to Background (μc $\times 10^{-4}$)	
		Well	Container							Peak	Total
3 × 3 well	1.75	1.75		In well	9600	24,150	0.382	0.48	7.76	0.5	3.21
3 × 3 well	4.5	4.5		In well	9500	25,700		0.48	7.76	0.5	
$1\frac{3}{4} \times 2$	4.0	4.0		In well	3230	12,864	0.245	0.186	2.9	0.5	2.25
3 × 3 solid	20		250	On top	4600	13,243	0.346	0.48	7.76	1.04	5.85
	100		250	On top	3023	9,390	0.320	0.48	7.76	1.59	8.26
	200		250	On top	1851	6,847	0.271	0.48	7.76	2.59	11.3
	500		1000	On top	1681	5,580	0.295	0.48	7.76	2.86	13.9
	1000		1000	On top	1056	3,570	0.295	0.48	7.76	4.55	21.7
2 × 2 solid	20		250	On top	1831	6,570	0.279	0.234	2.79	1.28	4.27
	100		250	On top	1152	4,417	0.261	0.234	2.79	2.03	6.33
	200		250	On top	759	3,132	0.242	0.234	2.79	3.09	8.9

TABLES OF SOLID ANGLES AND ACTIVATIONS

A. V. H. Masket[1] R. L. Macklin H. W. Schmitt

The interaction of radiation with a homogeneous cylindrical body presents a frequent calculational problem in nuclear physics. Scintillation and Geiger counters, neutron and gamma-ray sources, and reactor fuel elements are common examples. Two reciprocal cases are found; either the radiation originates in the cylinder and the intensity at a point (or points) is desired, or the radiation from a point source interacts with the material of the cylinder and this interaction is desired. Calculations are similar in the two cases.

For the case of first interactions and radiation following the usual $1/R^2$ law, the interaction can be formulated generally as follows, considering the radiation from a point source interacting with a body:

$$N = \left(\frac{Q}{4\pi\lambda}\right) \int_V dv \, \frac{e^{-l/\lambda}}{R^2}$$

$$= \frac{Q}{4\pi} \int_\Omega d\omega \, (1 - e^{-L/\lambda}),$$

where

N = primary interactions per second in the cylinder,

Q = quanta emitted per second from the point source,

λ = mean free path for the radiation in the (homogeneous) body,

V = volume of the body,

l = path length through the body from the radiating point to the volume element dv,

R = distance from the radiating point to the volume element dv,

L = path length through the body along an element of solid angle $d\omega$,

Ω = solid angle subtended by the body from the point source.

[1] ORINS summer participant from the University of North Carolina.

Two limiting cases are of interest. In one the interaction is weak; that is, l is always small compared with λ, and the exponential factor can be taken as unity. The remaining integral

$$I = \int_V \frac{dv}{R^2}$$

has been evaluated on the Oracle computer for a large range of cylinder dimensions and spacings. Tables of the results are being published in ORNL-2170.[2]

The second limiting case involves the converse relation l, always large compared with λ. In this case most of the body suffers no direct interaction, the surface layer being opaque, and the interaction reduces to

$$N = \frac{Q\Omega}{4\pi},$$

where Ω is the solid angle (in steradians) subtended by the cylinder from the point emitter. The solid angles subtended by disks and cylinders have been calculated for a large range of disk and cylinder dimensions and spacings. Tables of these results are also included in ORNL-2170.

With the aid of the tables and formulas given in this report,[2] the solid angle and linear activation for a right cylinder of any size from any point in space may readily be found. Simple approximations are given for dimensions beyond the ranges of the tables, and these are also useful if great accuracy in interpolation is required. By further integration of the results for a point source, the radiation interaction between a cylinder and other finite bodies may be found. Extension of the results to cases with small self-absorption and to cases where second interactions are important is briefly discussed.

[2] A. V. H. Masket, R. L. Macklin, and H. W. Schmitt, *Tables of Solid Angles and Activations*, ORNL-2170 (Nov. 1956).

NUCLEAR ORIENTATION OF Np^{237}, U^{233}, AND U^{235} NUCLEI

L. D. Roberts J. W. T. Dabbs G. W. Parker

Work on the alpha-particle anisotropy from oriented Np^{237} and U^{233} nuclei has continued.[1,2] Several lines of attack on various problems associated with this work have been used.

NEPTUNIUM-237

An attempt to determine the direction of orientation of the Np^{237} nuclei in $NpO_2Rb(NO_3)_3$ by observing the temperature dependence of the alpha-particle anisotropy below 0.5°K was not successfully concluded because of a surprising difficulty in cooling this salt to these temperatures in an apparatus especially constructed for this measurement. In this apparatus, shown in Fig. 1, provisions were made both for indirect cooling of the nuclear sample by adiabatic demagnetization of a paramagnetic salt and for piping the light produced by the alpha particles striking a ZnS screen to an external photomultiplier. The spin Hamiltonian for $NpO_2Rb(NO_3)_3$ is effectively

$$(1) \qquad \mathcal{H} = AI_cS_c' + q\left[I_c^2 - I\left(\frac{I+1}{3}\right)\right],$$

where I_c is the projection of the nuclear spin along the crystalline c axis, S_c' is the effective projection of the magnetic electron spin, $\pm\frac{1}{2}$, along this same axis, and the coupling coefficients A and q have the values[3]

$$A = 0.167\ \text{cm}^{-1}, \quad q = -0.030\ \text{cm}^{-1}.$$

The relative signs of A and q are known,[3] but the absolute signs have been obtained from calculations of Eisenstein and Pryce.[4] The experiment mentioned above was to have confirmed these absolute signs as follows: Equation 1 leads to a calculated nuclear orientation $\Delta_2 I^2$ which is quite different, as a function of temperature, for the cases $q < 0$ and $q > 0$ (see Fig. 2). The shapes of the two curves are indistinguishable, within experimental error, down to about 0.5°K, and temperatures of this order were the lowest which have been shown to be obtained. The reasons appear to be twofold: first, the crystals appear to develop a mosaic structure on cooling which hinders heat transport severely, and, second, a number of experiments indicate that some source of internal heating is present. The latter is possibly the low-temperature "tail" of a phase transition which proceeds very slowly at liquid-helium temperatures, giving rise to the evolution of a few hundred ergs per minute in typical samples. It is hoped that a change to another crystal system will lead to a resolution of this problem. It is of interest to note that, in experiments performed below 1°K, the anisotropy of alpha-particle emission was always observed to increase as the temperature was lowered. This further increase of anisotropy was always perpendicular to the crystalline c axis and was such as to enhance the anisotropy already present at 1°K (ref 2).

$NpO_2Rb(NO_3)_3$ Magnetic Susceptibility

An associated problem to the one above was the question of the validity of the Hamiltonian (Eq. 1) at temperatures of ~1°K, since the microwave data on which Eq. 1 is based were taken at 20°K. In addition, the microwave data were obtained on a very small concentration of neptunium in $UO_2Rb(NO_3)_3$. It was verified in susceptibility measurements, using a highly sensitive mutual inductance bridge,[5] that pure $NpO_2Rb(NO_3)_3$ remains a normal paramagnetic salt down to a temperature of 1.2°K, following the Curie-Weiss law with a Weiss constant of only −0.067°K and a Curie constant of the magnitude expected from the microwave data.[3] The susceptibility measurements give $g_{\parallel}^2 + 2g_{\perp}^2 = 11.26 \pm 0.1$ for a powdered sample, whereas the microwave data lead to a value in the range 11.30 to 11.98. This suggests that there is no appreciable change in the electronic structure between the dilute and concentrated NpO_2^{++} salts. The small Weiss constant

[1] L. D. Roberts *et al.*, *Phys. Semiann. Prog. Rep. Sept. 10, 1955*, ORNL-1975, p 45.

[2] L. D. Roberts, J. W. T. Dabbs, and G. W. Parker, *Phys. Semiann. Prog. Rep. March 10, 1956*, ORNL-2076, p 3.

[3] B. Bleaney, *Phil. Mag.* **45**, 992 (1954).

[4] J. C. Eisenstein and M. H. L. Pryce, *Proc. Roy. Soc. (London)* **A229**, 20 (1955).

[5] R. A. Erickson, L. D. Roberts, and J. W. T. Dabbs, *Rev. Sci. Instr.* **25**, 1178 (1954).

UNCLASSIFIED
ORNL-LR-DWG 11817

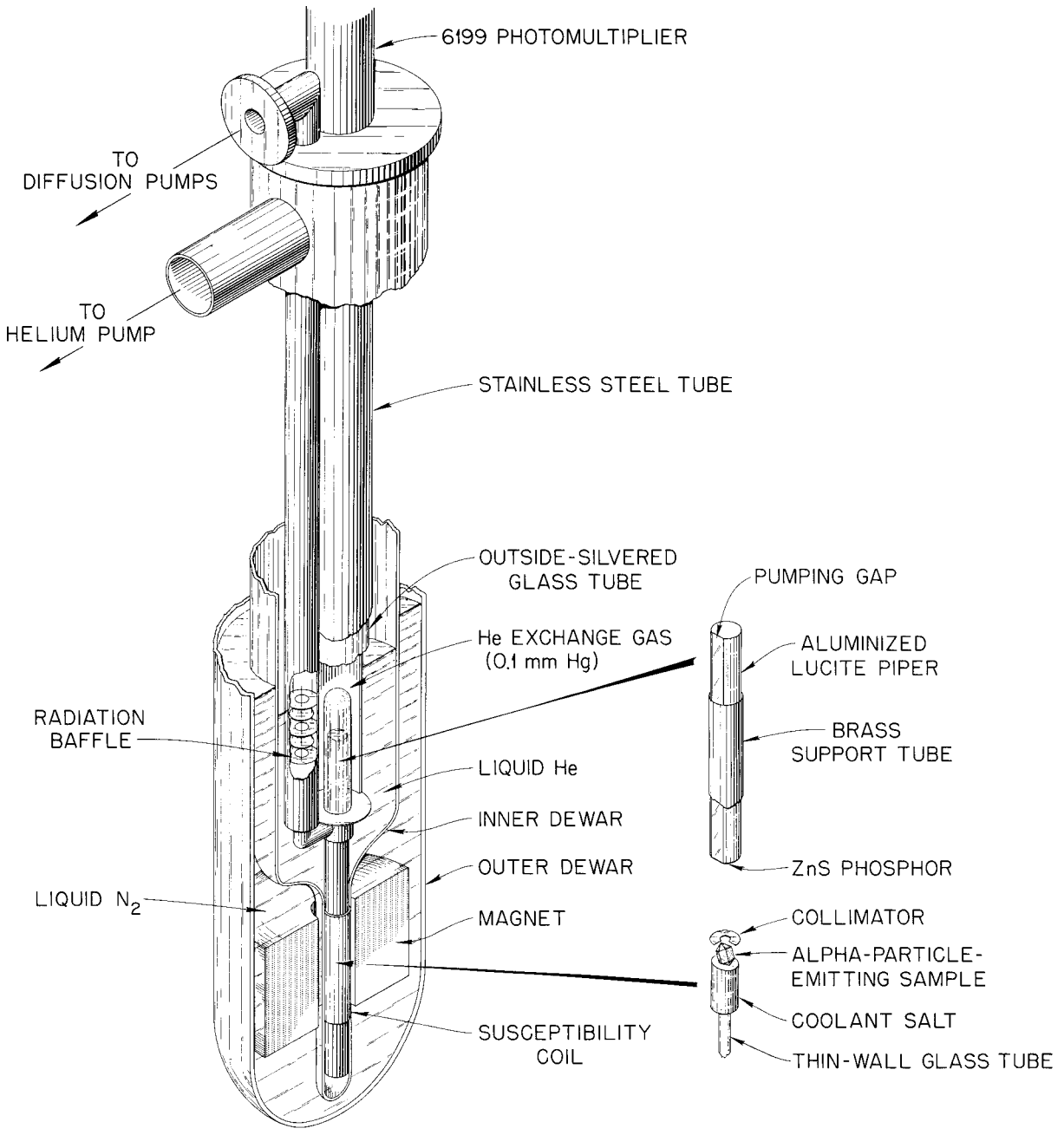

Fig. 1. Apparatus for Observing Anisotropy of Alpha Emission Below 1°K.

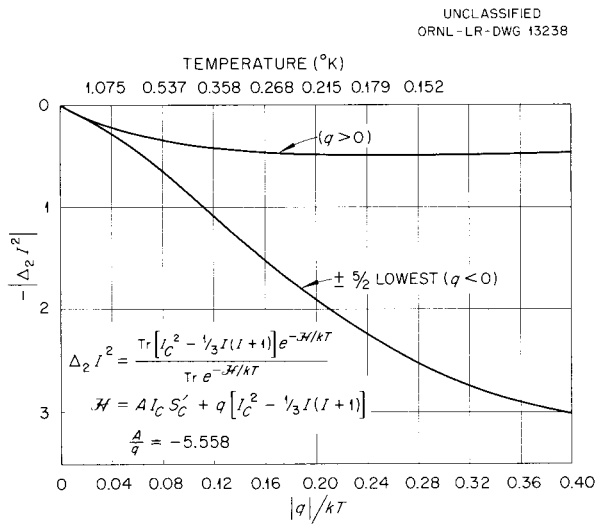

Fig. 2. Calculated Nuclear Alignment of Np^{237} for $q < 0$ and $q > 0$.

and the measured Curie constant thus indicate that the calculations leading to the curves of Fig. 2 are valid to temperatures of ~0.1°K.

URANIUM-233

As pointed out in the previous semiannual report,[6] the size of the coupling constant q in the Hamiltonian

$$\mathcal{H} = q\left[I_c^2 - I\left(\frac{I+1}{3}\right)\right] \tag{2}$$

for U^{233} in $UO_2Rb(NO_3)_3$ was unknown. The results given there tended to indicate that q was very large if the curvature observed in the ratio of intensities $R_{\parallel}/R_{\perp}$ relative to the crystalline c axis vs $1/T$ was real. Subsequent measurements in which a carbon resistance thermometer was placed adjacent to the U^{233} sample have established that this curvature was spurious and was due to a temperature difference of ~0.1°K between sample and bath, while it had previously been assumed that the sample temperature and the bath temperature were the same. This temperature difference was found to be due to heat flow down the supports to the sample holder. Fundamentally, the difficulty is due to the very small thermal conductivity of helium gas (~25 μw·deg^{-1}·cm^{-1}) at temperatures near 1°K. Modifications to the above apparatus[7] were made which reduced the heat input to the sample holder, and, as mentioned above, a thermometer was installed. In addition, a collimator was added between the ZnS alpha-detector layer and the crystal in such a way that a constant, known solid angle for counting was obtained for all orientations of the crystal. If the alpha-particle-emitting layer on the surface of the crystal is thicker than one alpha-particle range, it can easily be seen that the counting rate observed will be independent of crystal angle if there is no nuclear orientation (i.e., at high temperatures). In this case geometry corrections are calculable, and the collimator was designed to make them small.[8,9] Two examples of observed angular distributions from U^{233} nuclei are given in Figs. 3 and 4. It is seen that the amplitude of the $P_2(\cos\theta)$ term increases as the temperature is lowered; in fact, this increase is found to be linear in $1/T$, as shown in Fig. 5, where the intensity along the c axis of the crystal is shown relative to the intensity at 90 deg to the c axis as a function of $1/T$.

[6] L. D. Roberts, J. W. T. Dabbs, and G. W. Parker, *Phys. Semiann. Prog. Rep. March 10, 1956*, ORNL-2076, p 5.

[7] L. D. Roberts, *op. cit.*, Fig. 1, p 3.

[8] M. E. Rose, *Geometrical Corrections for Anisotropically Emitting Sources*, ORNL-2050 (March 1, 1956).

[9] M. E. Rose, *Phys. Semiann. Prog. Rep. March 10, 1956*, ORNL-2076, p 1.

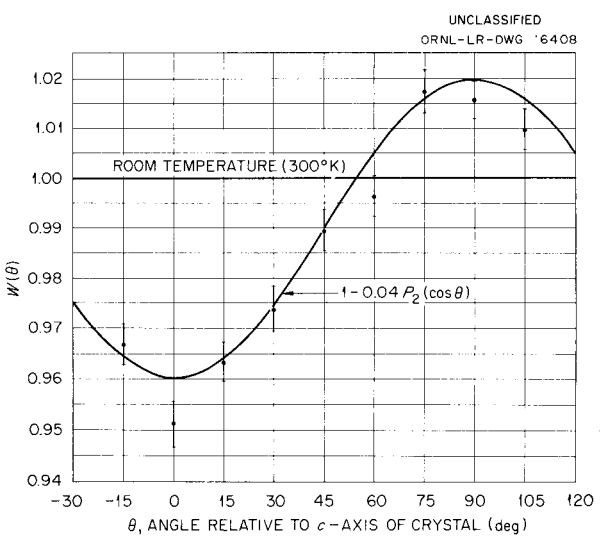

Fig. 3. Angular Distribution of Alpha Particles from Oriented U^{233} Nuclei.

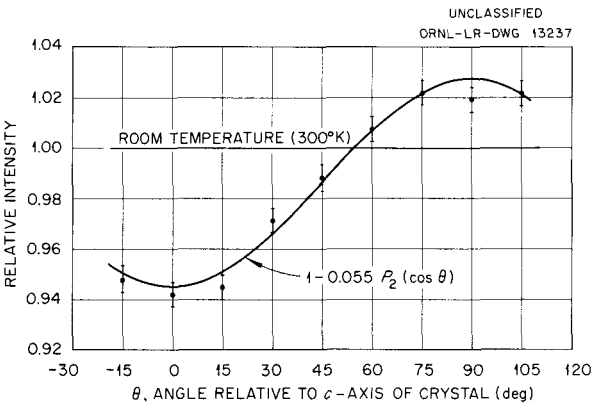

Fig. 4. Angular Distribution of Alpha Particles from Oriented U^{233} Nuclei.

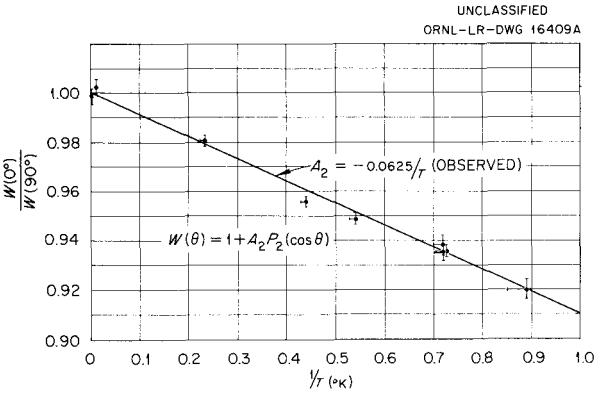

Fig. 5. Anisotropy of Alpha-Particle Emission as a Function of $1/T$.

Specific Heat and Quadrupole Coupling in $U^{235}O_2^{++}$ and $U^{233}O_2^{++}$

In order to interpret the above results, it is necessary to know the degree of nuclear alignment of U^{233} to be expected as a function of temperature. This can be calculated from the spin Hamiltonian. In that the salt $UO_2Rb(NO_3)_3$ is not paramagnetic, the quadrupole coupling term (Eq. 2) is the only important one.[2] Here $q < 0$, since the nuclear quadrupole moments of both U^{235} and U^{233} are positive,[10] and the moment of the electronic bond structure to which the nuclei are coupled is thought to be positive.[2,4] In principle, $|q|$ may be obtained from quadrupole resonance measurements, but such measurements are difficult and have not been made. From our alpha-particle anisotropy measurements previously reported,[2] a preliminary minimum value of $q \sim 0.04$ cm^{-1} was estimated. A Schottky-type specific-heat anomaly in an appropriate temperature range is to be expected from any splitting of energy levels; in the present case a measurable specific heat of the form

$$C \cong Nk \frac{Tr H^2}{k^2 T^2}, \tag{3a}$$

or

$$\frac{CT^2}{R} \simeq \frac{2.069}{15} q^2 I(I+1) \left[\frac{4}{3} I(I+1) - 1\right], \tag{3b}$$

in the accessible temperature region of 0.3 to 1.0°K (where $|q|/kT \ll 1$) is calculated. Here q is in cm^{-1}. In the case of U^{233}, however, the high specific alpha activity of this nucleus prevents carrying out the measurement, and it was decided to measure the specific heat of a salt containing $U^{235}O_2^{++}$ ions. The first attempts were with $U^{235}O_2Rb(NO_3)_3$; however, it was found difficult to carry out these measurements because of a relatively large internal heat generation, as mentioned above. This measurement of the specific heat associated with the quadrupole coupling was then made on $U^{235}O_2F_2$, since the properties of the UO_2^{++} bond were expected to be essentially independent of the compound, and it was known from previous higher-temperature specific-heat measurements[11] that no phase transition existed for this salt. The result was calculated from the relation

$$\frac{CT^2}{R} = 43.45 q^2, \tag{4}$$

which is the value deduced from Eq. 3b with $I = 7/2$ and with the Hamiltonian of Eq. 2; q is in cm^{-1}.

The apparatus is shown in Fig. 6. Novel features of this apparatus include a liquid-nitrogen-cooled solenoid for the adiabatic demagnetization and a continuously pumped chamber through which the heater leads were brought into the sample space, thus obviating vacuum problems due to superfluid helium leaks. In addition, the apparatus is easily

[10] K. L. Vander Sluis and J. R. McNally (private communication).

[11] P. F. Wacker and R. K. Cheney, *J. Research Natl. Bur. Standards* 39, 317, esp 319 (1947).

demountable. In this experiment a sample of $U^{235}O_2F_2$ was connected thermally to a cooling salt, $Mn(NH_4)_2(SO_4)_2 \cdot 6H_2O$, and an electrical heating coil. The magnetic susceptibility of the cooling salt served as a thermometer. After adiabatic demagnetization to about 0.3°K, measured quantities of heat were introduced with the heater, and the temperature changes for each heating were determined. Subtraction of the heat capacity of the cooling salt and metal parts from the measured total gave the heat capacity of the sample of UO_2F_2. Since the lattice specific heat below ~1°K is negligible, the entire heat capacity could be attributed to the quadrupole coupling.

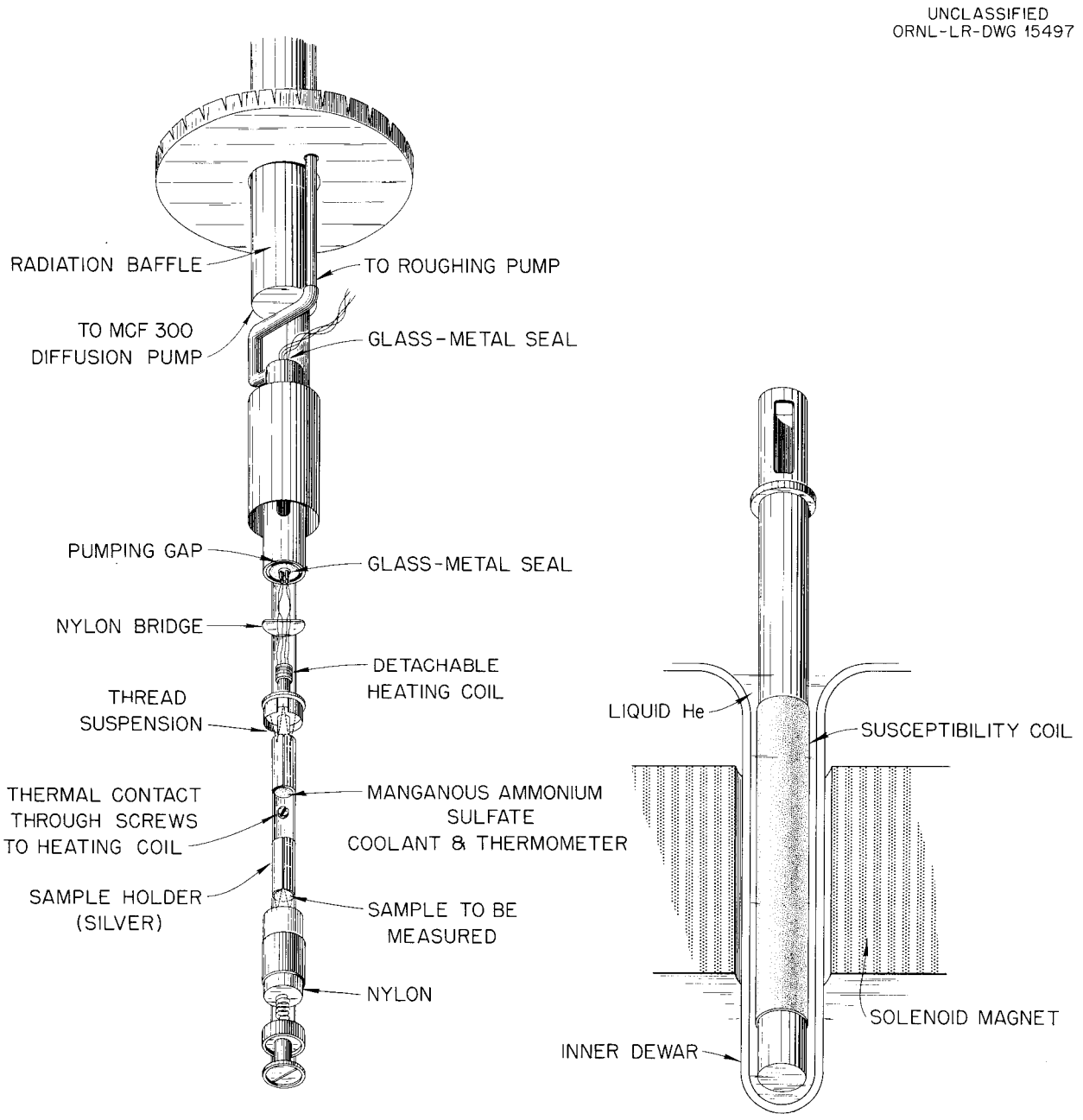

Fig. 6. Apparatus for Specific-Heat Measurements Below 1°K.

From these measurements, a value $q(U^{235}O_2^{++}) = -0.015 \pm 0.0015\ cm^{-1}$ was determined, and it is assumed that this coupling coefficient is the same in $U^{235}O_2Rb(NO_3)_3$.

To obtain $q(U^{233}O_2^{++})$ it was then necessary to take into account the ratio of the quadrupole moments of U^{233} and U^{235} nuclei. Kaliteevski and Chaika[12] observed the hyperfine structure of optical spectra in both these isotopes and gave calculations for the ratios of their magnetic dipole and electric quadrupole moments. Unfortunately, the hyperfine multiplets for U^{235} were not completely resolved, and an incorrect spin assignment for U^{235} was used in their calculations. We have recalculated these ratios from their optical data on the 5915.4-Å transition and find, for the nuclear quadrupole moments Q,

$$(5) \qquad \frac{Q(233)}{Q(235)} = 0.7 \pm 0.3 ,$$

and, for the nuclear magnetic dipole moments μ,

$$(6) \qquad \frac{\mu(233)}{\mu(235)} = -1.74 \text{ (no error assigned)} ,$$

using $I(233) = 5/2$ and $I(235) = 7/2$.

Vander Sluis and McNally[10] have re-examined their plates on this same transition, with the following results:

$$(7) \qquad \frac{Q(233)}{Q(235)} = 0.8 \pm 0.3 ,$$

and

$$(8) \qquad \frac{\mu(233)}{\mu(235)} = -1.63 \text{ (no error assigned)} .$$

Recent unpublished work by Dorain, Hutchison, and Wong[13] on paramagnetic resonance in U^{+++} has definitely established the above spins to be correct and, in addition, has given

$$(9) \qquad \frac{Q(233)}{Q(235)} = 0.855 \pm 0.15 ,$$

and

$$(10) \qquad \left|\frac{\mu(233)}{\mu(235)}\right| = 1.536 \pm 0.005 .$$

It can be shown that

$$(11) \qquad \frac{q(233)}{q(235)} = \frac{Q(233)}{Q(235)} \cdot \frac{I(2I-1)}{I'(2I'-1)} = \frac{42}{20}\,\frac{Q(233)}{Q(235)} ,$$

where $I' = 5/2$ and $I = 7/2$. Since the paramagnetic resonance result has the smallest error of the above three determinations of $Q(233)/Q(235)$, we have used this value, Eq. 11, and our measured value of $q(U^{235}O_2^{++})$ to obtain

$$(12) \qquad q(U^{233}O_2^{++}) = -0.027 \pm 0.006\ cm^{-1} .$$

The error is predominantly due to the uncertainty in the quadrupole moment ratio.

Analysis of Alpha-Particle Anisotropy in Aligned U^{233} Nuclei

The alpha-particle decay of U^{233} has been discussed, for example, by Hollander, Perlman, and Seaborg,[14] Bohr, Fröman, and Mottelson,[15] and Goldin, Novikova, and Tretyakov.[16]

Figure 7 shows the decay scheme as given by Bohr *et al.*[15] and by Goldin *et al.*,[16] where I is the total angular momentum, K is the projection of I on the nuclear symmetry axis, and l is the angular momentum carried off by the alpha particle.

[12] N. I. Kaliteevski and M. P. Chaika, *Bull. Leningrad Univ.*, No. 11, 121–137 (1955).

[13] P. B. Dorain, C. A. Hutchison, Jr., and E. Wong, *Phys. Rev.* (to be published).

[14] J. M. Hollander, I. Perlman, and G. T. Seaborg, *Revs. Mod. Phys.* **25**, 469 (1953).

[15] A. Bohr, P. O. Fröman, and B. R. Mottelson, *Kgl. Danske Videnskab. Selskab Mat. fys. Medd.*, **29**, No. 10, (1955).

[16] L. L. Goldin, G. I. Novikova, E. F. Tretyakov, *Phys. Rev.* **103**, 1004 (1956).

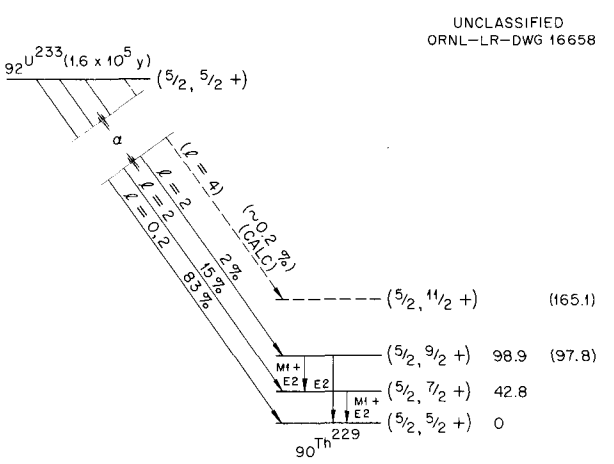

Fig. 7. Decay Scheme of U^{233}.

First we note that the alpha decay is interpreted[15] as taking place to the ground-state rotational band in Th^{229} with no parity change, which Bohr *et al.*[15] refer to as a favored transition. Next we note that Bohr *et al.* suggest that predominantly $l = 0, 2$ for the ground-state transition and that $l = 2$ for the second and third excited states. The transitions to these three lowest states are the only ones of sufficient intensity to be of importance to our experiments; and as the assignment of these l values by Bohr *et al.* is of particular interest to us, we will briefly review their work. They have noted that virtually all the even-even alpha emitters above radium decay to a rotational band in the ground states of the daughter, the transition probability to the lowest state with $l = 0$ being ~75% of the total, the transition probability to the next state with $l = 2$ being ~24%, and that to all the higher transitions with $l = 4, 6, 8, \ldots$ adding up to much less than 1%. Thus transitions with $l = 0$ or 2 are greatly preferred for the even-even nuclei. They then suggest that an odd-mass alpha emitter consists of a nuclear core plus an odd particle and that, in favored alpha transitions, only the even-even core takes part in the alpha formation. With this picture they extrapolate the behavior of the even-even alpha emitters to those of odd mass. Then for a favored transition from an alpha emitter in the state I_i, K_i to a daughter in a state I_f, $K_f = K_i$ they give an approximate relation for the transition probability P:

$$P = P_0(Z,E) \sum_l C_l \left(C^{I_i l I_f}_{K_i 0 K_f} \right)^2 , \tag{13}$$

$$\log P_0(Z,E) = C(Z) - \frac{D(Z)}{\sqrt{E}} , \tag{14}$$

where Z is the nuclear charge and E is the energy of the alpha particle in a given transition; $C^{I_i l I_f}_{K_i 0 K_f}$ is a vector addition coefficient and the C_l are empirical constants taken from the remarkably consistant behavior of the even-even emitters. The Geiger-Nuttall constants, C and D, are selected to be in accord with the alpha emitters, with $84 \leqq Z \leqq 98$ and to make $C_0 = 1$. It is then found that $C_2 \cong 0.7$ and $C_4 \sim 0.01$ to 0.1, while C_6 and higher are only of the order of 0.01. Equation 13 then enables one to predict the admixture of $l = 0, 2, 4, \ldots$ in a given transition, and, because of the smallness of the coefficients above C_2, Bohr *et al.* suggest that only $l = 0$ and 2 make an important contribution. Using their values[15] for C and D and the I, K quantum numbers of Fig. 7, we calculate from Eq. 13 the admixture of $l = 0, 2$ for the U^{233} ground-state transition and find that Eq. 13 gives 80% of $l = 0$ and 20% of $l = 2$.

L. D. Landau and K. A. Ter-Martirosian have each suggested theoretical relationships predicting intensities in alpha decay.[16] The relation of Landau, which is based on the idea of a presumably higher barrier penetration in alpha emission near the tips of a prolate spheroidal nucleus, does not give information relative to l admixtures. Also, his model would seem to predict an anisotropy of alpha emission from oriented U^{233} of opposite sign to that which we observe. The relation of Ter-Martirosian, which can in principle predict l admixtures, contains several unspecified adjustable constants. Thus neither of these relationships appears to be suitable for interpreting our results.

Equation 13 is definite and has had some qualitative success in predicting intensities in a number of alpha decay schemes as well as an alpha-gamma angular correlation result in Am^{241}. Thus we will use this relation in discussing our results, although it is only semiquantitative.

With the assumption, then, of the decay scheme of Fig. 7, it is possible to give a specific description of our results in terms of the general formalism of angular momentum theory.[17] To terms in $1/T$ and for the three lowest states, the angular distribution $W(\theta)$ (where θ is the angle measured from the axis of quantization, the crystalline c axis) may be given as

$$W(\theta) = 0.835 \left[W_{00}^{5/2\to5/2} + \delta^2 W_{22}^{5/2\to5/2} - 2\delta \cos(\sigma_2 - \sigma_0) W_{02}^{5/2\to5/2} \right] + 0.149\, W_{22}^{5/2\to7/2} + 0.016\, W_{22}^{5/2\to9/2} , \tag{15}$$

where the W superscripts give $I_i \to I_f$ and the

[17] M. E. Rose, *Phys. Semiann. Prog. Rep. March 10, 1956*, ORNL-2076, p 1.

notation is that of refs 17 and 18, with δ the effective ratio of the amplitude of the $l = 2$ wave to that of the $l = 0$ wave. The factor $\cos(\sigma_2 - \sigma_0)$ due to the coulomb field is very close to -1. Substituting numerical values, this reduces to

$$(16)\quad W(\theta) = 1 - \frac{0.795\delta^2 + 4.415\delta + 0.226}{1 + 0.835\delta^2}\,\frac{q}{kT}P_2(\cos\theta)\ ,$$

with k the Boltzmann constant, and T the absolute temperature. As discussed earlier, q is thought to be negative.

Our results as expressed in Fig. 5 permit the identification

$$(17)\quad \frac{0.795\delta^2 + 4.145\delta + 0.226}{1 + 0.835\delta^2}\cdot\frac{q}{k} = 0.0625.$$

Figure 8 gives a plot of Eq. 17 and shows the correlation of alpha-particle results of Fig. 5 with our specific-heat measurement of q/k and the value of δ calculated from Eq. 13. Figure 9 gives a plot of the alpha-anisotropy coefficient, A_2T, that is, the coefficient of $P_2(\cos\theta)/T$ of Eq. 16 vs δ for our measured value of

$$\frac{q}{k} = -0.0388 \pm 0.0086°K\ ,$$

and again compares this result with our measured value of A_2T:

$$A_2T = \frac{-q}{k}\,\frac{0.795\delta^2 + 4.145\delta + 0.226}{1 + 0.835\delta^2}\ .$$

From Fig. 8 we note that the minimum quadrupole coupling $q(U^{233}O_2^{++})/k$ consistent with our measured alpha anisotropy (Fig. 5) is $0.037 \pm 0.0015°K$ or $0.026 \pm 0.001\ cm^{-1}$, which

[18] L. D. Roberts, J. W. T. Dabbs, and G. W. Parker, *Phys. Semiann. Prog. Rep. March 10, 1956*, ORNL-2076, p 3.

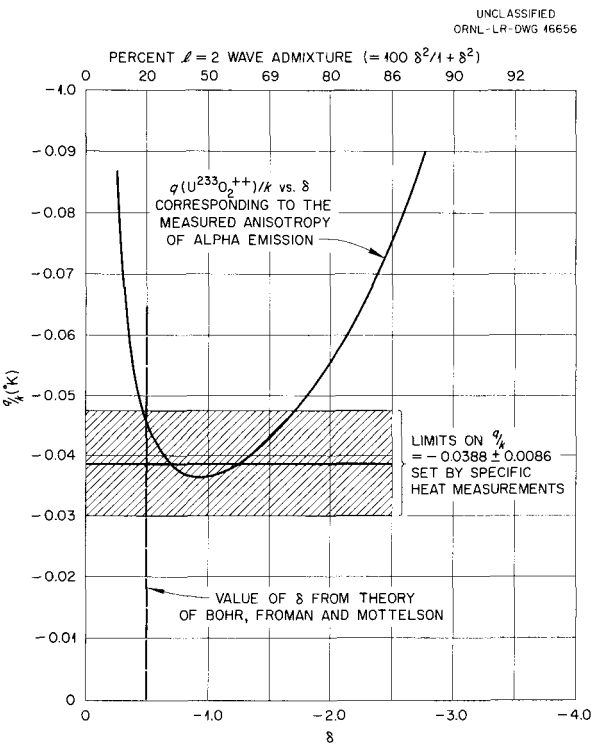

Fig. 8. Specific-Heat Constant, q/k, as a Function of δ.

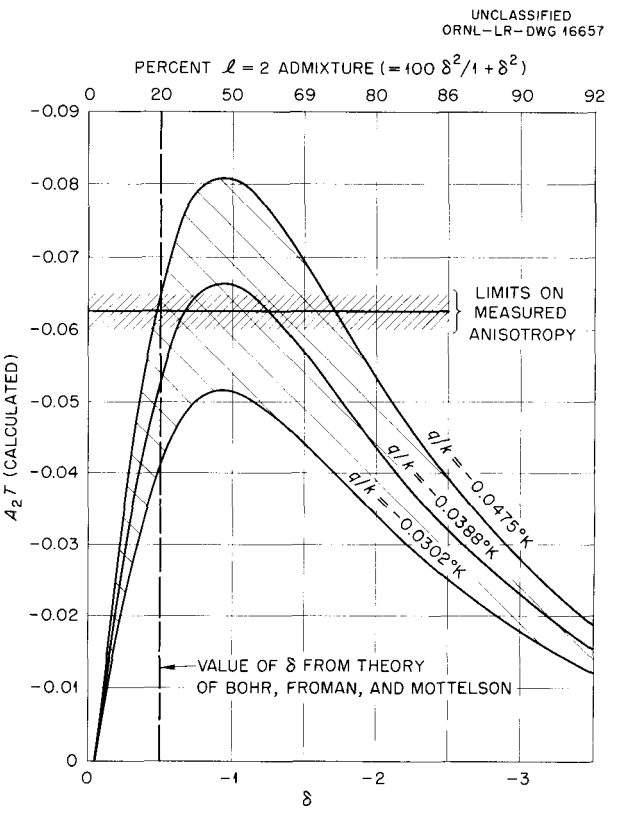

Fig. 9. Calculated Anisotropy Coefficient A_2T as a Function of δ.

sets this minimum at a smaller value than our previous estimate of 0.04 cm^{-1}. Thus the measured $q(U^{233}O_2^{++})/k$ from the specific-heat measurements is very close to this minimum. Conversely, we find from Fig. 9 that the observed alpha-anisotropy coefficient A_2T is near the maximum value that would be permitted by our measured $q(U^{233}O_2^{++})/k$ with the optimum value of $\delta = -0.95$.

Further, Fig. 9 illustrates the fact that our results lead to a δ lying in the range

$$-0.45 \geqq \delta \geqq -1.75 \ .$$

These values correspond to an $l = 2$ or d-wave admixture of

$$17\% \leqq \frac{100\delta^2}{1 + \delta^2} \leqq 75\% \ ,$$

which includes the value of 20% from the theory of Bohr *et al.* To this degree, our nuclear alignment results seem to be in accord with their picture of alpha-decay intensities. It should be noted that both our result for this admixture and the observed intensities in the decay of a number of odd nuclei (see Table IV, ref 15) give values which are in general somewhat higher than their theory predicts.

A serious disagreement between the interpretation of our experiments and theory is with regard to the most obvious aspect of our results, namely, the sign of A_2T. Suggestions have been made by Hill and Wheeler,[19] Christy,[20] and Landau[16] that, for a nucleus of prolate spheroidal shape, coulomb barrier effects would lead to predominant alpha emission from the nuclear tips, with the major lobe of intensity parallel to the nuclear symmetry axis. Then if the nuclei are aligned with the symmetry axis parallel to the crystalline c axis, one would certainly expect the qualitative result that the predominant alpha emission would be along the c axis also. As was presented before,[17,18,21] our experiments give just the opposite result; indeed, it would appear that the anisotropy has nearly the largest permissible value in this direction. Thus it is worthwhile to see at what point the actual disagreement most likely occurs.

First of all, we note that the microwave measurement of the quadrupole coupling by Bleaney *et al.*[22] for NpO_2^{++} and the $q(U^{233}O_2^{++})$ which we have obtained from specific-heat measurements presented in this report are of such magnitude that substantial nuclear alignment would certainly be possible at 1°K for both systems. Nuclear spin-lattice relaxation times will certainly be very short, compared with 1 sec for NpO_2^{++}, due to the magnetic coupling in this group. In the UO_2^{++} specific-heat measurements, the fact that the specific heat was measurable down to 0.3°K demonstrates that the addition of 0.1% NpO_2^{++} to the UO_2^{++} sample provided a sufficient spin-lattice relaxation mechanism for equilibrium within a few seconds. Thus the nuclear alignment to be expected from statistical mechanical calculations must occur.

Our observations of the anisotropy of alpha emission have now been performed on some ten different crystals in some 30 separate experiments, and all the results are in agreement. Thus it would seem to be a statistical certainty that the gross effect of nuclear alignment is the predominant emission of alpha particles perpendicular to the crystalline c axis.

The results of Vander Sluis and McNally[23] and of Kaliteevski and Chaika[24] from optical spectroscopy seem to indicate quite clearly that the sign of the intrinsic nuclear quadrupole moment of U^{233} is positive. Unfortunately, no direct experimental information is available as to the sign of the Np^{237} nuclear quadrupole moment, although the fact that U^{233}, U^{235}, Am^{241}, and Am^{243} are observed to have Q positive suggests that $Q(Np^{237})$ is positive also.

The only remaining qualitatively important factor is the nature of the electronic charge density in the UO_2^{++} and NpO_2^{++} bonding orbitals. The best theoretical discussions available, for example,

---

[19] D. L. Hill and J. A. Wheeler, *Phys. Rev.* 89, 1102 (1953).

[20] R. F. Christy, *Phys. Rev.* 98, 1205 (1955).

[21] Papers presented by L. D. Roberts, J. W. T. Dabbs, G. W. Parker, and R. D. Ellison; J. W. T. Dabbs, L. D. Roberts, and G. W. Parker; and M. E. Rose, L. D. Roberts, and J. W. T. Dabbs, *Washington APS Meeting*, May 1956.

[22] B. Bleaney, *Phil. Mag.* 45, 992 (1954).

[23] K. L. Vander Sluis and J. R. McNally (private communication).

[24] N. I. Kaliteevski and M. P. Chaika, *Bull. Leningrad Univ.*, No. 11, 121–137 (1955).

those of Coulson[25] and Eisenstein and Pryce,[26] indicate that the major charge density due to the bonding orbitals lies along the O-Np-O or O-U-O axis, which would then lead to $q < 0$ and the alignment of the nuclear symmetry axis along the oxygen-oxygen direction. Even though these arguments seem quite strong, there is perhaps less direct experimental evidence in support of these bonding charge density calculations than that which exists in support of the other aspects of our experiment. Thus we conclude that our experiments place these bonding orbital calculations and the barrier treatment of alpha emission[19,20] in disagreement. For the moment, it does not seem possible to make an absolutely firm decision as to which of these two conflicting concepts is correct. It is possible to observe, however, that the spheroidal barrier is perhaps not the most important factor in the direction of alpha emission from the nucleus, and that there is in fact no direct experimental support for the idea that it should be. The bonding orbital calculations, on the other hand, are made by a theory which – while difficult – has had wide and definite success. In the particular cases of UO_2^{++} and NpO_2^{++}, these orbital calculations seem to be capable of describing a rather wide variety of microwave resonance, magnetic susceptibility, crystal structural, and chemical phenomena. It is true that these phenomena generally reflect the properties of the electronic wave functions at large distances from the nucleus, whereas nuclear quadrupole coupling reflects the character of these wave functions at much smaller distances. From these orbital calculations the over-all quadrupole moment of the UO_2^{++} or NpO_2^{++} bond is positive. It seems improbable that this sign would then be negative for the region near the uranium or neptunium nucleus.

Recently, Rasmussen and Segall[27] have discussed the alpha decay of spheroidal nuclei. From inward integrations based on experimental alpha-group intensities in the decay of Th^{228} and Cm^{242}, they obtain calculated alpha-probability distributions on the spheroidal nuclear surface. While their calculations do not directly apply to the decay of U^{233}, it is interesting to note that all of their five calculated distributions are strongly peaked, and three of them are peaked near the nuclear equator. This latter type of distribution on the nuclear surface would permit a qualitative agreement among our results, the bonding calculations, and the spheroidal barrier picture.

[25] C. A. Coulson, private communication.

[26] J. C. Eisenstein and M. H. L. Pryce, *Proc. Roy. Soc.* (*London*) **A229**, 20 (1955).

[27] J. O. Rasmussen and B. Segall, *Phys. Rev.* **103**, 1298 (1956).